AD-A246 775

NPS OC-91-002

NAVAL POSTGRADUATE SCHOOL
Monterey, California

DTIC
ELECTE
MAR 0 4 1992
S
D
D

THESIS

A NUMERICAL STUDY OF TIME-DEPENDENT WIND
FORCING OFF THE WEST COAST
OF PORTUGAL, 1987-1988

by

Stephen L. Buss

June, 1991

Thesis Advisor: Mary L. Batteen

Approved for public release; distribution is unlimited.

92-05293

92 3 02 053

NAVAL POSTGRADUATE SCHOOL
Monterey, California

Rear Admiral R. W. West   Provost H. Shull
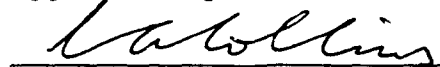Superintendent

The work reported herein was prepared for the Office of Naval Research
and funded by Naval Postgraduate School.

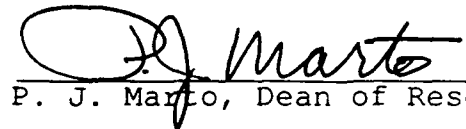Reproduction of all or part of this report is authorized.

Principal author for this report was:

_____
S. L. Buss, LT, USN

Approved by:

_____
C. A. Collins, Chairman
Department of Oceanography

Released by: P. J. Marto, Dean of Research

REPORT DOCUMENTATION PAGE

1a. REPORT SECURITY CLASSIFICATION UNCLASSIFIED		1b. RESTRICTIVE MARKINGS	
2a. SECURITY CLASSIFICATION AUTHORITY		3. DISTRIBUTION/AVAILABILITY OF REPORT Approved for public release; distribution is unlimited.	
2b. DECLASSIFICATION/DOWNGRADING SCHEDULE			
4. PERFORMING ORGANIZATION REPORT NUMBER(S) NPS OC-91-002		5. MONITORING ORGANIZATION REPORT NUMBER(S)	
6a. NAME OF PERFORMING ORGANIZATION Naval Postgraduate School	6b. OFFICE SYMBOL (If applicable) OC	7a. NAME OF MONITORING ORGANIZATION Office of Naval Research	
6c. ADDRESS (City, State, and ZIP Code) Monterey, CA 93943-5000		7b. ADDRESS (City, State, and ZIP Code) 800 N. Quincy Street Arlington, VA 22217-5000	
8a. NAME OF FUNDING/SPONSORING ORGANIZATION Naval Postgraduate School	8b. OFFICE SYMBOL (If applicable)	9. PROCUREMENT INSTRUMENT IDENTIFICATION NUMBER O & MN, Direct Funding	

8c. ADDRESS (City, State, and ZIP Code) Monterey, CA 93943-5000	10 SOURCE OF FUNDING NUMBERS			
	Program Element No	Project No	Task No	Work Unit Accession Number

11. TITLE (Include Security Classification)

A Numerical Study of Time-Dependent Wind Forcing off the West Coast of Portugal, 1987-1988

12. PERSONAL AUTHOR(S)

13a. TYPE OF REPORT Master's Thesis	13b. TIME COVERED From To	14. DATE OF REPORT (year, month, day) June 1991	15. PAGE COUNT 122

16. SUPPLEMENTARY NOTATION

The views expressed in this thesis are those of the author and do not reflect the official policy or position of the Department of Defense or the U.S. Government.

17. COSATI CODES			18. SUBJECT TERMS (continue on reverse if necessary and identify by block number)
FIELD	GROUP	SUBGROUP	Eastern Boundary Current Eddies, Wind Forcing, Canary Current

19. ABSTRACT (continue on reverse if necessary and identify by block number)

A process-oriented numerical study of time-dependent wind forcing is conducted using a ten-layer, beta plane, primitive equation ocean model to provide insight into mesoscale eddy generation off the west coast of Portugal from 1987 to 1988. The wind forcing used was derived from synoptic surface pressure analyses off Lisbon, Portugal. Results obtained show that eddies generated during the coastal upwelling season (generally occurring during the spring and summer) decay during the winter. Only cyclonic eddies form during the 1987 and 1988 upwelling seasons. The eddies are generated through a combination of barotropic and baroclinic instability mechanisms. Since the wind forcing of the five-month-long 1987 upwelling season generates larger and stronger eddies than the wind forcing of the seven-month-long 1988 upwelling season, eddy characteristics appear to be more influenced by the characteristics (e.g., intensity, duration and frequency of occurrence) of the wind forcing than by the total length of the upwelling season. This study affirms the importance of wind stress forcing to the overall surface circulation and eddy generation in the coastal ocean regime off the west coast of Portugal.

20 DISTRIBUTION/AVAILABILITY OF ABSTRACT ☒ UNCLASSIFIED/UNLIMITED ☐ SAME AS REPORT ☐ DTIC USERS	21 ABSTRACT SECURITY CLASSIFICATION UNCLASSIFIED	
22a NAME OF RESPONSIBLE INDIVIDUAL M.L. Batteen	22b TELEPHONE (Include Area code) 408-646-2768	22c OFFICE SYMBOL OC/Bv

DD FORM 1473, 84 MAR   83 APR edition may be used until exhausted
All other editions are obsolete

A Numerical Study of Time-Dependent Wind
Forcing off the West Coast
of Portugal 1987-1988

by

Stephen L. Buss
Lieutenant, United States Navy
B.S., United States Naval Academy, 1982

Submitted in partial fulfillment
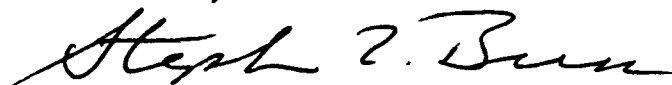of the requirements for the degree of

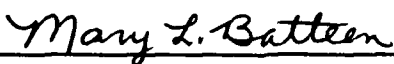MASTER OF SCIENCE IN PHYSICAL OCEANOGRAPHY
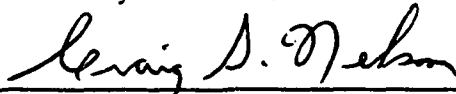
from the

NAVAL POSTGRADUATE SCHOOL
June 1991

Author: _____

Stephen L. Buss

Approved by: _____

Mary L. Batteen, Thesis Advisor

_____

Craig S. Nelson, Second Reader

_____

Curtis A. Collins, Chairman
Department of Oceanography

ABSTRACT

A process-oriented numerical study of time-dependent wind forcing is conducted using a ten-layer, β-plane, primitive equation ocean model to provide insight into mesoscale eddy generation and duration off the west coast of Portugal from 1987 to 1988. The wind forcing used was derived from synoptic surface pressure analyses off Lisbon, Portugal. Results obtained show that eddies generated during the coastal upwelling season (generally occurring during the spring and summer) decay during the winter. Only cyclonic eddies form during the 1987 and 1988 upwelling seasons. The eddies are generated through a combination of barotropic and baroclinic instability mechanisms. Since the wind forcing of the five-month-long 1987 upwelling season generates larger and stronger eddies than the wind forcing of the seven-month-long 1988 upwelling season, eddy characteristics appear to be more influenced by the characteristics (e.g., intensity, duration and frequency of occurrence) of the wind forcing than by the total length of the upwelling season. This study affirms the importance of wind stress forcing to the overall surface circulation and eddy generation in the coastal ocean regime off the west coast of Portugal.

iii

TABLE OF CONTENTS

LIST OF TABLES

LIST OF FIGURES

ACKNOWLEDGEMENTS

I. INTRODUCTION

The importance of oceanic Eastern Boundary Current (EBC) regions to human life cannot be overestimated. The biological productivity of these areas is substantial, in fact, it is more highly concentrated in these regions than almost anywhere else in the world ocean. The four million pounds of anchovy removed over a one-year period from an 800 by 30 mile coastal strip (~0.02% of the world ocean surface area) comprising the inshore waters off Peru amounted to one-seventh of the total world landings of fish for that same year (Wooster and Reid, 1963). These nutrient-rich waters, with their close proximity to land, provide economic and physical sustenance to large portions of the world's population.

EBC regions are important militarily as well. Coastal processes occurring in EBC areas are of particular importance to the Navy. In fact, naval research planning and programming guidance from the Chief of Naval Research has targeted coastal processes because they "...impact heavily amphibious operations, shallow water ASW, and the structure of the ocean circulation/composition in the mid-field region." (Chief of Naval Research, 1987).

It is no wonder that there is significant scientific interest in EBCs and the surrounding coastal oceanic environment. A region so important economically and militarily must be completely understood in order to maximize its productivity and increase its usefulness.

A. BACKGROUND

Upper-layer circulation in the subtropical oceans of the world may be characterized by large anticyclonic gyres with predominantly zonal currents at the northern and southern boundaries and meridional currents at the eastern and western boundaries (Figure 1). The meridional current along the western boundary is called a Western Boundary Current (WBC), while the meridional current along the eastern boundary is called an Eastern Boundary Current (EBC).

There are four "classical" subtropical EBCs, which include the following:

- **California Current** (off the west coast of North America)

- **Peru Current** (off the west coast of South America)

- **Benguela Current** (off the west coast of South Africa)

- **Canary Current** (off the west coast of Europe and North Africa).

The EBC of the Indian Ocean is anomalous and, although it is frequently mentioned in articles (e.g., Wooster and Reid, 1963) on upwelling and EBCs, it is largely a source of illustrative contrast. It is of little wonder, yet worthy of note, that most EBC studies have been biased towards subtropical EBCs. This is, in part, due to the relatively mild conditions and general convenience under which these currents may be observed. The poleward reaches of the Canary Current are the focus of this study.

1. Common Features of EBCs

Well-developed, sub-tropical EBCs have compensating equatorward flow for the strong poleward flow found on the western boundary of the gyres (Wooster and Reid,

2

1963). They are fed by the west wind drifts, which in the case of the Canary Current is the North Atlantic Drift (Pickard and Emery, 1982).

Generally, isotherms run meridionally along eastern boundaries. This is contrasted by the predominantly zonal orientation of the isotherms found farther west (Wooster and Reid, 1963).

Surface salinities are strongly influenced by source waters and the seasonal impact of coastal upwelling, which can increase or decrease surface salinity depending on the variation of salinity with depth (Wooster and Reid, 1963). In most EBC regions salinity decreases with increasing depth, so that upwelling causes a decrease in surface salinity. The west coast of North America is an exception where salinity increases with depth, so that upwelling in this region produces an increase in surface salinity (Pickard and Emery, 1982). Upwelling is covered in greater detail below.

Generally, the EBCs are slow, broad and shallow with low volume transport. This is in contrast to the Western Boundary Currents (WBCs), like the Gulf Stream, which are narrow, swift and deep with high volume transports (Wooster and Reid, 1963).

2. Upwelling Processes

Upwelling is classically defined as the vertical advection of colder, nutrient-rich water from subsurface layers to the surface layer caused by horizontal divergence in the surface layer (Smith, 1968). At the coast, the horizontal divergence in the surface layer is caused by wind-stress induced offshore Ekman transport. The surface layer affected by Ekman transport is roughly the same thickness as the mixed layer, on the order of 50-100 m depth (Brink, 1983).

There are three oceanic regions where upwelling is a dominant process: along the equator, in regions of strong cyclonic wind stress curl and along subtropical eastern ocean boundaries. Coastal upwelling along eastern boundaries is a significant bio-physical process and perhaps the biggest reason for the military, economic and biological importance of the regions. Since coastal upwelling at oceanic eastern boundaries is dominated by the coastal wind stress (Smith, 1968), it is a highly time-dependent process. Periods of predominantly equatorward (upwelling favorable) winds tend to induce upwelling while periods of predominantly poleward winds tend to reduce or eliminate upwelling and force downwelling. The effects of coastal upwelling are confined primarily in the cross-shore direction to distances on the order of 10-50 km. This distance is the baroclinic Rossby radius of deformation, the horizontal scale at which the ocean can respond to wind stress (Huyer, 1983).

3. General Circulation

The focus of this study is the very northern reaches of the Canary Current off the west coast of the Iberian Peninsula. A short review of the general circulation of the atmosphere and ocean in the vicinity of the Iberian Peninsula is presented here as an aid to understanding the motivation for this investigation.

The atmospheric circulation over the Eastern North Atlantic Ocean is dominated by a high pressure center located in the vicinity of the Azores. This high pressure center, frequently called the Azores High, tends to move southward and weaken in winter, which allows the Icelandic Low to assert greater influence on the atmospheric circulation off the west coast of the Iberian Peninsula (Figures 2 and 3). The seasonal

4

variation in the location, intensity and areal coverage of the Azores High and the Icelandic Low controls the seasonal variation in wind stress. Seasonal variations in the wind stress dominate the general ocean surface circulation. Periods of predominantly poleward wind stress (generally occurring in fall and winter) force poleward flow. Periods of predominantly equatorward wind stress (generally occurring in spring and summer) force equatorward flow and initiate the coastal upwelling that dominates this "classical" EBC region. Figure 4 shows the seasonal variation of wind stress off the Iberian Peninsula (Bakun and Nelson, 1991). Superimposed on the seasonal variation of the wind stress there can be 2-20 day events and relaxations of equatorward winds, and reversals to poleward winds similar to those found off Oregon (Huyer, 1983).

The poleward alongshore surface flow generated by the predominantly poleward wind stress during fall and winter has mean velocities of ~10 cm/s or less (Barton, 1989; Haynes and Barton, 1990; Frouin et al., 1990). Poleward alongshore flow also occurs during the upwelling season (spring and summer), but instead of being the dominant surface flow, it can be a poleward undercurrent. This poleward flow has mean velocities of ~2-10 cm/s (Miencke et al., 1975; Fiuza, 1982; Ambar, 1985, cited by Barton, 1989). The predominantly equatorward surface flow which occurs primarily during the upwelling season (spring and summer) has mean velocities of ~10 cm/s (Wooster et al., 1976).

Recently, significant attention has been paid to the formation and growth of cold-water filaments and cyclonic and anticyclonic eddies in EBC regions. These have been seen in hydrographic surveys (Figure 5) as well as in remotely-sensed observations

5

(Figure 6) in the coastal ocean off the west coast of Portugal. Fiuza and Sousa (1989) and Barton (1986) have observed that the filaments of cold water extend westward from the coast. The influence of mesoscale eddies on the filaments has been noted by Fiuza and Sousa (1989) but questions remain as to the extent of that influence.

In addition to cold water filaments, there is significant interest in the poleward flow along the west coast of the Iberian Peninsula. Haynes and Barton (1990) postulated that the poleward flow was the result of thermohaline forcing which was generated by the weakening or reversal of the summertime equatorward winds. Frouin *et al.* (1990) investigated observations of a wintertime poleward surface flow off the coasts of Portugal and Spain and concluded that onshore Ekman convergence induced by southerly winds accounted for one-fifth of the transport and that the addition of geostrophic adjustment of the large-scale zonal flow provided a better quantitative agreement with the observations. The poleward current observed by Frouin *et al.* (1990) was 25-40 km wide, 200 m deep and characterized by velocities of 20-30 cm/s.

Numerical studies have been conducted on the coastal ocean processes occurring off the west coast of the Iberian Peninsula. In particular, Lopes da Costa (1989) investigated the role of time dependent wind forcing from February to December 1986, in the generation of eddies, jets, fronts, and upwelling filaments off the west coast of the Iberian Peninsula. He found that: the vertical extent and cross-section of the model-simulated surface equatorward jet was increased and the poleward undercurrent was reduced by equatorward wind events; the vertical extent of the surface equatorward jet was reduced, the cross-sectional area of the poleward undercurrent increased and the

6

poleward current shoaled nearshore in response to relaxations of the equatorward winds; and a complete reversal of equatorward winds or periods of poleward winds created a poleward surface current nearshore and displaced the equatorward current offshore. Additionally, he observed the generation of eddies during the middle of the upwelling season that weakened by the end of the upwelling season. Accompanying the growth and decay of these eddies was a weakening or disappearance of the equatorward surface current and the development of a poleward surface current nearshore.

B. OBJECTIVES

The importance of wind stress to the surface circulation and eddy generation in the coastal ocean is undeniable. While there are other processes at work in the coastal regime, it is the wind stress that induces the coastal upwelling in EBC regions and generates the surface currents and eddies in these regions.

The primary objective of this study is to gain a greater understanding of the influence of time-dependent wind stress on the general upper layer circulation and mesoscale eddy-generation processes in the ocean off the coast of Portugal. In particular, by continuing the time-dependent wind forcing for follow-on years 1987 and 1988 of the same primitive equation model (described in the next chapter) used by Lopes da Costa (1989), the following questions can be investigated: Do the eddies which remained at the end of 1986 completely decay before the next upwelling season or are they simply rejuvenated and maintained by the equatorward winds? What is the generation

mechanism for the eddies? Does the length of the upwelling season influence the characteristics of the eddies?

The organization of the study is as follows. In Chapter II the ocean model and the analysis techniques are described. In Chapter III the results of the model simulation along with an analysis of the results are shown. A summary is presented in Chapter IV.
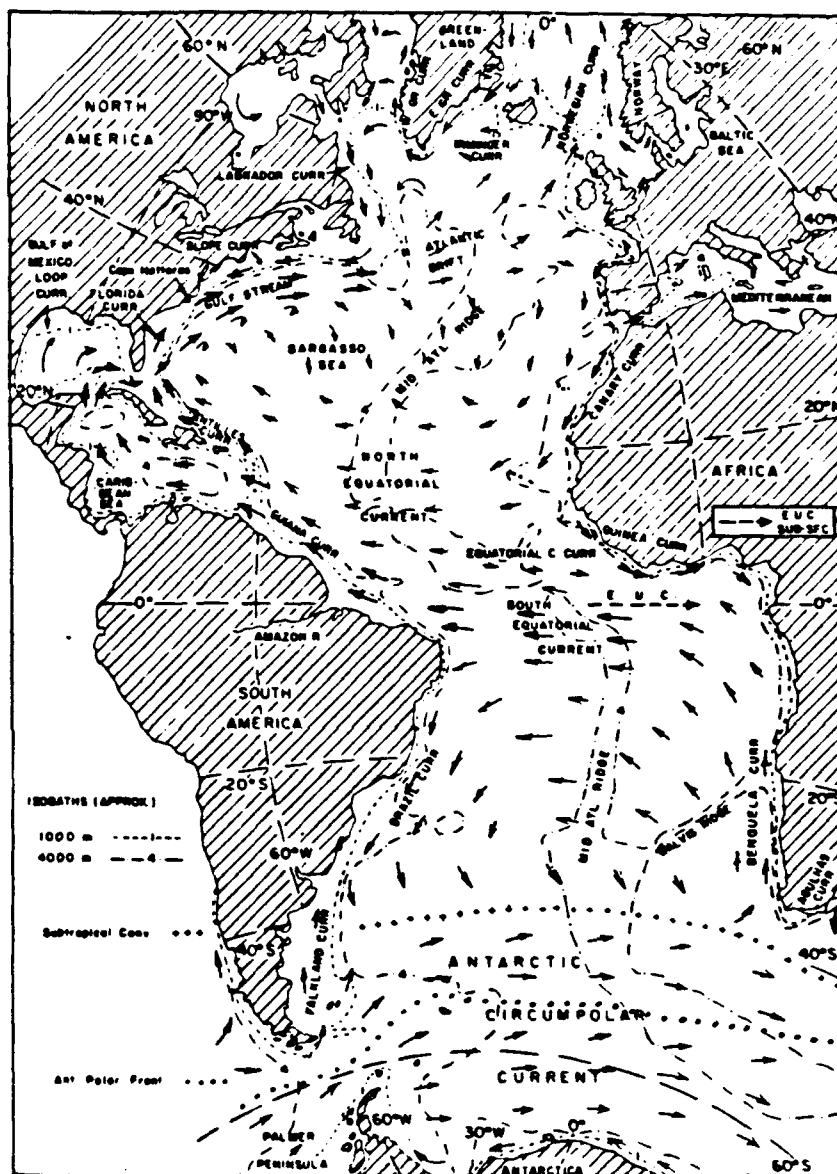
Figure 1. Atlantic Ocean surface circulation. (Pickard and Emery, 1982)
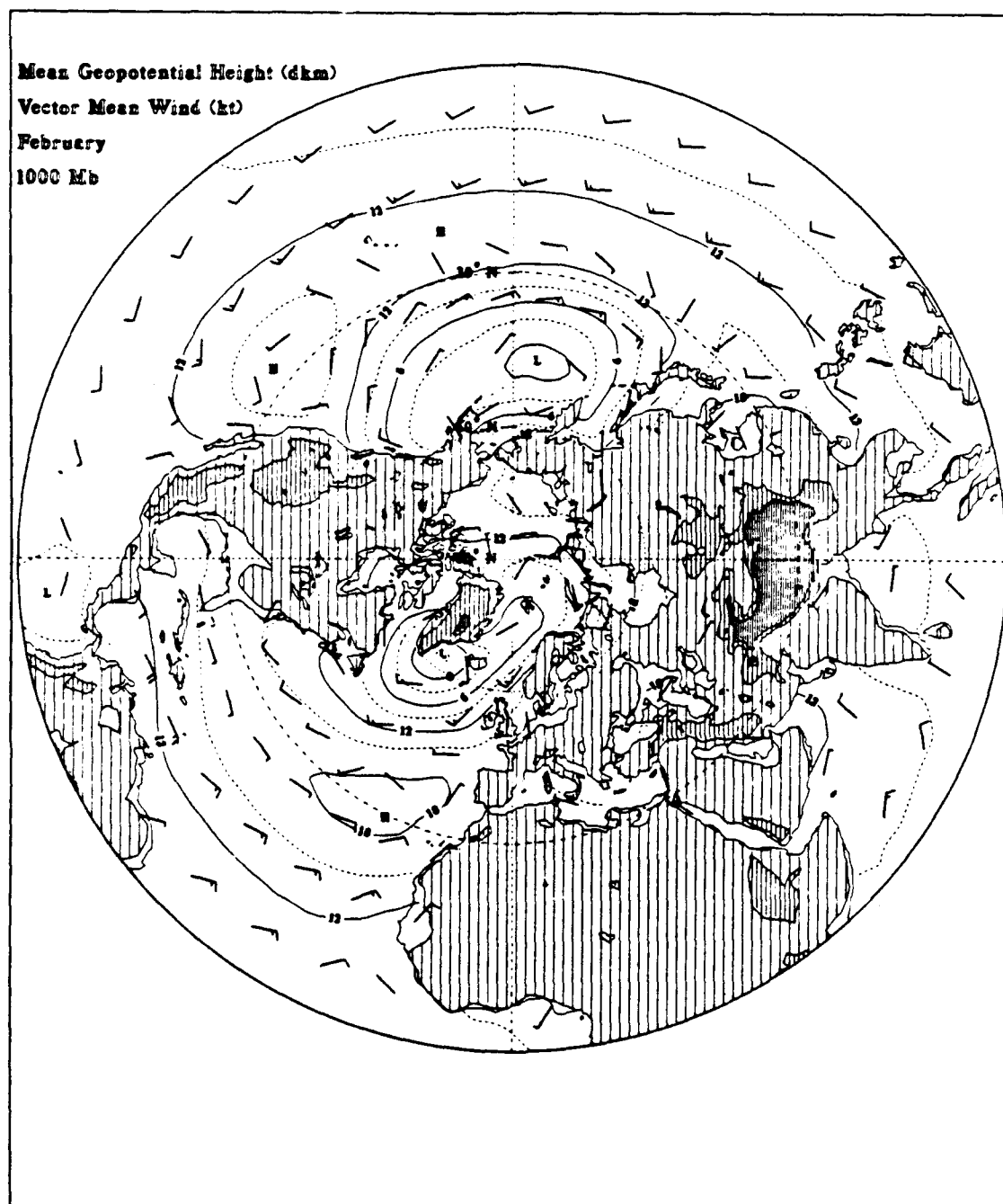
Figure 2. 1000 mb geopotential height (dekameters) averaged over 1980-1985 on a 2.5° global grid for February. (NOCD, Asheville, N. C., 1989)
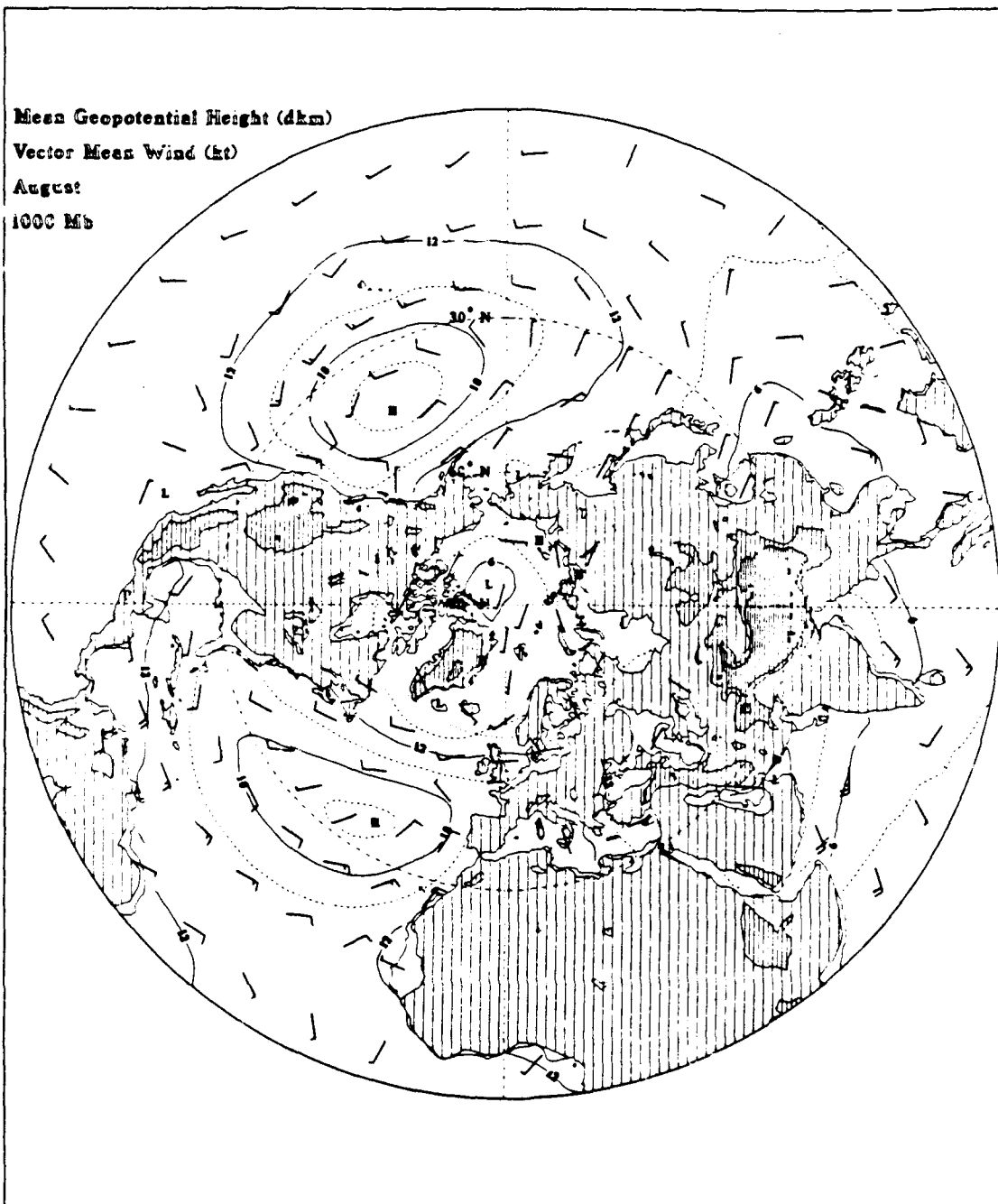
Figure 3. 1000 mb geopotential height (dekameters) averaged over 1980-1985 on a 2.5° global grid for August. (NOCD, Asheville, N. C., 1989)
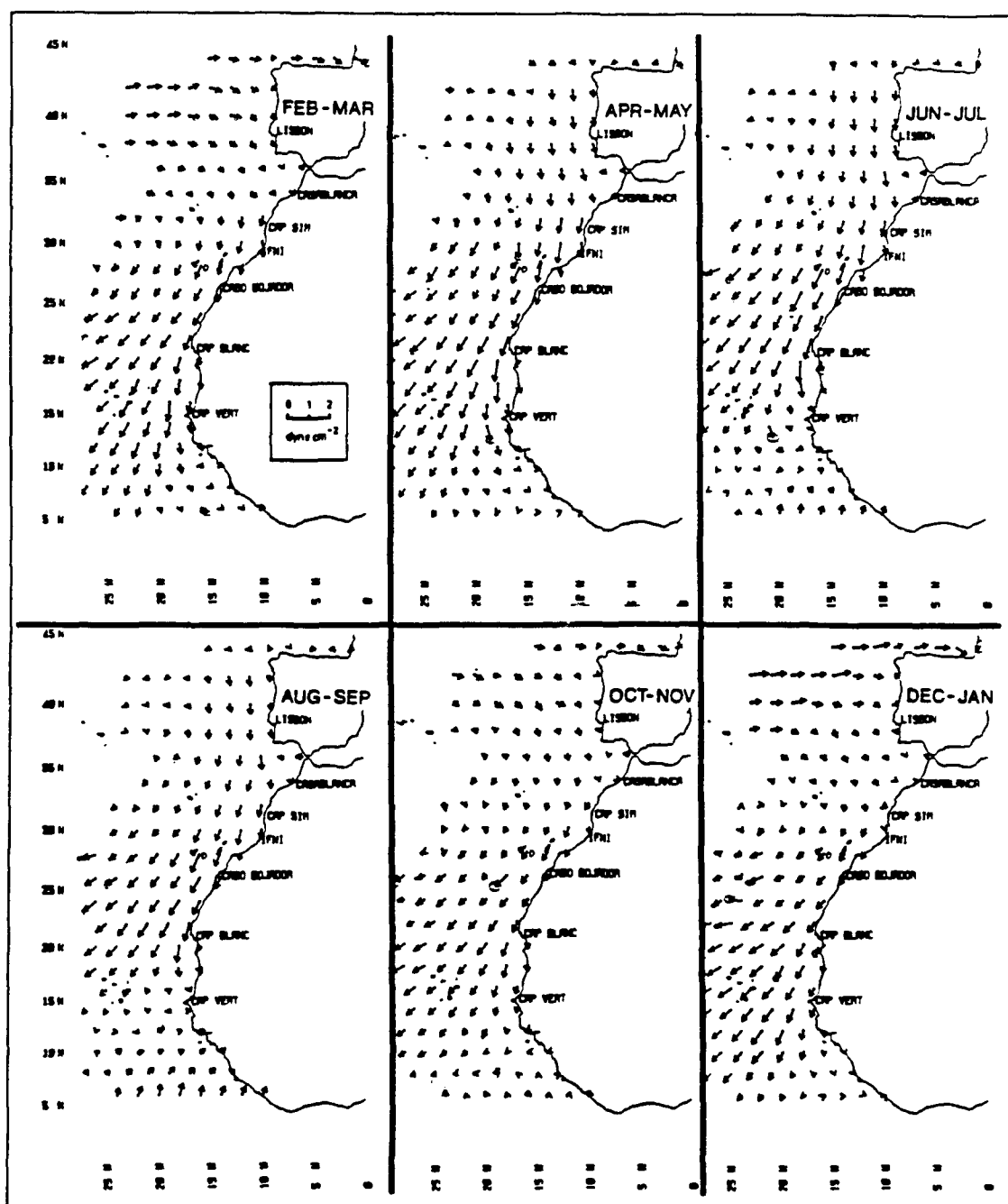
Figure 4. Seasonal variation of wind stress (dyne cm⁻²) over the northern reaches of the Canary Current (Bakun and Nelson, 1991)
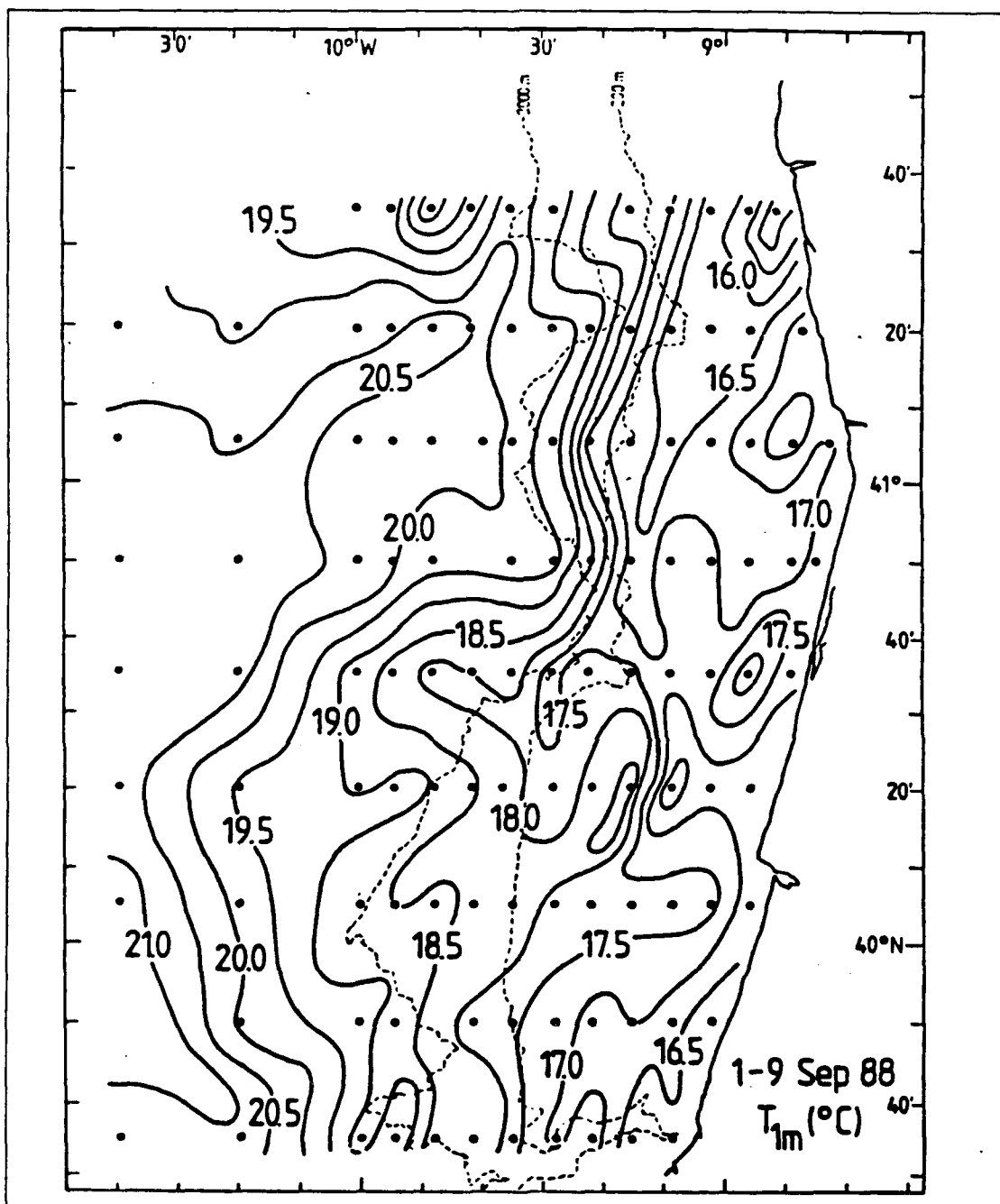
Figure 5. Sea surface temperature (°C) distribution off the northern coast of Portugal from "in situ" measurements made in Sept. 1988 (Fiuza and Sousa, 1989).
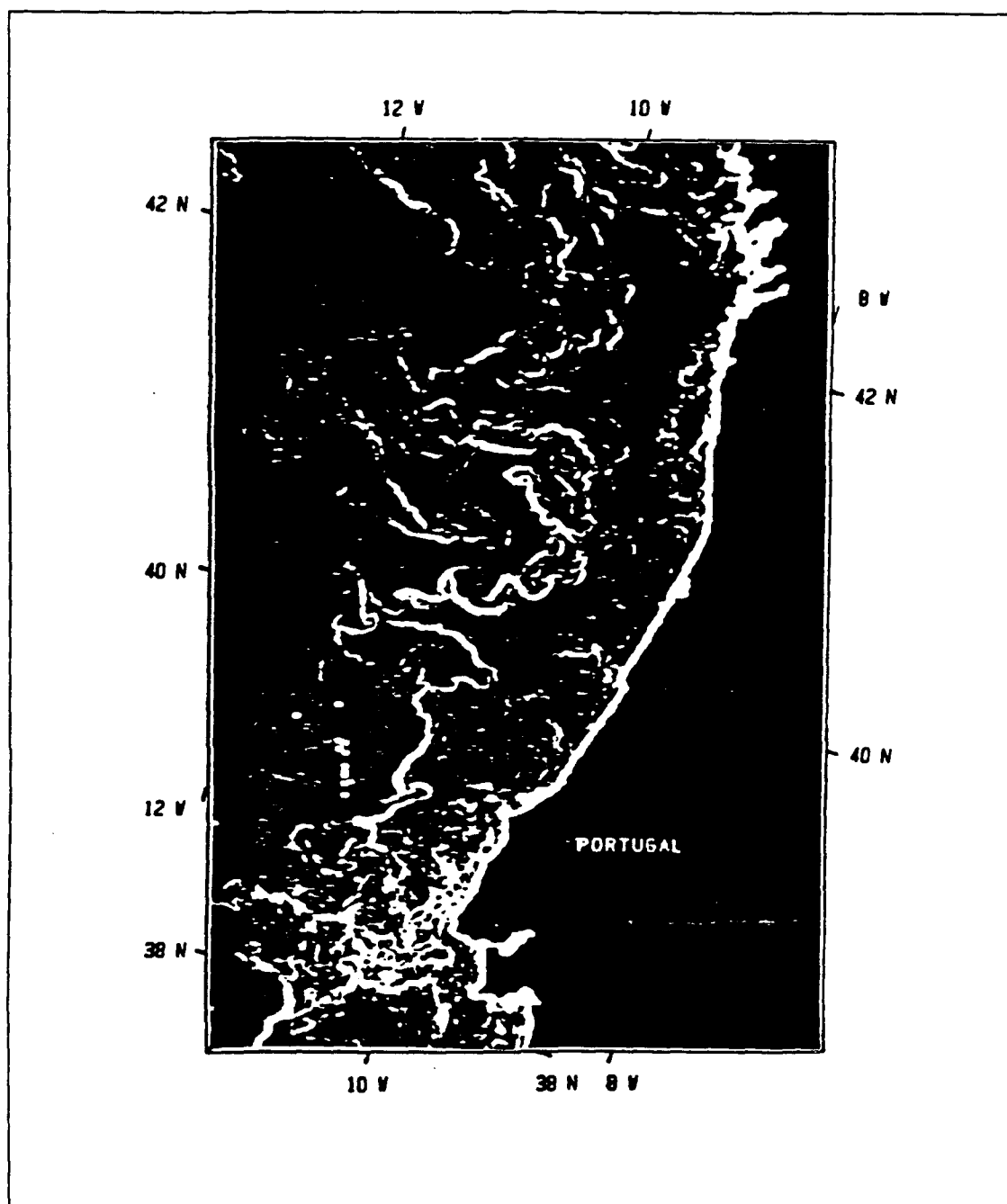
Figure 6. Sea surface temperature gradient patterns showing filament structure off Portugal in Sept. 1982 (Barton, 1986).

II. METHODS

A. THE NUMERICAL MODEL

The numerical model used in this investigation is a primitive equation (PE) model originally developed by Haney (1985) for a closed basin and adapted by Batteen *et al.* (1989) for limited area EBC regions. A more rigorous description of the model is available in the references mentioned above. Here, a brief summary of relevant features is presented.

To permit dynamic and thermodynamic process-oriented studies, the model uses non-adiabatic PEs with the following approximations and assumptions:

- hydrostatic and traditional assumptions characteristic of PE models in general (Phillips, 1966);

- Boussinesq approximation;

- density as a function of temperature only;

- β-plane approximation.

In the model's equations, the spatial variables x, y and z form a right-handed cartesian coordinate system with the positive x-direction towards shore, positive y-direction poleward alongshore and positive z-direction upwards. The variables u, v and w represent the x, y and z components of velocity, respectively. Additionally, t represents time, T temperature, p pressure and ρ density. Table 1 fully defines the remaining

15

constants used in the model. The governing equations form a closed system of six

equations and six unknowns (u, v, w, p, ρ and T) that may be written as:

$$\frac{du}{dt} = -\frac{1}{\rho_0}\frac{\partial p}{\partial x} + fv - A_m\nabla^4 u + K_m\frac{\partial^2 u}{\partial z^2} + \delta_d(u) \tag{1}$$

$$\frac{dv}{dt} = -\frac{1}{\rho_0}\frac{\partial p}{\partial y} - fu - A_m\nabla^4 v + K_m\frac{\partial^2 v}{\partial z^2} + \delta_d(v) \tag{2}$$

$$\frac{\partial p}{\partial z} = -\rho g \tag{3}$$

$$\frac{\partial u}{\partial x} + \frac{\partial v}{\partial y} + \frac{\partial w}{\partial z} = 0 \tag{4}$$

$$\rho = \rho_0(1 - \alpha(T - T_0)) \tag{5}$$

$$\frac{dT}{dt} = -A_H\nabla^4 T + K_H\frac{\partial^2 T}{\partial z^2} + Q_S + \delta_d(T). \tag{6}$$

In equation (6) the heating due to solar radiation (Q_S) as a function of depth is:

$$Q_s = \frac{1}{\rho_0 C}\frac{\partial S}{\partial z}, \tag{7}$$

16

and the total downward flux of solar radiation (S) in equation (7) is:

$$S = S_0(Re^{z/z_1} + (1-R)e^{z/z_2}) . \qquad (8)$$

In equation (8), the downward flux of solar radiation at the surface is S_0, the fraction of incoming radiation absorbed in the upper few meters is 0.62 (R=0.62) and the fraction of incoming radiation that penetrates to deeper levels is 0.38 ((1-R)=0.38) with z_1=1.5 m and z_2=20 m following Paulson and Simpson (1977). In equations (1), (2) and (6) the terms $\delta_d(u)$, $\delta_d(v)$ and $\delta_d(T)$ represent the vertical turbulent mixing of zonal momentum, meridional momentum and heat, respectively (Lopes da Costa, 1989).

The finite differencing scheme used in the model is a space-staggered B-scheme (Arakawa and Lamb, 1977; Batteen and Han, 1981). There are ten layers separated by constant z-levels at 13, 46, 98, 182, 316, 529, 870, 1416, 2283, and 3656 m.

1. Boundaries

a. Horizontal

The northern, southern and western boundaries of the model domain are open with some spatial smoothing applied within 5 grid points of the boundary (approximately 50 km). The eastern boundary is closed. It is modeled as a straight vertical wall.

b. *Vertical*

At the top (z = 0) of the model domain, the boundary conditions are:

$$K_m \frac{\partial u}{\partial z} = 0 \tag{9}$$

$$K_m \frac{\partial v}{\partial z} = \frac{\tau^y}{\rho_0} \tag{10}$$

$$K_H \frac{\partial T}{\partial z} = -Q_B \tag{11}$$

$$w = 0 \tag{12}$$

In equation (8) above, τ^y is the alongshore component of the wind stress. The wind forcing used in the model will be discussed in the next chapter. In equation (11), Q_B is the net upward flux of long wave radiation, sensible heat, and latent heat across the surface.

The boundary conditions at the bottom (z = -H) of the model domain are:

$$K_m \frac{\partial u}{\partial z} = C_D (u^2 + v^2)^{1/2} (u\cos\gamma - v\sin\gamma) \tag{13}$$

$$K_m \frac{\partial v}{\partial z} = C_D (u^2 + v^2)^{1/2} (v\cos\gamma - u\sin\gamma) \tag{14}$$

18

$$K_H \frac{\partial T}{\partial z} = 0 \qquad\qquad (15)$$

$$w = 0 \qquad\qquad (16)$$

In equations (13) and (14) (based on Weatherly, 1972), C_D is the bottom drag coefficient. The remaining symbols and constants are defined in Table 1.

2. Model Domain

The domain of the model is a rectangular box covering approximately 6 degrees of longitude beginning at 9° W, and ~9.5 degrees of latitude beginning at 34.7°N. This forms a region extending approximately 512 km offshore and 1024 km along the coast (Figure 7). The domain is flat-bottomed with a uniform depth of 4500 m.

3. Initialization

An exponential temperature field, based on Levitus (1982) climatology (Figure 8 where 42.5°N, 12.5°W is the north location and 37.5°N, 12.5°W is the south location), of the form shown in Figure 9 is used to initialize the model. The functions used to initialize each of the ten levels are:

19

$$T(z) = 9.8 + 7.7e^{(z/300)}, \quad (-500m \leq z \leq 0m) \tag{17}$$

$$T(z) = 11.25 + 7.857 \times 10^{-4}(z + 500), \quad (-1200m \leq z < -500m) \tag{18}$$

$$T(z) = 2.5 + 8.2e^{(\frac{(z + 1200)}{600})}, \quad (-4500m \leq -1200m). \tag{19}$$

B.   ANALYSIS TECHNIQUES

Energy analyses will be applied to model output to gain insight into the predominant eddy-generating mechanisms.   The technique to be used provides an understanding of the interactions between the time-averaged flow and the mesoscale eddies and is based on that of Han (1975) and Semtner and Mintz (1977).   In this analysis, eddy-generating mechanisms will be identified by the type of energy transfer taking place, following Batteen and Rutherford (1990).   In particular, the transformation of eddy available potential energy into eddy kinetic energy is an indicator of baroclinic instability and the transformation of time mean kinetic energy into eddy kinetic energy is an indicator of barotropic instability.   Following the Semtner and Mintz (1977) notation:

$\overline{(\ )}$	time average
$(\ )'$	time deviation
$(\hat{\ })$	horizontal space average
$(\ )^*$	horizontal space deviation,

20

the kinetic, time mean and eddy kinetic energy calculations are:

$$K = \frac{u^2 + v^2}{2} \tag{20}$$

$$\overline{K} = \frac{\overline{u}^2 + \overline{v}^2}{2} \tag{21}$$

$$K' = \frac{\overline{u'^2} + \overline{v'^2}}{2}. \tag{22}$$

The eddy available potential energy is calculated by:

$$P' = \alpha g [\frac{1}{2} \overline{(T'^*)^2} (\frac{\partial \overline{T}}{\partial z})^{-1}]. \tag{23}$$

The transfer from time mean to time eddy kinetic energy, an indicator of barotropic instability, is calculated by:

$$\{\overline{K} \to K'\} = \overline{v} \cdot (\nabla \cdot \overline{v'v'} + \frac{\partial}{\partial z} \overline{w'v'}). \tag{24}$$

The transfer from eddy available potential to eddy kinetic energy, an indicator of baroclinic instability, is calculated by:

$$\{P' \to K'\} = \alpha g [\overline{T'w'}]. \tag{25}$$

21

Equation (20) is used to calculate time series of total kinetic energy for 1987 and 1988. By examining the quasi-steady state prior to and during eddy generation, energy transfer plots calculated from equations (24) and (25) can be used to determine the predominant instability mechanism.

Table 1. Values of constants used in model (from Lopes da Costa, 1989).

	Value	Name
Ω	$2\,\pi\;day^{-1}$	earth rotation rate
C	$0.958\;cal\;gm^{-1}\;(°K)^{-1}$	specific heat of sea water
C_D	1.3×10^{-3}	drag coefficient
L	$595.\;cal\;gm^{-1}$	latent heat of sea water
T_o	$278.2°K$	constant reference temperature
ρ_o	$1.23 \times 10^{-3}\;gm\;cm^{-3}$	density of air
ρ_o	$1.0276\;gm\;cm^{-3}$	density of sea water at T_o
α	$2.01 \times 10^{-4}\;(°K)^{-1}$	thermal expansion coefficient
K	10	number of levels in vertical
ΔX	$8. \times 10^{5}\;cm$	zonal grid spacing
ΔY	$1.6 \times 10^{6}\;cm$	meridional grid spacing
D	$4.5 \times 10^{5}\;cm$	total ocean depth
ϕ_o	$34.7°\;N$	latitude of southern boundary
ϕ_-	$44.3°\;N$	latitude of northern boundary
λ_o	$9.0°\;W$	longitude of eastern boundary
λ_-	$15.0°\;W$	longitude of western boundary
Δt	$800.\;s$	time step
f	$0.93 \times 10^{-4}s^{-1}$	Coriolis parameter
g	$980.\;cm\;s^{-2}$	acceleration of gravity
A_M	$2. \times 10^{17}\;cm^4\;s^{-1}$	biharmonic momentum diffusion coefficient
A_H	$2. \times 10^{17}\;cm^4\;s^{-1}$	biharmonic heat diffusion coefficient
K_M	$0.5\;cm^2\;s^{-1}$	vertical eddy viscosity
K_H	$0.5\;cm^2\;s^{-1}$	vertical eddy conductivity
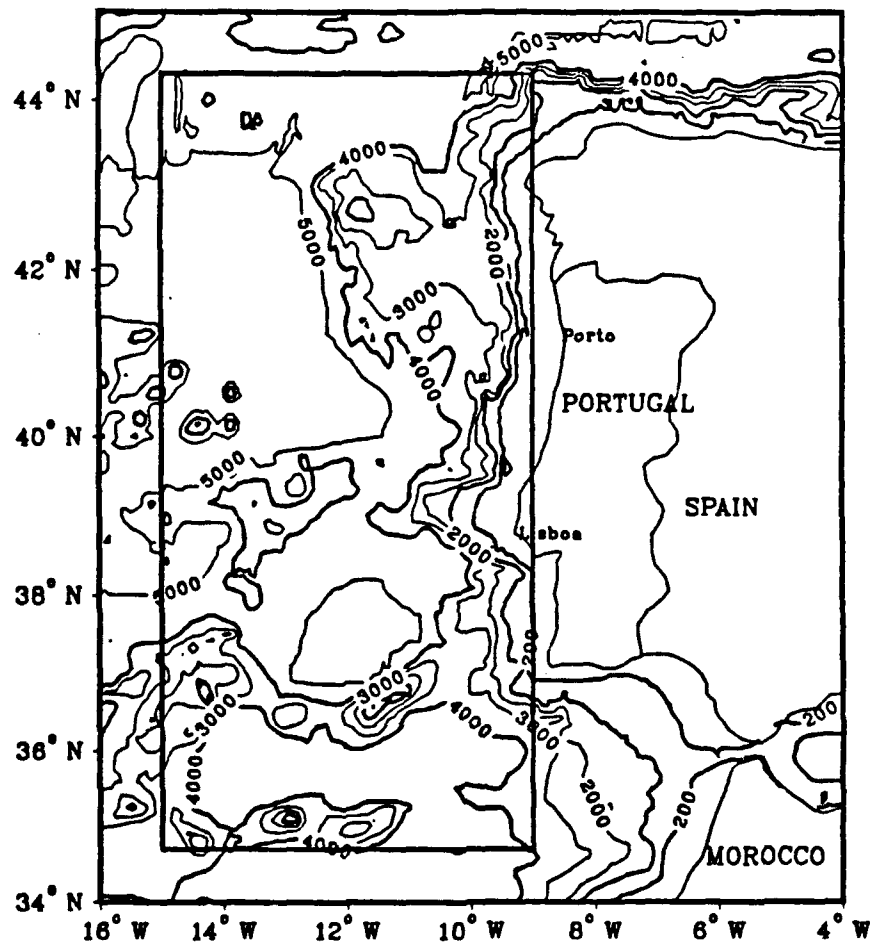
Figure 7. Model domain. Bathymetric contours in meters.

24
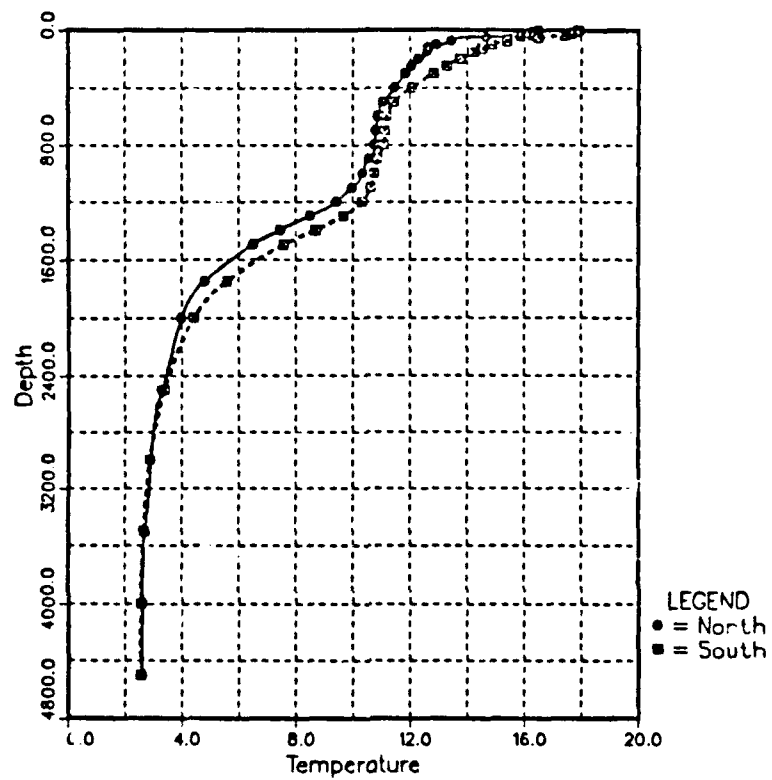
Figure 8. Climatological temperature (°C) profiles with depth (m) off Portugal (from Levitus, 1982).
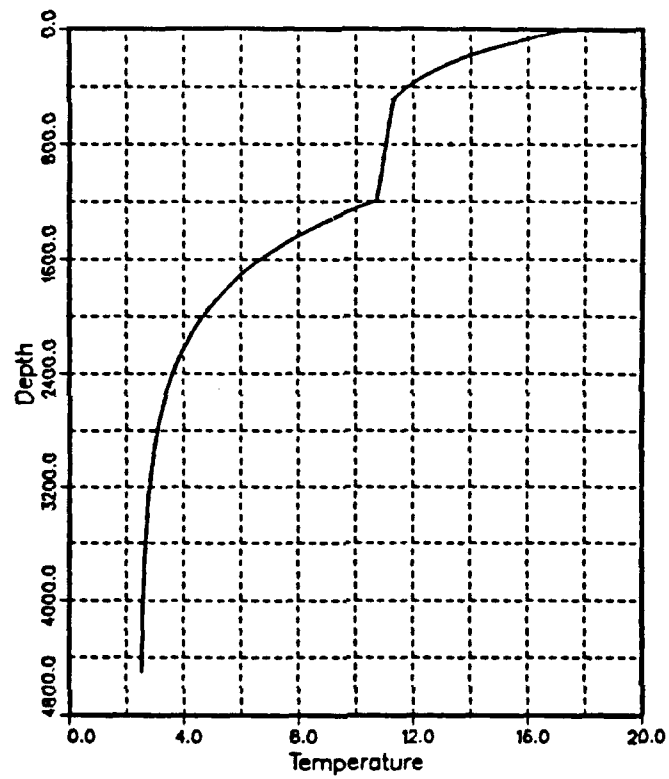
Figure 9. Temperature (°C) profile with depth (m) (from Lopes da Costa, 1989).

26

III. RESULTS

The model was forced using a time-varying value of the alongshore component of the wind stress derived at six-hourly intervals (four times a day) from the Fleet Numerical Oceanography Center (FNOC) surface pressure analyses for 1987 and 1988. Following Bakun (1973), the wind velocity was computed by multiplying the geostrophic wind speed by 0.7 and rotating its direction 15° to the left to account for friction. The wind forcing was applied uniformly throughout the domain to within 5 grid points of the northern and southern boundaries. This wind-band forcing was used to allow the propagation of coastal Kelvin waves. The propagation of the Kelvin waves allows an alongshore pressure gradient to be established, permitting a coastal trapped jet and relatively realistic undercurrent to be generated (Batteen *et al.*, 1991). In the absence of this banding, an alongshore current would develop that would be unrealistically strong and deep (Batteen *et al.*, 1991).

To facilitate discussion of the model's response, the model forcing was temporally subdivided into four phases. They are:

- **Pre-Upwelling Phase**: defined by the beginning of the calendar year and the end of predominantly poleward winds.

- **Upwelling Favorable (Pre-Eddies) Phase**: defined by the beginning of predominantly equatorward winds and the initial appearance of eddies.

- **Upwelling Favorable (Eddies Present) Phase**: defined by the initial appearance of eddies and the end of predominantly equatorward winds.

27

- **Post-Upwelling Phase**: defined by the beginning of predominantly poleward winds and the end of the calendar year.

Consistent with the expected atmospheric circulation (Figures 2 and 3), the monthly means for both the time series (Figures 10 and 11) and numerical summaries (Tables 2 and 3) of the alongshore component of wind off Lisbon, Portugal for 1987 and 1988 show a peak in equatorward winds in the summer months and generally poleward winds in the winter. As described earlier, the equatorward wind stress creates conditions favorable for coastal upwelling. In 1987, the period of predominantly equatorward winds is approximately five months long (from May to September) and in 1988, equatorward winds dominate for approximately seven months (from March to September).

A. PRE-UPWELLING PHASE

1. 1987 Pre-Upwelling Phase

The 1987 Pre-Upwelling phase lasts until the end of April (day 120). Although the March mean is slightly equatorward, the poleward mean for April (Figure 10) prolongs the 1987 Pre-Upwelling phase until the end of April (day 120). As seen in the expanded time series (Figures 12 and 13), this phase may be characterized by several 8-10 day bursts of poleward winds, several 3-4 day bursts of poleward winds and many high frequency fluctuations. Based on analysis of the model's output, it will be seen that the response time of the ocean to the wind stress is on the order of one day; as a result, the higher frequency fluctuations will not be investigated. Two examples of the model's output in response to 3-4 and 8-10 day bursts of poleward winds are presented.

28

a.   8-10 Day Bursts of Poleward Winds

The poleward burst of interest occurred between days 50 and 60 (19 February to 1 March). During this period, almost exclusively poleward winds occurred, with one relatively small amplitude (1 m/s) equatorward fluctuation (Figure 12). The resulting flow is best illustrated with horizontal plots of the alongshore component of velocity and vertical cross-sections of the alongshore component of velocity and temperature (Figures 14 and 15).

The flow at 75 m depth at the beginning of this poleward burst is predominantly equatorward within 64 km of shore (Figure 14a). There is also predominantly equatorward flow at the surface (Figure 15a) with an equatorward jet between the coast and approximately 30 km offshore. This jet extends to an average depth of approximately 250 m, deeper to the north and somewhat shallower to the south (Figures 14a and 15a). In addition to the nearshore equatorward flow, there is evidence of a weak poleward undercurrent at the coast between depths of approximately 250 and 750 m (Figure 15a). The isotherms bend upward within 40 km of the coast (Figure 15c), consistent with the equatorward flow. This trend extends down to a depth of 500 m.

By the end of the poleward burst (day 60), the flow response shifts from a coastal equatorward flow to a poleward flow (Figure 14b). A cross section of the meridional velocity for day 60 (Figure 15b) shows predominantly poleward flow at the surface and evidence of a poleward jet between the coast and 60 km offshore. The isotherms between the surface and 125 m depth bend downward (Figure 15d), as expected.

29

b. *3-4 Day Bursts of Poleward Winds*

As shown in Figures 12 and 13, the winds were predominantly equatorward during the middle of March (day 75), until a poleward burst occurred between days 93-97 (3 April to 7 April). The flow at 75 m depth (Figure 16a) at the beginning of this burst is predominantly equatorward, with equatorward meridional velocities of ~4 cm/s along the coast. As a result of the poleward burst (days 93-97), this coastal flow reversed direction and became a 4 cm/s poleward flow (Figure 16b). The coastal equatorward flow on day 93 extended down to approximately 250 m depth (Figure 17a). Following the burst, the resulting poleward flow extended to approximately 700 m depth (Figure 17b). The response of the isotherms near the coast is consistent with the shift in direction of the wind stress. In particular, the slight upward trend evident on day 93 (Figure 17c) no longer exists on day 97 (Figure 17d).

c. *1987 Pre-Upwelling Phase Eddies*

An objective of this study is to determine the relationship between eddies generated in different upwelling seasons. There are several residual eddies present (Figure 18a) during the first phase of 1987 that were produced by 1986 eddy-generating mechanisms. These residual eddies disappear by the middle of March (Figure 18b).

2. 1988 Pre-Upwelling Phase

The forcing characteristics for 1988 (Figure 19) are similar to 1987 with two notable exceptions. First, the Pre-Upwelling Phase for 1988 is approximately one-fourth as long as the pre-upwelling phase for 1987, lasting until the end of January. Second, the

poleward bursts are of the order of only 2-5 days in length instead of the 8-10 day time scales for 1987. Two examples are presented.

a. 2-Day Poleward Burst

The meridional velocity field for 4 January (Figure 20a) indicates a residual poleward flow along the northern coast, that intensifies and spreads equatorward by 6 January as a result of the 2-day burst of poleward winds (Figure 20b). Dynamic height plots (Figures 21a and 21b) also support this observation as do vertical cross-sections of velocity (Figures 22a and 22b). By January 4 (Figure 22a), largely poleward surface flow in association with a subsurface equatorward flow is evident. By January 6 (Figure 22b), the surface poleward flow has increased in vertical extent and the equatorward flow has been substantially reduced as well as displaced offshore. The vertical cross-sections of temperature are consistent with the downwelling expected in association with poleward winds. Figure 22c shows a slight downturn at the coast in the surface isotherm which is more pronounced by day 6 (Figure 22d).

b. 4-Day Poleward Burst

This poleward burst occurred between 23 and 27 January (days 23 and 27 in Figure 19). The situation prior to the poleward burst is different than that prior to the 2-day burst presented above. Here the initial coastal flow is predominantly equatorward (as opposed to poleward on 4 January) in the near-surface layer (Figures 23a and 24a). By 27 January, following the burst of poleward winds, there is a reversal of the near-surface flow from equatorward to poleward near the coast (compare Figures 23a

31

and b and 24a and b). The effect here is the same as before, i.e., there is a reduction and movement offshore of the equatorward jet and an intensification and surfacing of the poleward flow. The response of the isotherms is the same as earlier, except that they initially bend upward at the coast due to offshore Ekman transport (Figure 24c). Following the burst there is a downward trend (Figure 24d).

c. 1988 Pre-Upwelling Phase Eddies

As in 1987, there are weak residual eddies in the nearshore flow during early 1988, which were produced by 1987 eddy-generating mechanisms (Figures 25a). The eddies left over from 1987 disappear towards the end of January (Figure 25b).

3. Pre-Upwelling Phase Summary

The response of the model to wind forcing during the Pre-Upwelling phase in 1987 and 1988 is similar. Most of the poleward bursts result in a reduction in intensity and/or displacement of an equatorward jet and the intensification and/or surfacing of a poleward flow. In each case the isotherms responded as expected. In some cases, an initial upward trend was simply removed as opposed to being replaced by a downward trend. In other cases the initial downward trend was intensified. When there was an extended duration of poleward wind, the isotherms displayed the downward trend at the coast that is associated with the downwelling induced by the poleward flow.

In both 1987 and 1988, there were eddies present that were produced by the previous year's eddy-generating mechanisms (1986 and 1987 respectively). These

residual eddies disappeared towards the end of the Pre-Upwelling phases during both 1987 and 1988.

B. UPWELLING FAVORABLE (PRE-EDDIES) PHASE

1. 1987 Upwelling Favorable (Pre-Eddies) Phase

The Upwelling Favorable (Pre-Eddies) phase, which begins around day 120 and lasts until approximately day 214, may be characterized by a series of events, relaxations and reversals of the equatorward winds (Figures 26 and 27). The response of the model to these events and relaxations is very similar to the response during the pre-upwelling phase except that predominantly equatorward winds have set up a quasi-steady surface equatorward jet at the coast which, by the end of the phase is accompanied by a subsurface poleward flow. An additional oceanic response is apparent when reviewing temperature fields. As a result of the upwelling, subsurface isotherms have broached the surface. The location of the intersection of an isotherm with the surface moves onshore or offshore in response to poleward or equatorward winds, respectively.

a. Two-Day Reversal

A short burst of poleward winds began on day 144 and continued until day 146 (24 May to 26 May). For the two weeks prior to the burst, the winds had been predominantly equatorward (Figure 26). The response of the velocity field is similar to the Pre-Upwelling phase; i.e., there is a reduction in the intensity of the equatorward jet (Figures 28a and 28b). Temperature cross-sections on days 144 and 146 show the onshore movement of the 17.5 °C isotherm due to the reversal (Figures 28c and 28d).

33

b. General Response

The result of sustained equatorward wind stress forcing is best observed towards the end of the phase. By 26 June, the equatorward jet has become established and a subsurface poleward undercurrent has developed (Figure 29a). Ten days later, the poleward undercurrent has increased in intensity but has shoaled somewhat (Figure 29b), due to the relaxation in equatorward winds on 4 and 5 July (days 185 and 186 in Figure 27). Velocity cross-sections for 16 July (Figure 29c) show a poleward undercurrent that lies closer to the surface. This response is likely due to two relaxations of the equatorward winds which occurred between 6 and 16 July (days 187 and 197 in Figure 27). Finally, within a week of the end of the phase, the equatorward jet has intensified while the poleward undercurrent has all but disappeared (Figure 29d). This intensification of the equatorward jet is likely a response to the intensification of the equatorward forcing, as seen in Figure 27.

2. 1988 Upwelling Favorable (Pre-Eddies) Phase

The Upwelling Favorable (Pre-Eddies) phase for 1988 begins around 1 February (day 32 in Figure 30) and lasts until the end of September (day 245 in Figure 32). Since the monthly mean for February is only -0.1 m/s, the demarcation between the Pre-Upwelling phase and the Upwelling Favorable phase is not as sharp as in 1987. In general, the response of the model to poleward bursts during the upwelling favorable phase is characterized by the onshore and offshore movement of isotherms and the presence of a quasi-steady surface equatorward jet and associated subsurface poleward flow.

a. Six-Day Reversal

A six-day reversal from equatorward to poleward winds occurred between 29 April and 5 May (days 120 and 126 in Figure 31). The temperature field illustrates the response of the model during this reversal. In general, the surface isotherms moved onshore in response to reduced offshore Ekman transport. The vertical cross-section of temperature for 29 April (Figure 33a) shows two isotherms (17.5 °C and 17.0 °C) surfaced near the coast. Following the reversal, the 17.5 °C isotherm has moved closer to shore and the 17.0 °C isotherm has submerged (Figure 33b).

b. General Response

The general oceanic response of the model to the 1988 wind stress forcing may be characterized, as in 1987, by the appearance and disappearance of the equatorward jet and poleward undercurrent combination. The first appearance of this flow combination occurs from late March to early April (Figure 34a). It disappears by the first part of May (Figure 34b). Of particular note is the reversal of predominantly equatorward winds towards the end of April (days 100-113 in Figure 31). By mid-June both the equatorward jet and poleward undercurrent reappear (Figure 34c) and disappear again shortly thereafter. Another wind reversal is coincident with this feature (days 160-165 in Figure 31).

3. Upwelling Favorable (Pre-Eddies) Phase Summary

Although the response of the model to upwelling favorable wind forcing during the second phase is generally similar to the response during the first phase, there

are several differences that warrant the distinction between the two phases. To begin with, the wind stress is more predominantly equatorward (upwelling favorable) during the upwelling phase. During both 1987 and 1988, the maximum poleward winds exceed the maximum equatorward winds during the pre-upwelling phases. During the upwelling phase, the situation is reversed, and the maximum equatorward winds exceed the maximum poleward winds. The mean winds throughout the upwelling phase are equatorward as well (Tables 2 and 3). As a result, the Upwelling Favorable (Pre-Eddies) phase is characterized by a quasi-steady equatorward jet (4-13 cm/s) near the coast which is accompanied by a poleward undercurrent (1-5 cm/s) by the end of the phase. There is also an onshore or offshore movement of the surfaced isotherms in response to poleward or equatorward winds, respectively.

C. UPWELLING FAVORABLE (EDDIES PRESENT) PHASE

1. 1987 Upwelling Favorable (Eddies Present) Phase

For 1987, the Upwelling Favorable (Eddies Present) phase begins around the first of August and ends in mid-October. The wind stress forcing during this phase may be characterized by a series of equatorward wind events separated by several 3-5 day reversals. The fluctuations in wind direction and speed are similar to the fluctuations found in the previous phase with one exception; instead of being increasingly equatorward, they are increasingly poleward (Figures 35 and 36).

36

a. General Response

Towards the end of the previous phase, the flow was characterized by a quasi-steady surface equatorward jet and a subsurface poleward current. The same situation is present during the early part of this phase. On day 240 (Figure 37a), there is evidence of only an equatorward jet within 20 km of the coast, which extends to 85 m depth. By day 244 (Figure 37b), the core of the equatorward jet has been displaced offshore, and a subsurface poleward flow has appeared and intensified to a 1-5 cm/s flow within 15 km of the coast and to 300 m depth.

Towards the end of the phase, a poleward current occurs less frequently and disappears for prolonged periods. An equatorward jet remains, but is substantially reduced in size. On day 215 (Figure 37c), at the beginning of the third phase, the equatorward jet extended 60 km horizontally and 300 m vertically. By day 258 (Figure 37d), the horizontal and vertical dimensions were reduced to 20 km and 150 m depth, respectively.

The large-scale response of the isotherms is consistent with the reduced upwelling that accompanies the decreasingly equatorward winds. Early in the phase (day 238), the 17 °C isotherm surfaced approximately 95 km offshore (Figure 38a). By day 277 (Figure 38b), one week prior to the end of the phase, it surfaced in two small areas of the domain, largely due to the presence of eddies.

b. 1987 Eddies

The single most distinguishing feature of the third phase is the presence of cyclonic eddies, which vary in number and intensity throughout the phase. Unlike

1986, which had both cyclonic and anticyclonic eddies (Lopes da Costa, 1989), no anticyclonic eddies were generated during 1987.

The eddies generated during this phase range from 10 km to 128 km in diameter. The vertical extent of the eddies varies from 200 m to 300 m in depth. The influence of these eddies on the mesoscale flow is significant and well illustrated in charts of sea surface temperature. As might be expected with cyclonic eddies, offshore displacement of isotherms is intensified on the poleward side of the eddies. For example, on day 244 the 17.0 °C surfaces closer to shore on the equatorward side of the eddies and farther from shore on the poleward side of the eddies (Figures 39a and 39b).

During the upwelling favorable phases in 1987, the following sequence of events or conditions leading up to the appearance of eddies was observed:

- The existence of both a surface equatorward jet and a subsurface poleward current (generated in the previous phase).

- The relaxation of the equatorward wind stress (beginning of August, around day 215).

- The shoaling and intensification of a subsurface poleward current (beginning of August, around day 215).

- The formation of eddies (beginning of August, around day 215).

2.   1988 Upwelling Favorable (Eddies Present) Phase

The Upwelling Favorable (Eddies Present) phase for 1988 is very short, beginning around the first of September (day 244) and concluding around the first of October (day 274) (Figures 40 and 41). The wind stress during this period is predominantly equatorward with no increasingly equatorward or increasingly poleward

38

trends. The wind forcing is characterized , a series of events and relaxations. The few reversals that do occur are minor in amplitude and of short duration (Figures 40 and 41).

a. General Response

As in 1987, the general response of the model to forcing during this phase is to modify an existing surface equatorward jet and a subsurface poleward current. The poleward flow surfaces and remains at or near the surface for the remainder of the phase. In early September (day 247), the velocity field cross-section (Figure 42a) shows the equatorward jet between 27 and 70 km offshore and a poleward current between the coast and 25 km offshore. This situation generally persists throughout the phase with the exception of approximately a week during mid-September. During this particular week the equatorward jet persists but the poleward flow is almost entirely eliminated (Figures 42b and 42c). The wind at this time is strongly equatorward (approximately 10 m/s). Following this event, there is a relaxation of the equatorward wind that permits the return of the poleward surface current, which remains until the end of the phase (Figure 42d).

The temperature field responded to the forcing in a manner similar to the results for 1987. At the beginning of the phase, the 17 °C isotherm extends as far as 160 km offshore near the middle of the domain (Figure 43a). By the end of the phase the same isotherm is approximately 100 km offshore, covering substantially less surface area (Figure 43b).

b. 1988 Eddies

Cyclonic eddies are generated during early September (Figure 44a) and again during the last part of September (Figure 44b). As in 1987, anticyclonic eddies are not generated during 1988. In general, these eddies are smaller and fewer in number than those generated during 1987. They are preceded by the same sequence of events described earlier for 1987.

3. Upwelling Favorable (Eddies Present) Summary

The wind stress forcing during this phase was different for 1987 and 1988. While the wind stress forcing in both years may be characterized by a series of events and relaxations, the forcing differs in three respects. First, the relaxations and reversals for 1988 are shorter and of lesser magnitude than those of 1987 (peak poleward wind for third phase 1988 was 3.8 m/s while for 1987 the peak poleward wind during the third phase was 12.6 m/s). Second, the wind stress forcing during the third phase of 1988 is neither decreasingly equatorward nor increasingly equatorward, whereas, the forcing for 1987 becomes decreasingly equatorward. Third, the Upwelling Favorable (Eddies Present) phase for 1987 is more than twice as long as in 1988 (two months compared to one month).

The general response of the model to the forcing mentioned above is similar in both years. In particular, a surface equatorward jet and subsurface poleward current are established by the end of the second phase. However, because of the differences in forcing during the third phase, the response of this flow combination is different in each

of the two years. In 1987, the poleward flow sometimes exists as an undercurrent and at other times shoals to the surface. In 1988, the flow combination appears intermittently with the poleward current almost exclusively at the surface.

The eddies during both 1987 and 1988 are different in size and in number. Eddies generated in 1987 are larger (approximately 60-100 km diameter) and greater in number (between four and five), while the eddies generated in 1988 are smaller (approximately 20-40 km diameter) and fewer in number (between two and three). During 1987, eddies are more persistent than those generated in 1988. The eddies for both years do have one similarity; they are all cyclonic. The same sequence of events acts as a prelude to eddy generation in both years:

- The appearance of both a surface equatorward jet and a subsurface poleward current.

- The relaxation of equatorward wind stress.

- The shoaling and/or intensification of the poleward current.

- The formation of eddies.

D. POST-UPWELLING PHASE

1. 1987 Post-Upwelling Phase

The 1987 Post-Upwelling phase begins in early October (day 286) and concludes at the end of December (day 365). The wind forcing is predominantly poleward in October and December with predominantly equatorward forcing in November (Figure 10, Table 2 and Figure 36). As in the Pre-Upwelling phase, the forcing is characterized by several 8-10 day bursts of poleward wind and many high frequency fluctuations.

a. General Response

The response of the model to Post-Upwelling forcing in 1987 is very similar to the response observed during the Pre-Upwelling phase. Generally, the upper level flow depends on the direction and duration of the wind forcing. For example, a cross-section of the meridional velocity field for day 331 (Figure 45a) shows 1-15 cm/s equatorward flow at the surface near the coast. This is in response to a nine-day burst of equatorward wind (Figure 36). Nine days later, following an eight-day poleward burst, the flow at the surface near the coast is now 1-7 cm/s poleward (Figure 45b).

b. Post-Upwelling Eddies

The cyclonic eddies present at the end of the third phase persist into the fourth phase. They do, however, decrease in intensity and number. On day 287 (Figure 46a) there are three large diameter (80-100 km) eddies and one smaller eddy (approximately 30 km in diameter). By day 362 (Figure 46b), there are only three large

42

eddies of decreased intensity. The decrease in intensity is evidenced by wider spacing between contour intervals as well as the decrease in number of contours.

2.   1988 Post-Upwelling

The wind forcing for the fourth phase of 1988 is different than that during 1987. Whereas this phase in 1987 may be characterized by a series of 8-10 day bursts of poleward winds, 1988 may be characterized as a period of decreasingly equatorward wind stress followed by a period of increasingly equatorward wind stress. The change from decreasingly equatorward winds to increasingly equatorward winds occurs around day 312 (Figure 41), almost in the middle of the Post-Upwelling phase.

a.   General response

Consistent with the wind, the meridional velocity fields show predominantly poleward flow in the surface layers during the first half of the phase (Figure 47a) and predominantly equatorward flow in the surface layers during the second half of the phase (Figure 47b). The response of the isotherms is consistent as well, showing downwelling in response to poleward winds (Figure 48a) and trends consistent with upwelling or at least reduced downwelling during periods of equatorward winds (Figure 48b).

b.   Post-Upwelling Eddies

At the conclusion of the third phase, there is one small (approximately 10 km in diameter) cyclonic eddy in the domain (at y~580 km in Figure 49a). Five days later, it has doubled in size (Figure 49b). Fifteen days later it has tripled in size and been

accompanied by several more cyclonic eddies (Figure 49c). This progression in size and number is accompanied by a decreased intensity, which is evidenced by the broader spacing between isobars and the decreased number of isobars visible between the beginning of the phase (Figure 49a) and the end of the phase (Figure 49d).

3. Post-Upwelling Summary

The wind stress forcing for the fourth phase of 1987 is characterized by 8-10 day bursts of equatorward and poleward winds. The wind stress forcing for the fourth phase of 1988 is characterized by a period of increasingly poleward winds followed by a period of increasingly equatorward winds.

The general response of the model to Post-Upwelling wind stress forcing is similar for both years. Predominantly poleward wind stress forces poleward flow, while predominantly equatorward wind stress forces equatorward flow. The isotherms responded accordingly; downwelling accompanied poleward wind stress and upwelling or reduced downwelling accompanied equatorward wind stress.

There were eddies present in both Post-Upwelling periods. Eddies present at the beginning of the fourth phase of 1987 decayed with time, while the eddies present at the beginning of the fourth phase of 1988 grew in size and number, yet decreased in intensity. The decrease in intensity was seen in both 1987 and 1988.

E. ENERGY ANALYSIS RESULTS

1. 1987 Eddy Generation

Eddies generated in 1987 first appear during early August (day 215). Between days 160 and 290, the kinetic energy (Figure 50) is quasi-steady. Beginning with day 227 and taking 20-day averages until day 287, plots of energy transfer in the upper five layers (above the permanent pycnocline) are used to show the dominant instability mechanisms (or in some cases, the lack of a dominant instability mechanism).

The first example, days 227 to 247 (Figures 51a and 51b), shows that both barotropic and baroclinic instability generate eddies in the coastal region between y~512 km and y~800 km. Baroclinic instability generates eddies in the coastal region equatorward of y~512 km and poleward of y~800 km. Offshore (x > 64 km), the generation of eddies is due to barotropic instability (Figure 51b). Eddy locations may be identified in planviews of zonal velocity (Figures 52a (day 227) and 52b (day 247)).

- The second example, covering days 247 and 267 (Figures 53a and 53b), shows predominantly baroclinic instabilities present throughout the nearshore region of the domain. These instabilities generated eddies in locations shown in Figures 52c and 52d. A third example (not shown) also shows predominantly baroclinic instabilities occuring throughout the nearshore region of the domain.

2. 1988 Eddy Generation

Eddies generated in 1988 appear at the beginning of September (day 245). The kinetic energy time series (Figure 54) is quasi-steady beginning at approximately day

45

180 and lasting until approximately day 300. Twenty-day averages of energy transfer from days 242 to 262 (Figures 55a and 55b) show mixed (both baroclinic and barotropic) instabilities in the poleward, coastal area of the domain and predominantly baroclinic instability in the equatorward, coastal area. Eddies are visible primarily in the poleward, coastal area of the domain (Figures 56a and 56b). From days 262 to 282, the energy transfer plots (Figures 57a and 57b) show predominantly baroclinic instability inshore and barotropic instability offshore. Eddies have developed slightly offshore (Figures 56c and 56b). Energy transfer plots for days 282 to 302 (not shown) indicate negative energy transfer (i.e., from eddy kinetic to either eddy available potential or time mean kinetic energy) throughout the domain, which is consistent with the absence of eddies during that period.
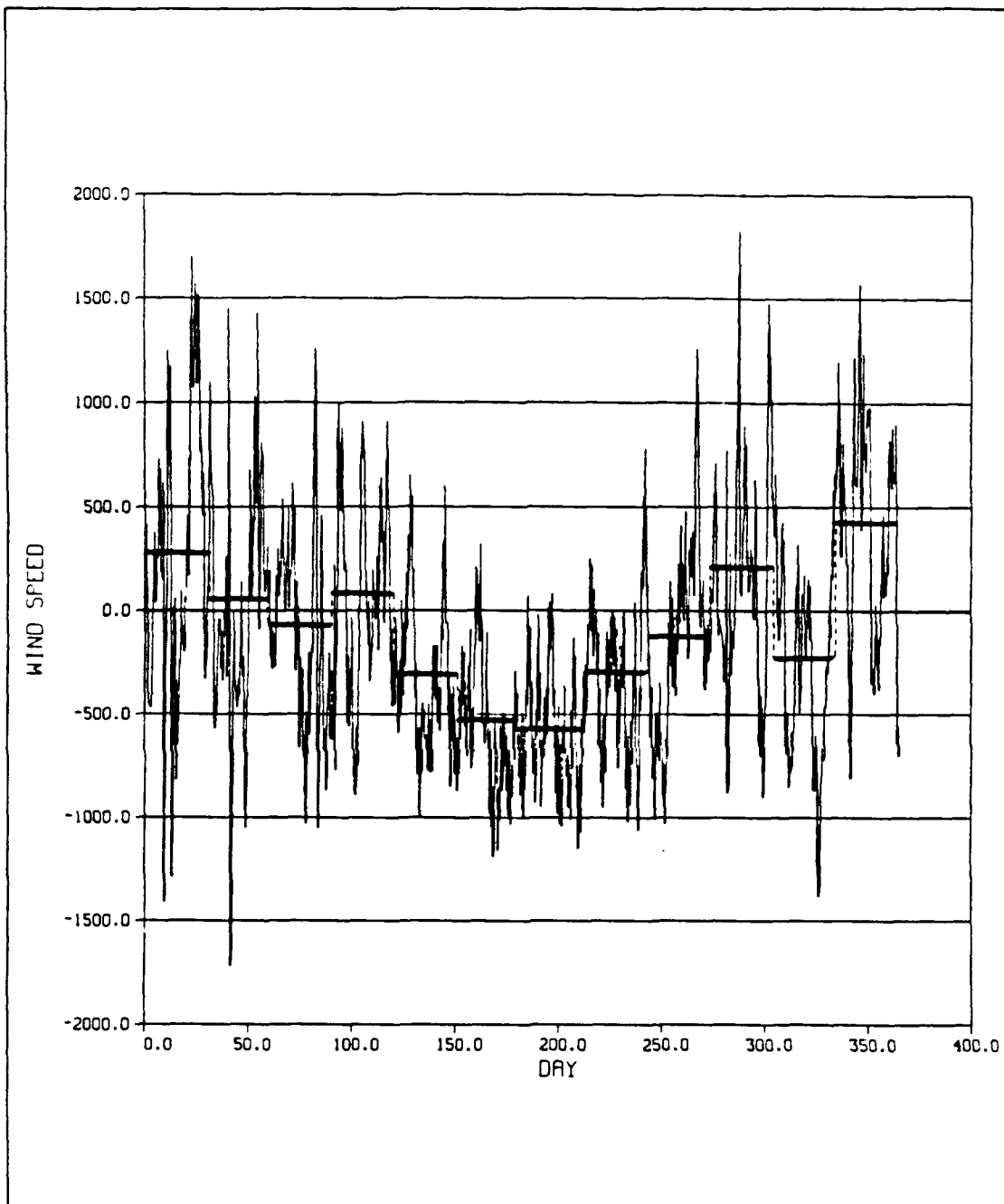
Figure 10. Time series of the six-hourly values of meridional wind velocity (cm/s) from 1 Jan. to 31 Dec. 1987 at 39°N, 10°W. Bars are monthly means.

47
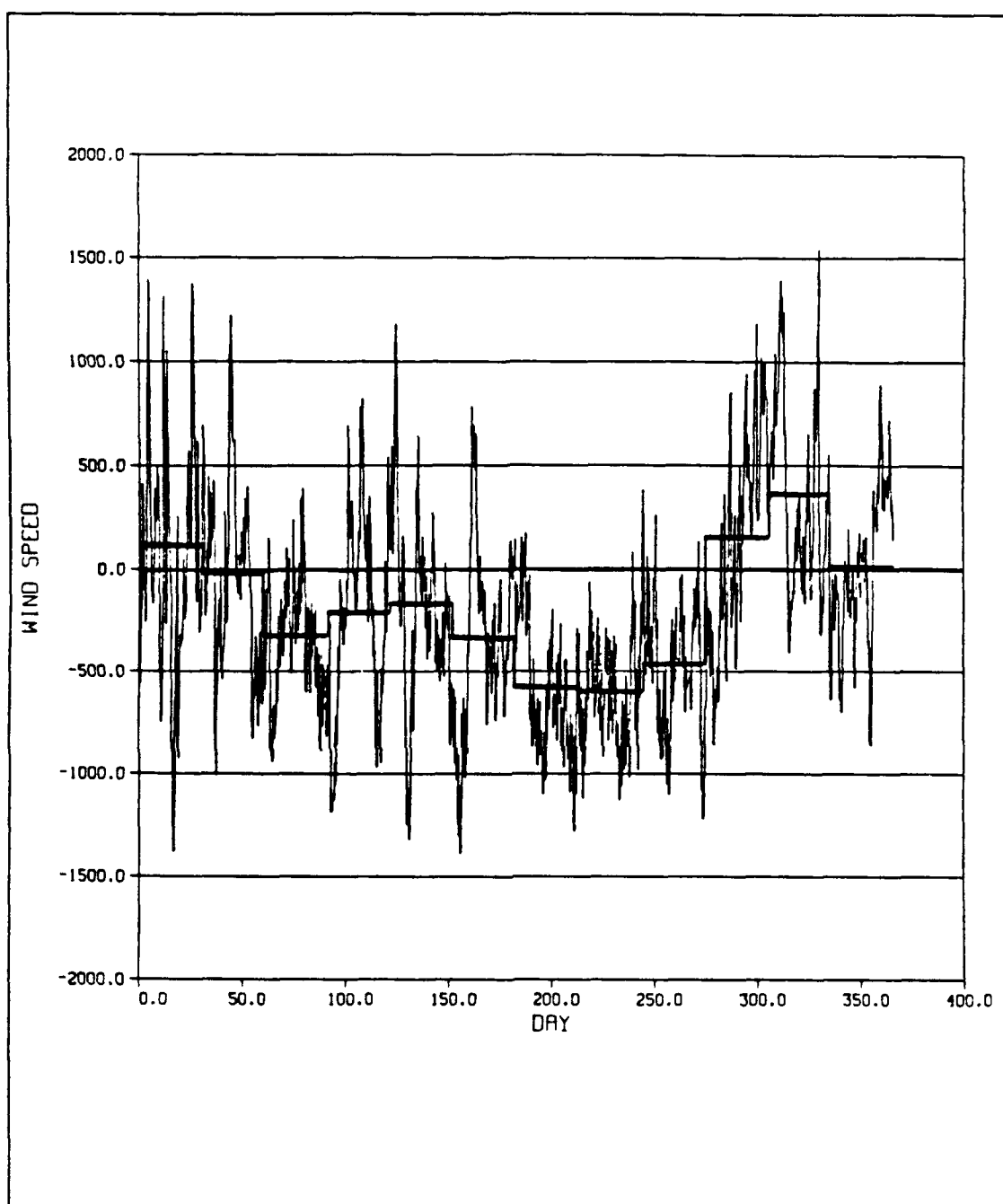
Figure 11. Time series of the six-hourly values of meridional wind velocity (cm/s) from 1 Jan. to 31 Dec. 1988 at 39°N, 10°W. Bars are monthly means.

48

Table 2. Statistical summary of equatorward (EW) and poleward (PW) wind forcing for 1987.

MONTH	MEAN (M/S)	STD DEV (M/S)	MAX PW WIND (M/S)	MAX EW WIND (M/S)	PCT TIME WITH EW WINDS
JAN	2.8	6.5	17.0	-14.1	34.7
FEB	.63	5.8	14.5	-17.2	52.7
MAR	-.60	4.5	12.6	-10.5	50.0
APR	.86	4.9	9.9	-8.9	45.8
MAY	-3.0	3.6	6.5	-10.0	80.6
JUN	-5.3	3.1	3.2	-11.9	93.3
JUL	-5.7	2.9	0.8	-11.5	95.2
AUG	-3.1	3.6	7.8	-10.6	83.1
SEP	-1.2	4.6	12.6	-10.3	63.3
OCT	2.1	5.0	18.3	-9.0	38.7
NOV	-2.3	5.8	6.6	-13.8	64.2
DEC	4.4	5.1	15.7	-8.1	22.6
JAN-DEC	-.45	5.7	18.3	-17.2	60.3

**Table 3.** Statistical summary of equatorward (EW) and poleward (PW) wind forcing for 1988.

MONTH	MEAN (M/S)	STD DEV (M/S)	MAX PW WIND (M/S)	MAX EW WIND (M/S)	PCT TIME WITH EW WINDS
JAN	1.2	5.7	13.9	-13.8	42.7
FEB	-.1	4.6	12.2	-10.1	50.9
MAR	-3.2	2.9	3.9	-9.4	86.3
APR	-2.1	4.8	8.2	-11.9	65.8
MAY	-1.7	4.8	11.8	-13.2	65.3
JUN	-3.3	4.6	7.8	-13.9	78.3
JUL	-5.7	3.3	1.7	-12.8	94.3
AUG	-5.9	2.5	1.8	-11.3	98.4
SEP	-4.6	3.2	3.8	-12.2	94.2
OCT	1.6	5.3	1.2	-8.6	41.1
NOV	3.6	4.7	15.4	-4.1	24.2
DEC	1.4	3.6	8.9	-8.6	51.6
JAN-DEC	-1.5	5.1	15.4	-13.9	66.2
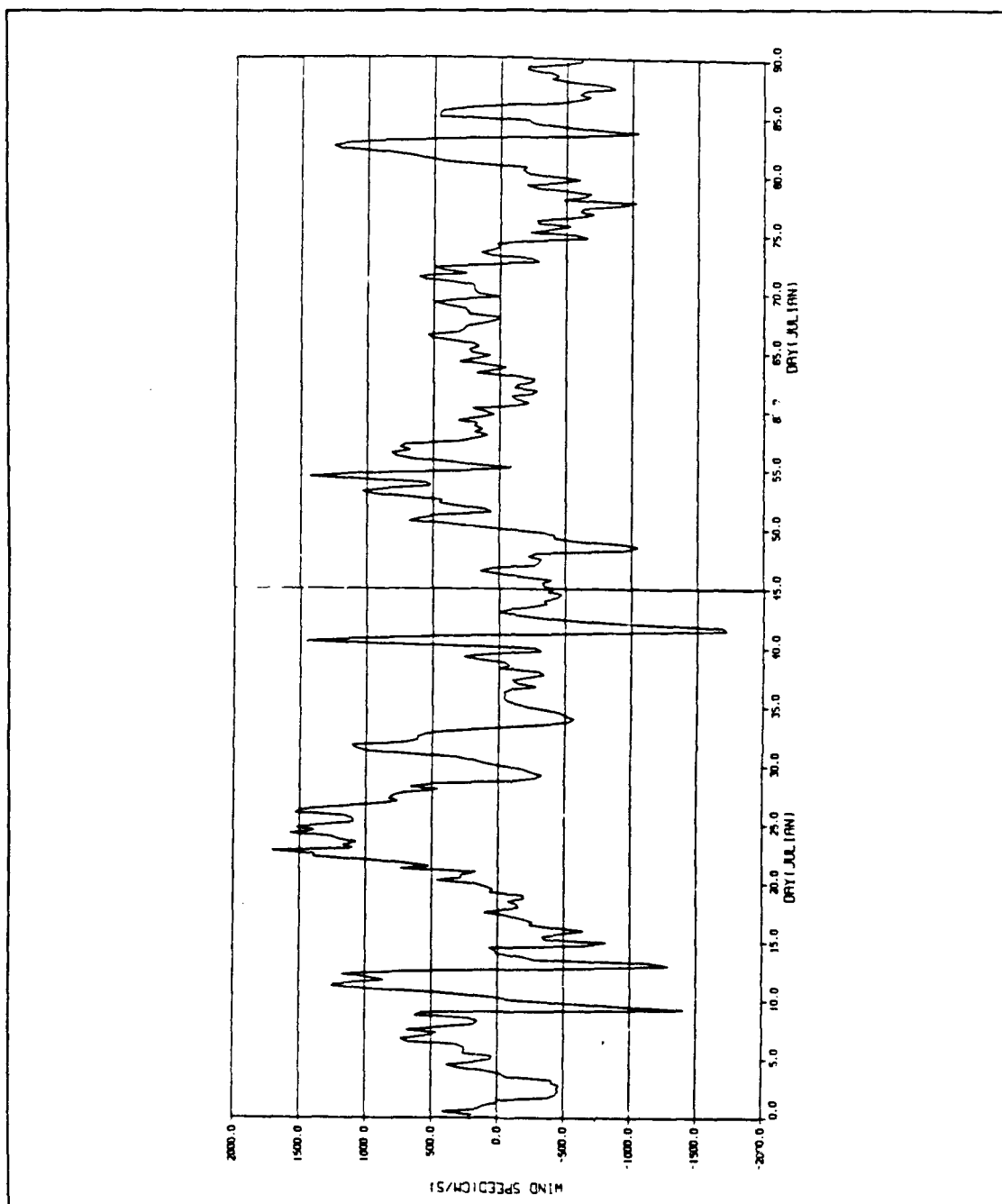
Figure 12. Expanded time series of meridional wind velocity (cm/s) for days 1-90 (1 Jan.-31 Mar.) 1987 at 39°N, 10°W.
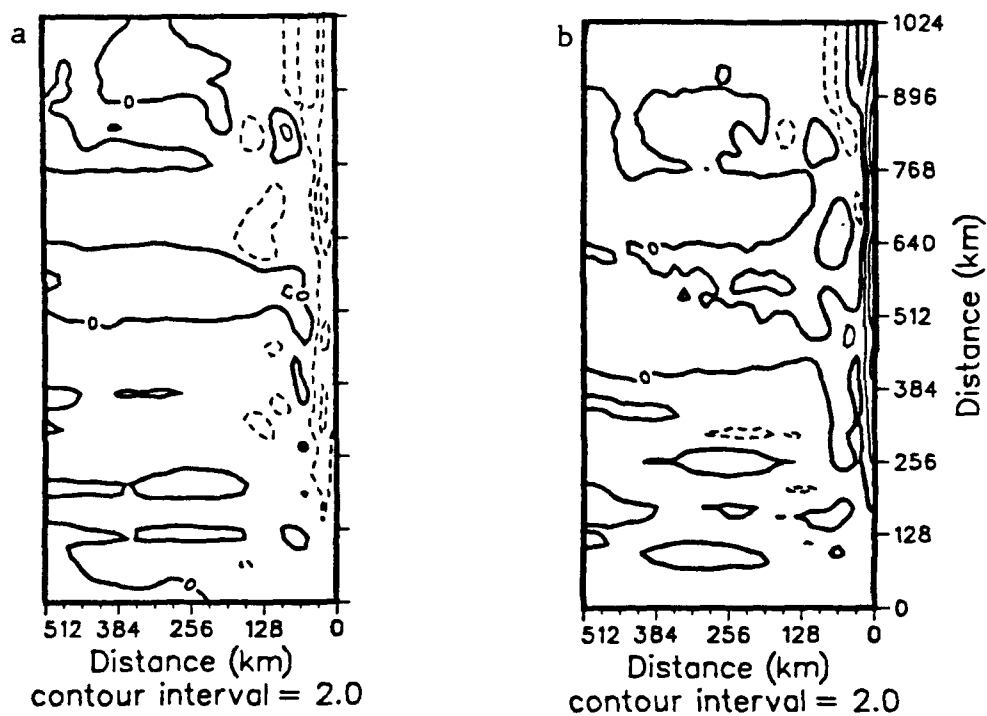
51
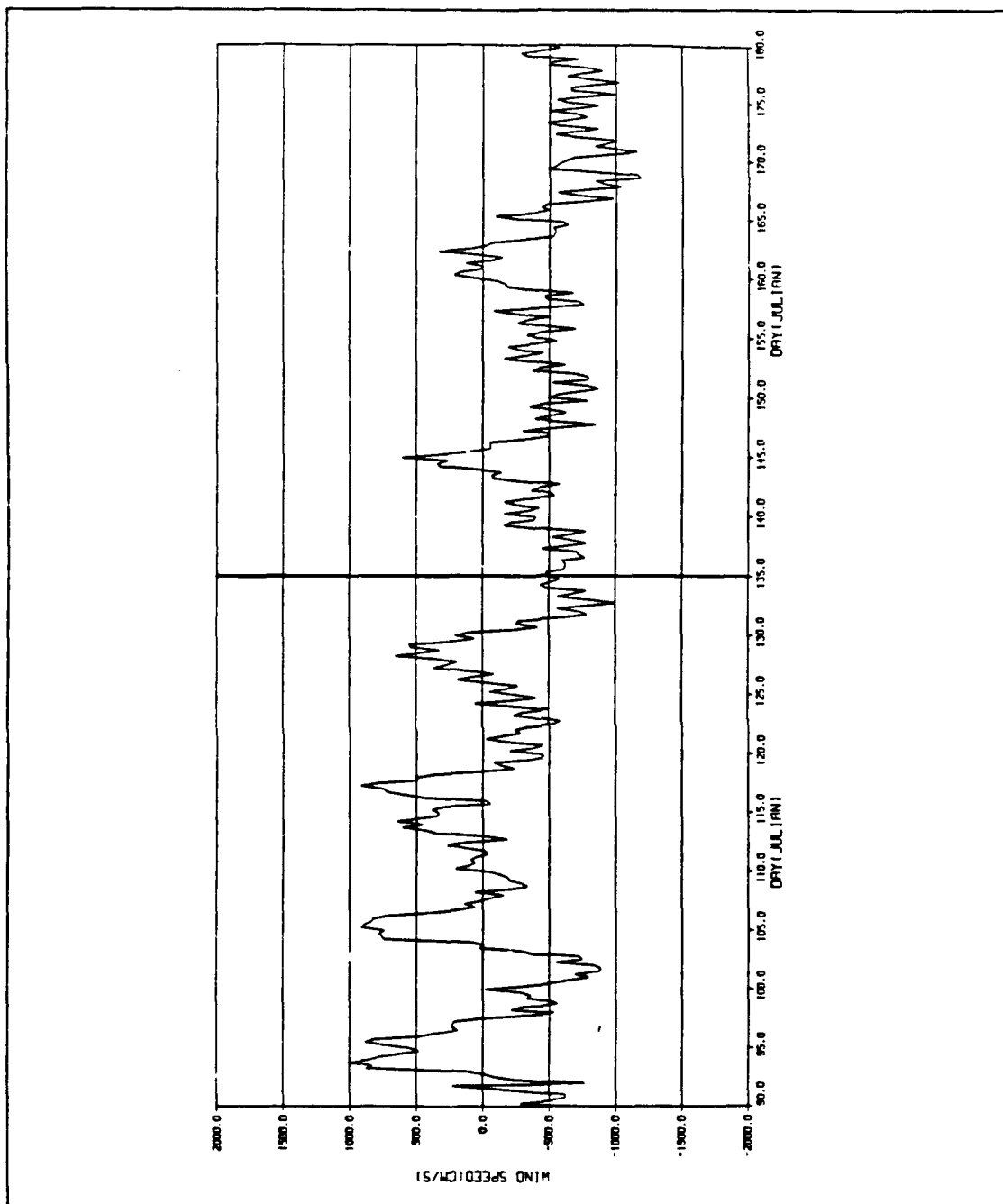
Figure 13. Expanded time series of meridional wind velocity (cm/s) for days 90-180 (31 Mar.-29 Jun.) 1987 at 39°N, 10°W.
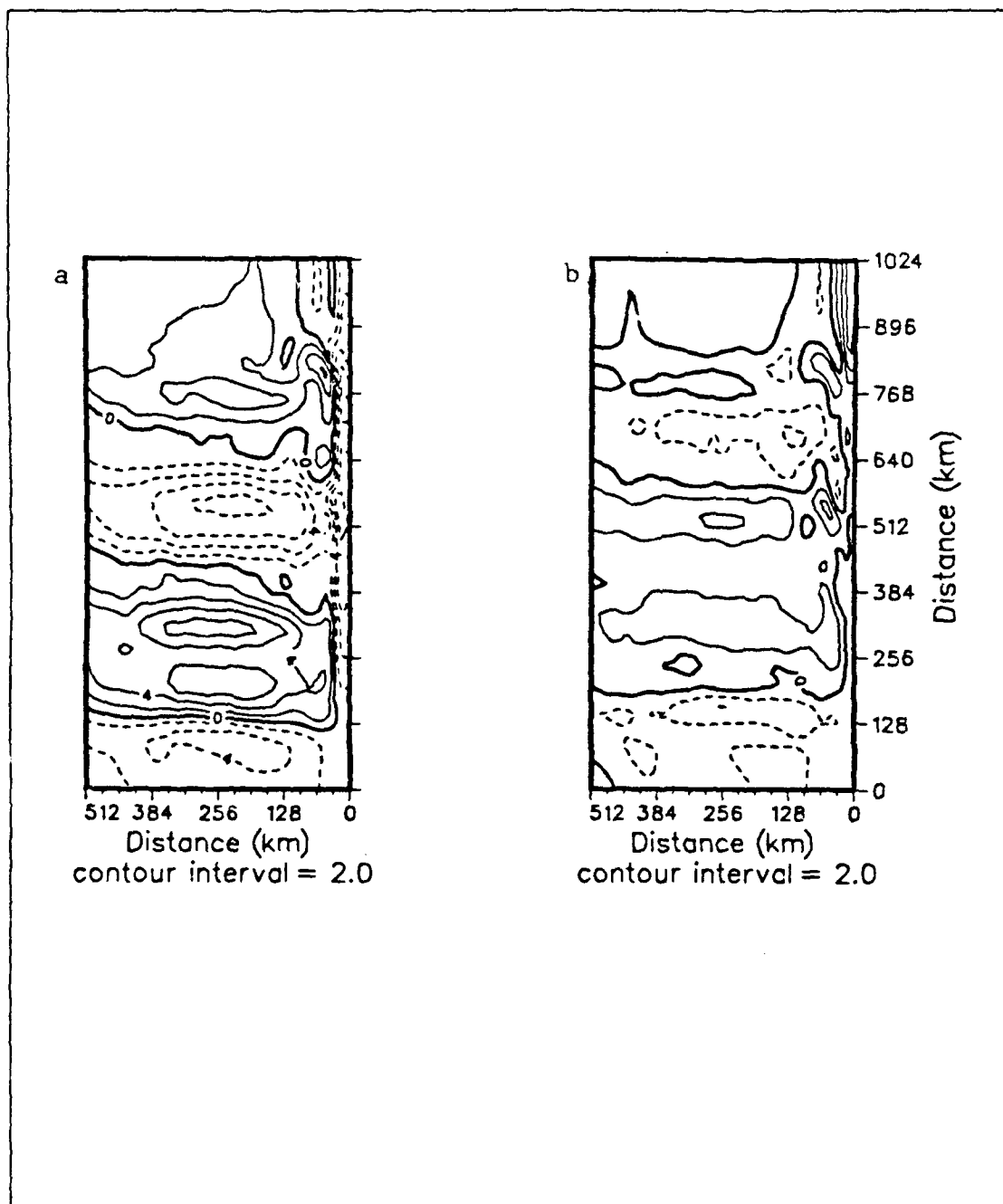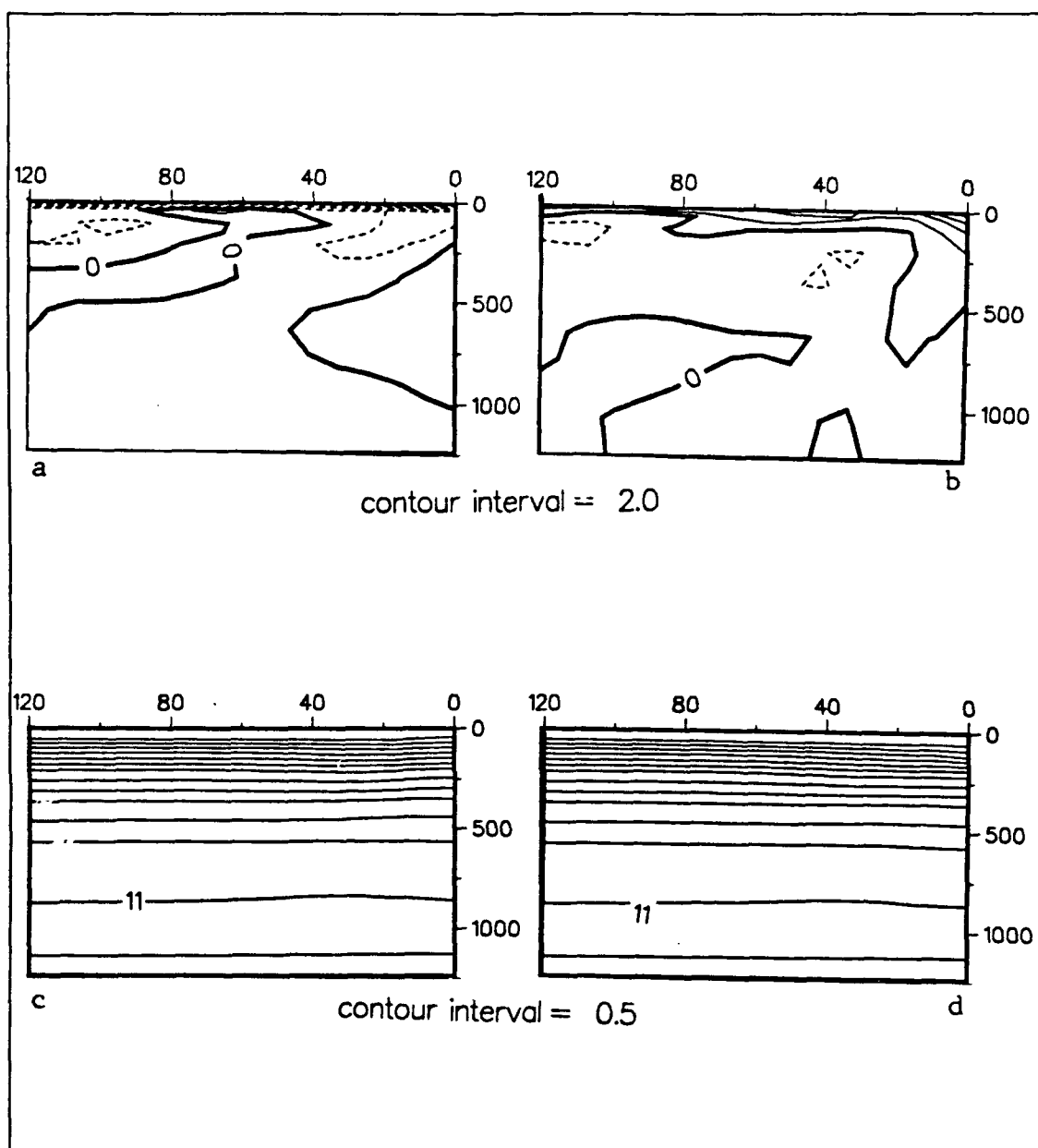
Figure 14. Isopleths of meridional velocity (cm/s) at 75 m depth for; **a)** 19 Feb. (day 50) and **b)** 1 Mar. (day 60) 1987. Dashed lines are negative contours.
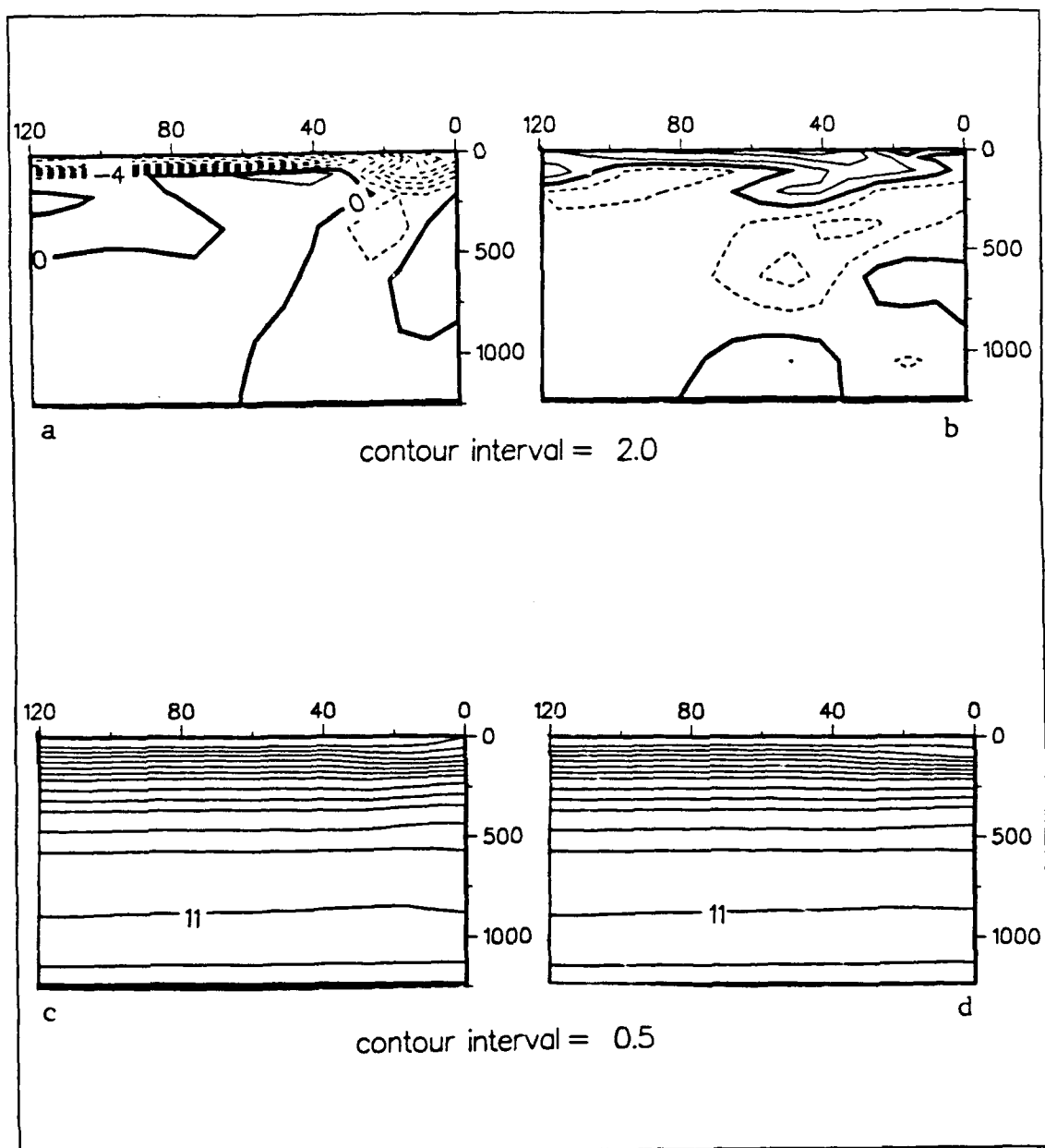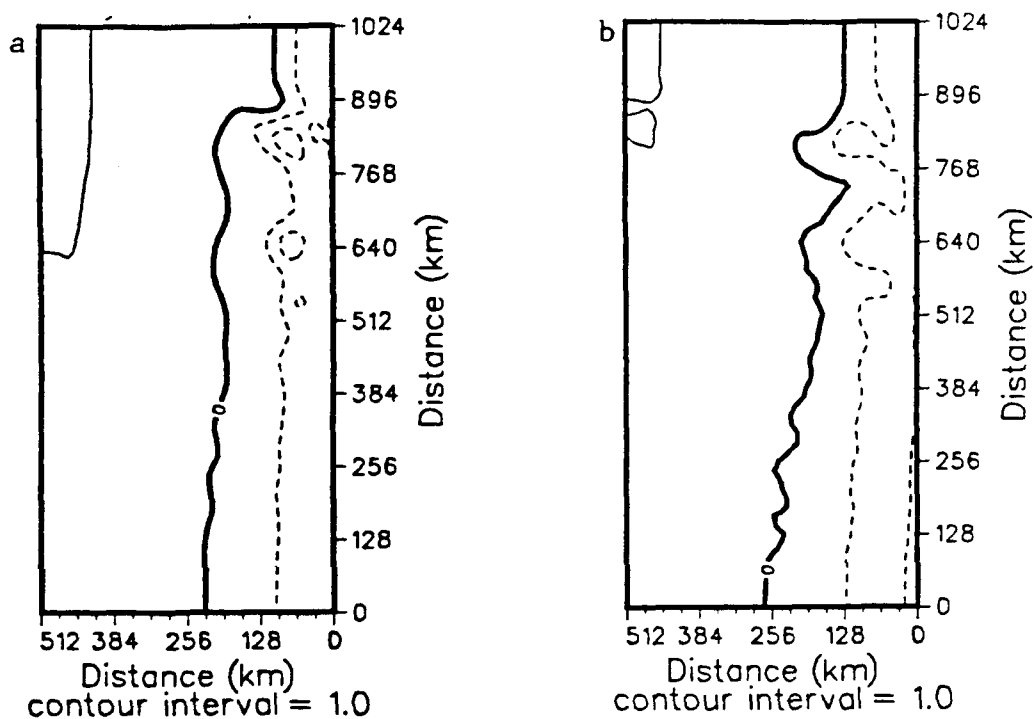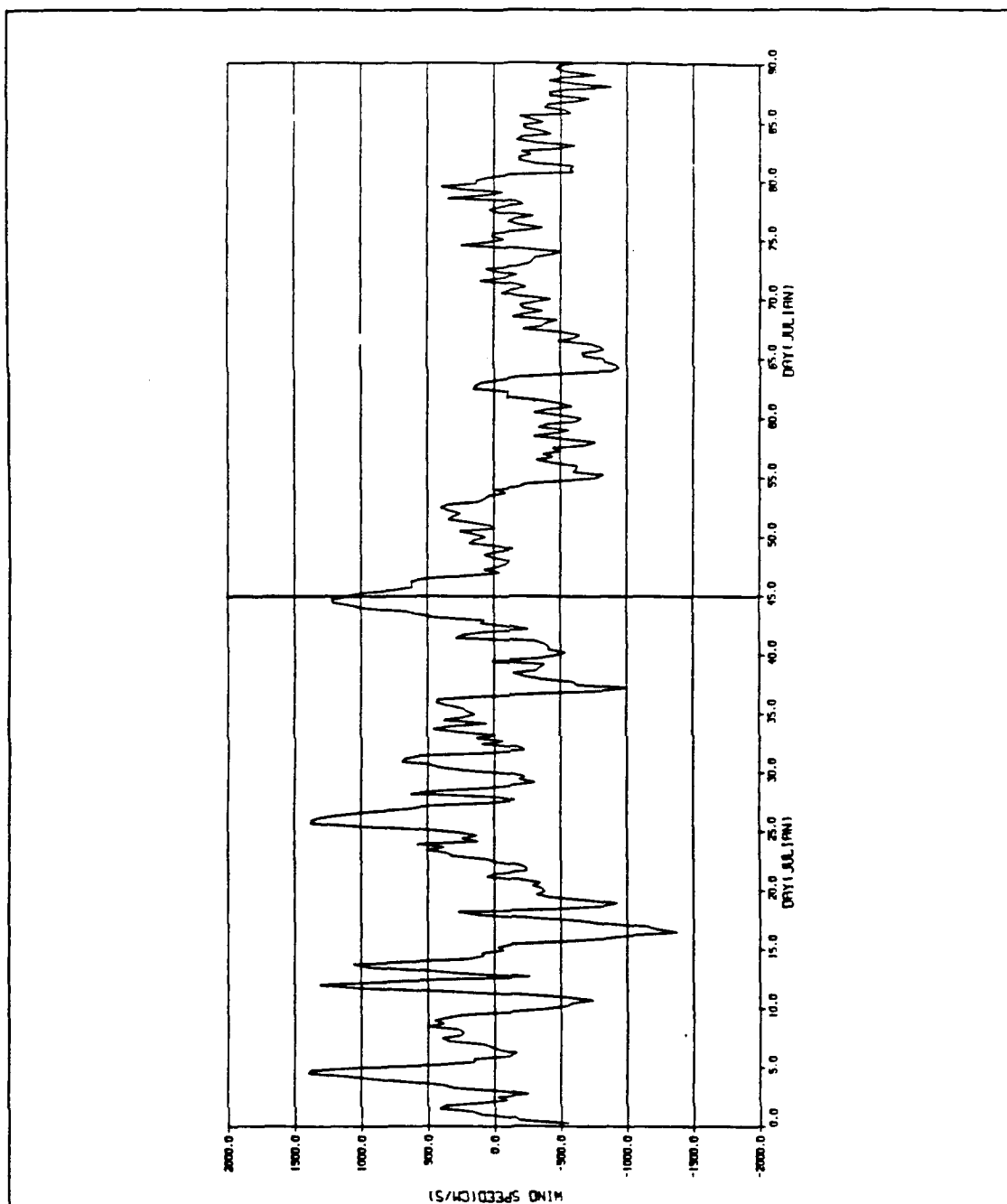
Figure 15. Vertical cross-shore sections at 40°N of meridional velocity (cm/s) (a,b) and temperature (°C) (c,d) for 19 Feb. (a,c) and 31 Mar. (b,d) 1987.

54

Figure 16. Isopleths of meridional velocity (cm/s) at 75 m for a) 3 Apr. (day 93) and b) 7 Apr. (day 97) 1987. Dashed lines are negative contours.

55

Figure 17. Vertical cross-shore sections at 40°N of meridional velocity (cm/s) (**a,b**) and temperature (°C) (**c,d**) for 3 Apr. (**a,c**) and 7 Apr. (**b,d**) 1987.
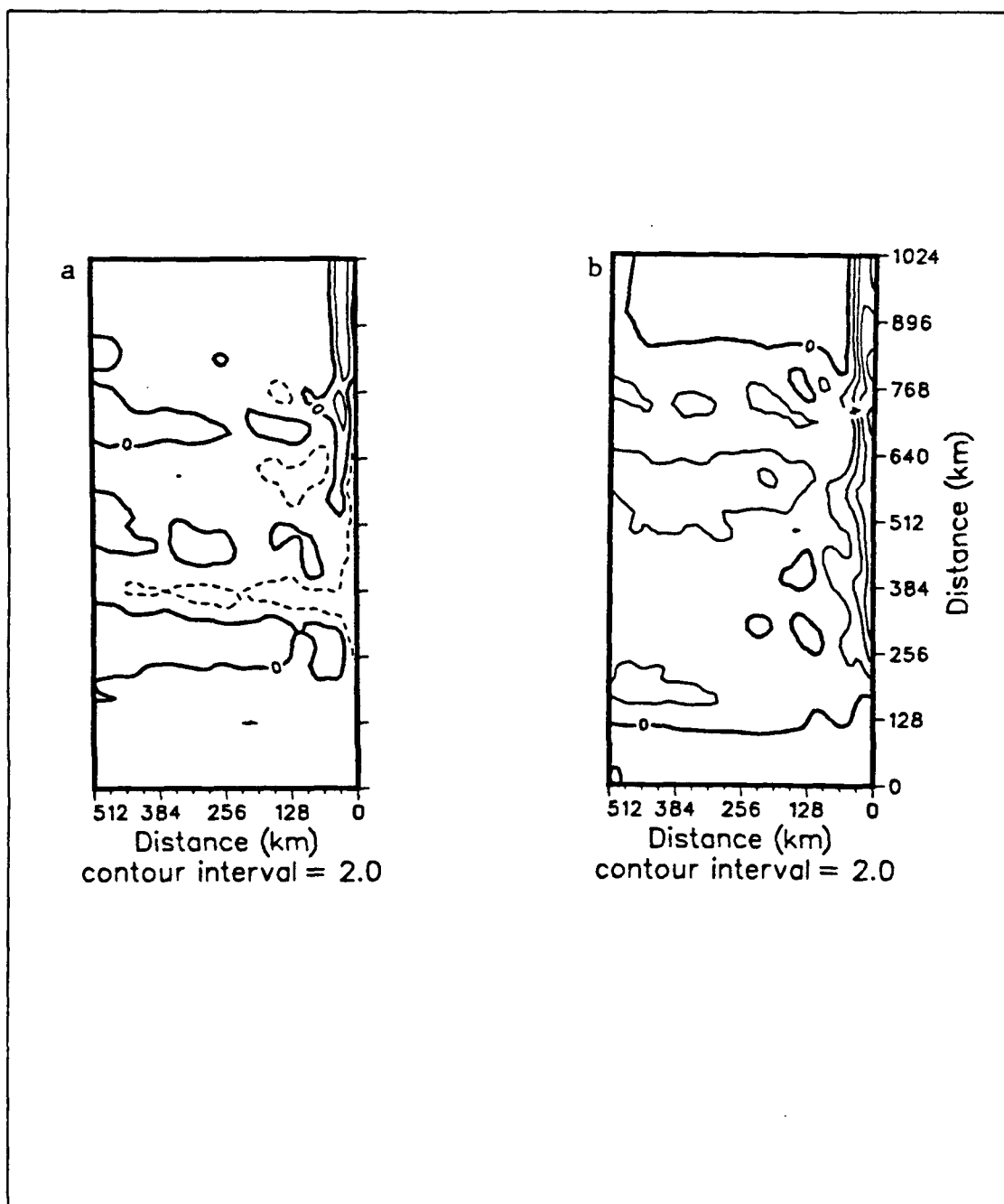
Figure 18. Surface isopleths of dynamic height (cm) relative to 2400 m for **a)** 10 Jan. (day 10) and **b)** 28 Mar. (day 87) 1987. Dashed lines are negative contours.
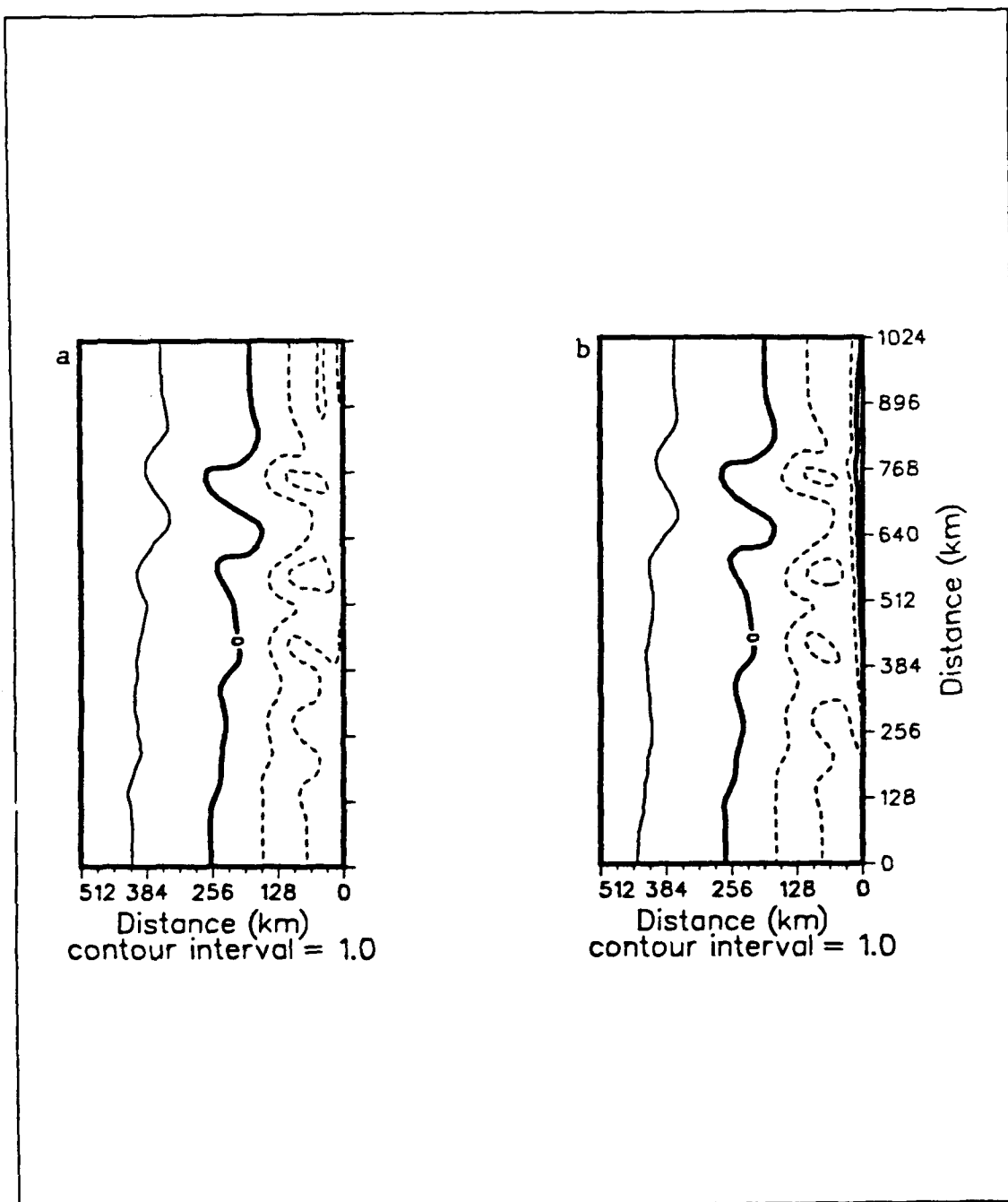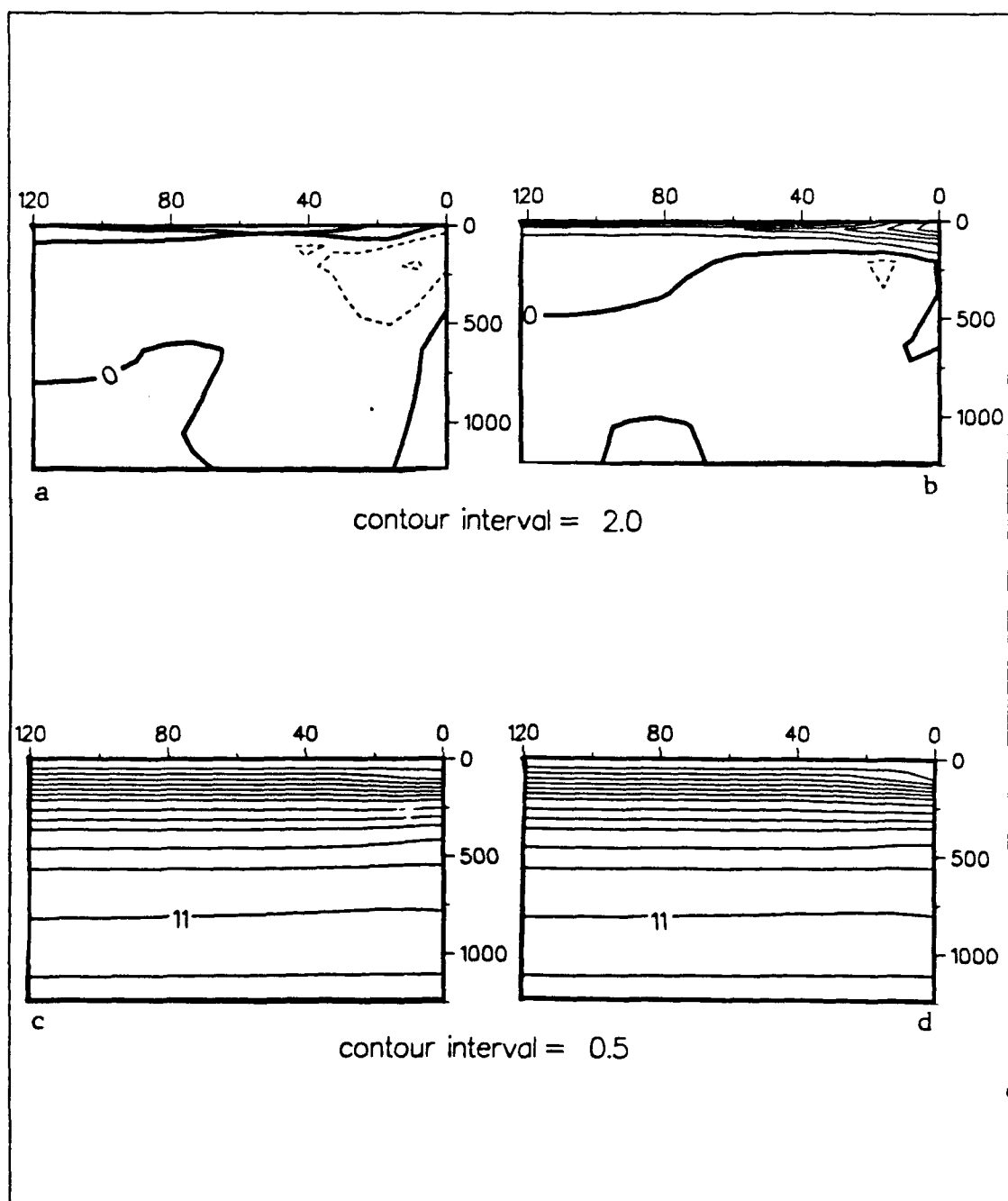
Figure 19. Expanded time series of meridional wind velocity (cm/s) for days 1-90 (1 Jan.-30 Mar.) 1988.
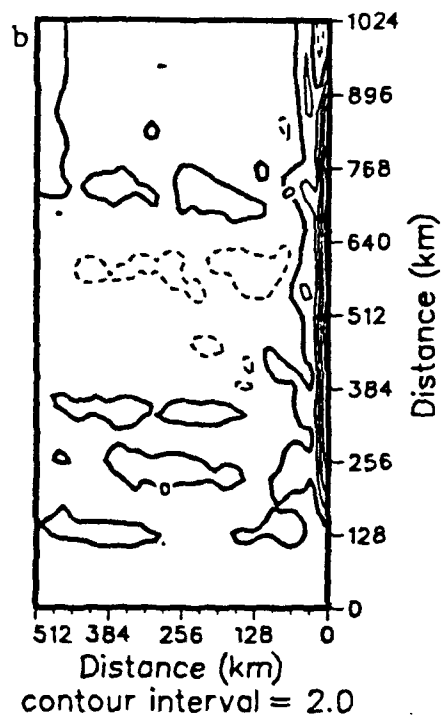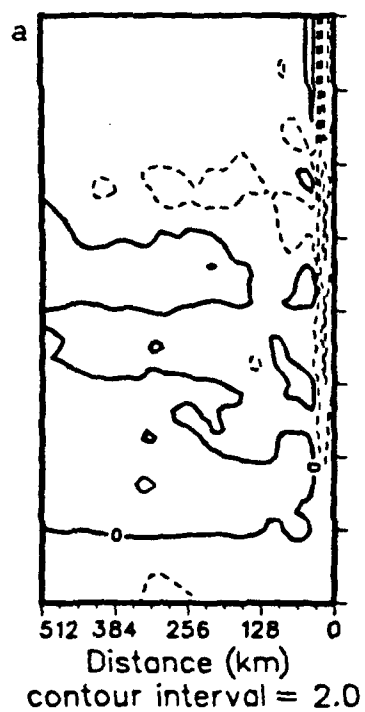
58

Figure 20. Isopleths of meridional velocity (cm/s) at 75 m depth for; **a)** 4 Jan. (day 4) and **b)** 6 Jan. (day 6) 1988. Dashed lines are negative contours.
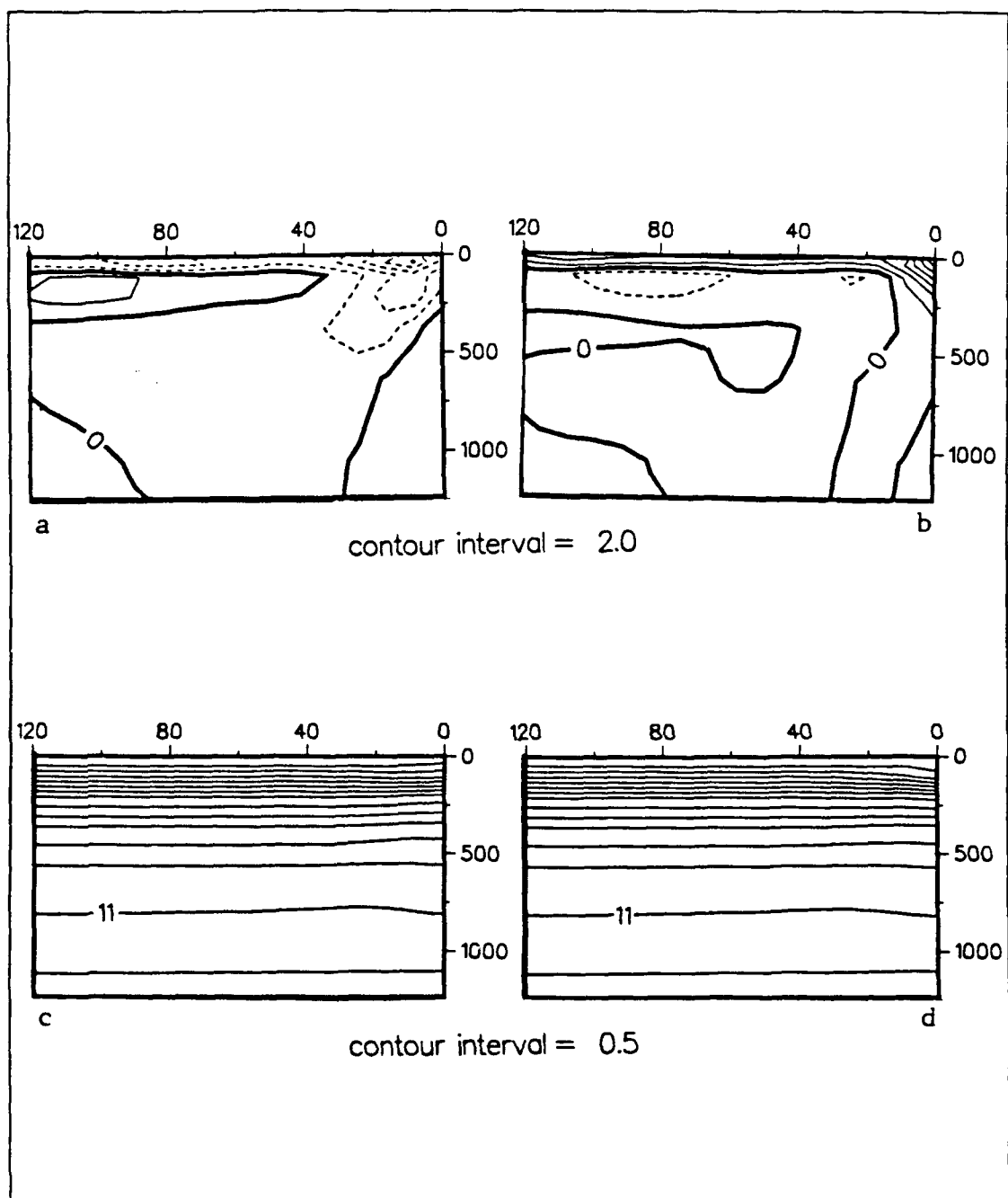
59

Figure 21. Surface isopleths of dynamic height (cm) relative to 2400 m for a) 4 Jan. (day 4) and b) 6 Jan. (day 6) 1988. Dashed lines are negative contours.
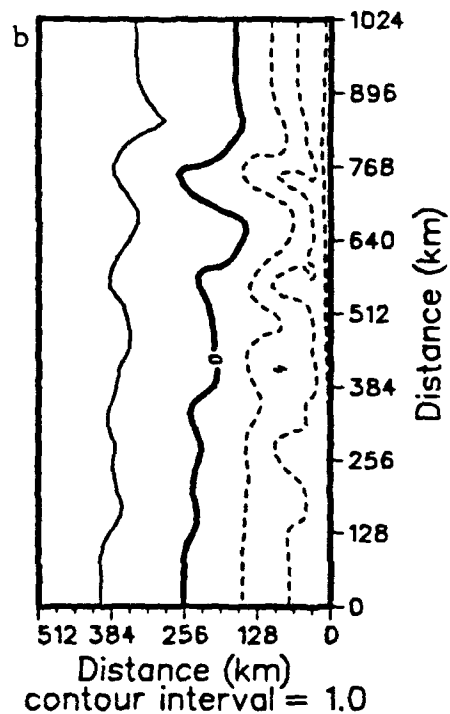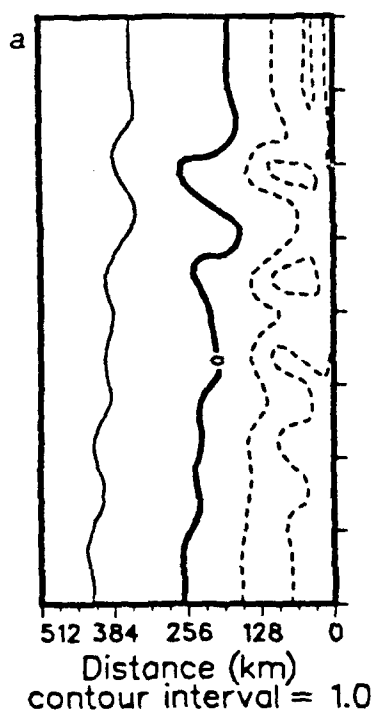
60

Figure 22. Vertical cross-shore sections at 40°N of meridional velocity (cm/s) (a,b) and temperature (°C) (c,d) for 4 Jan. (a,c) and 6 Jan. (b,d) 1988.

61

Figure 23. Isopleths of meridional velocity (cm/s) at 75 m depth for a) 23 Jan. (day 23) and b) 27 Jan. (day 27) 1988. Dashed lines are negative contours.

Figure 24. Vertical cross-shore sections at 42°N of meridional velocity (cm/s) (a,b) and temperature (°C) (c,d) for 23 Jan. (a,c) and 27 Jan. (b,d) 1988.

Figure 25. Surface isopleths of dynamic height (cm) relative to 2400 m for a) 2 Jan (day 2) and b) 22 Jan. (day 22) 1988. Dashed lines are negative contours.
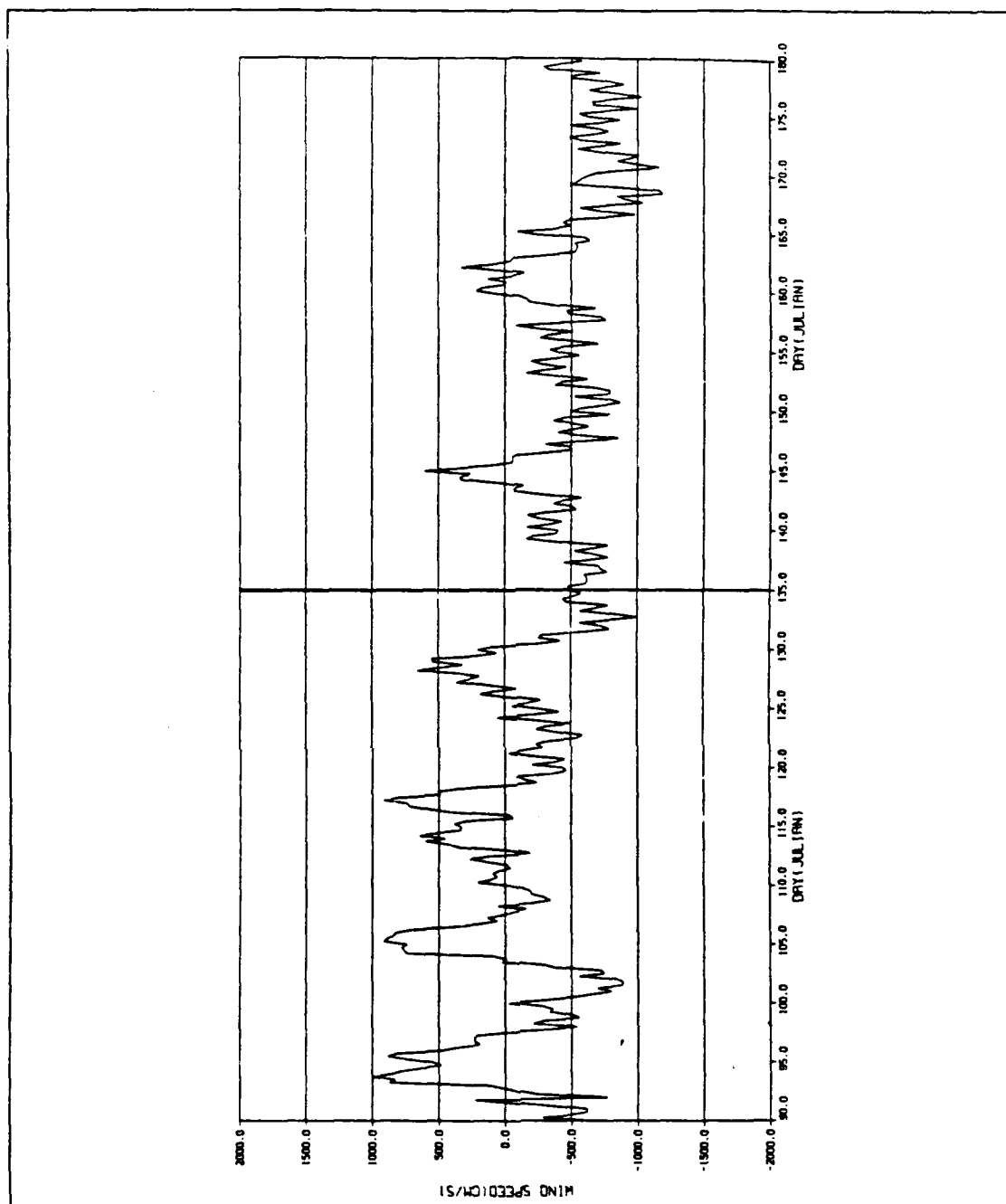
Figure 26. Expanded time series of meridional wind velocity (cm/s) for days 90-180 (31 Mar.-29 Jun.) 1987.
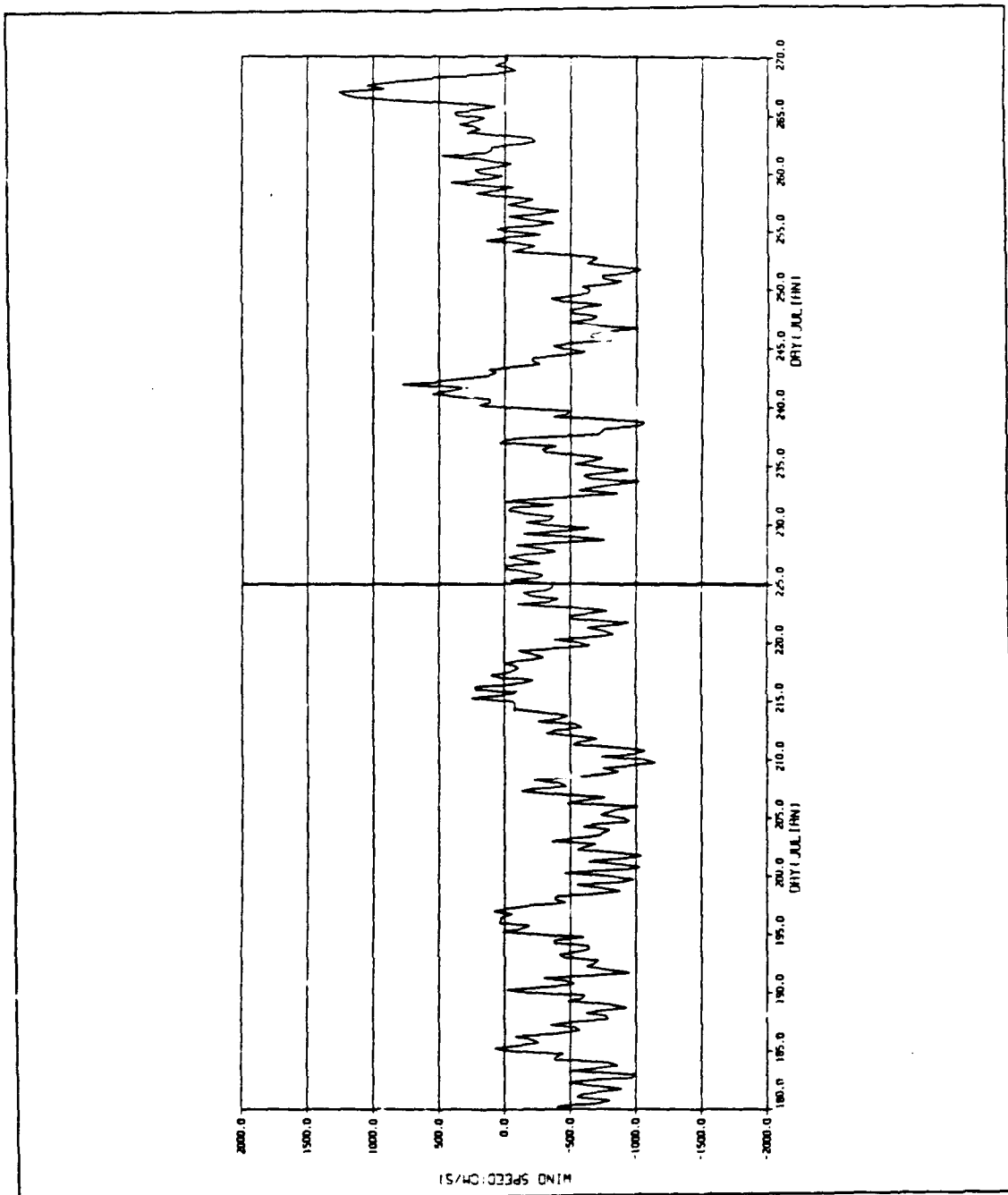
Figure 27. Expanded time series of meridional wind velocity (cm/s) for days 180-270 (29 Jun.- 27 Sep.) 1987.

Figure 28. Vertical cross-shore sections at 40°N of meridional velocity (cm/s) (**a,b**) and temperature (°C) (**c,d**) for 24 May (**a,c**) and 26 May (**b,d**) 1987.

contour interval = 2.0

Figure 29. Vertical cross-sections at 42°N of meridional velocity (cm/s) for **a)** 26 Jun.,**b)** 6 Jul., **c)** 16 Jul., and **d)** 26 Jul. 1987. Dashed=negative contours.

68
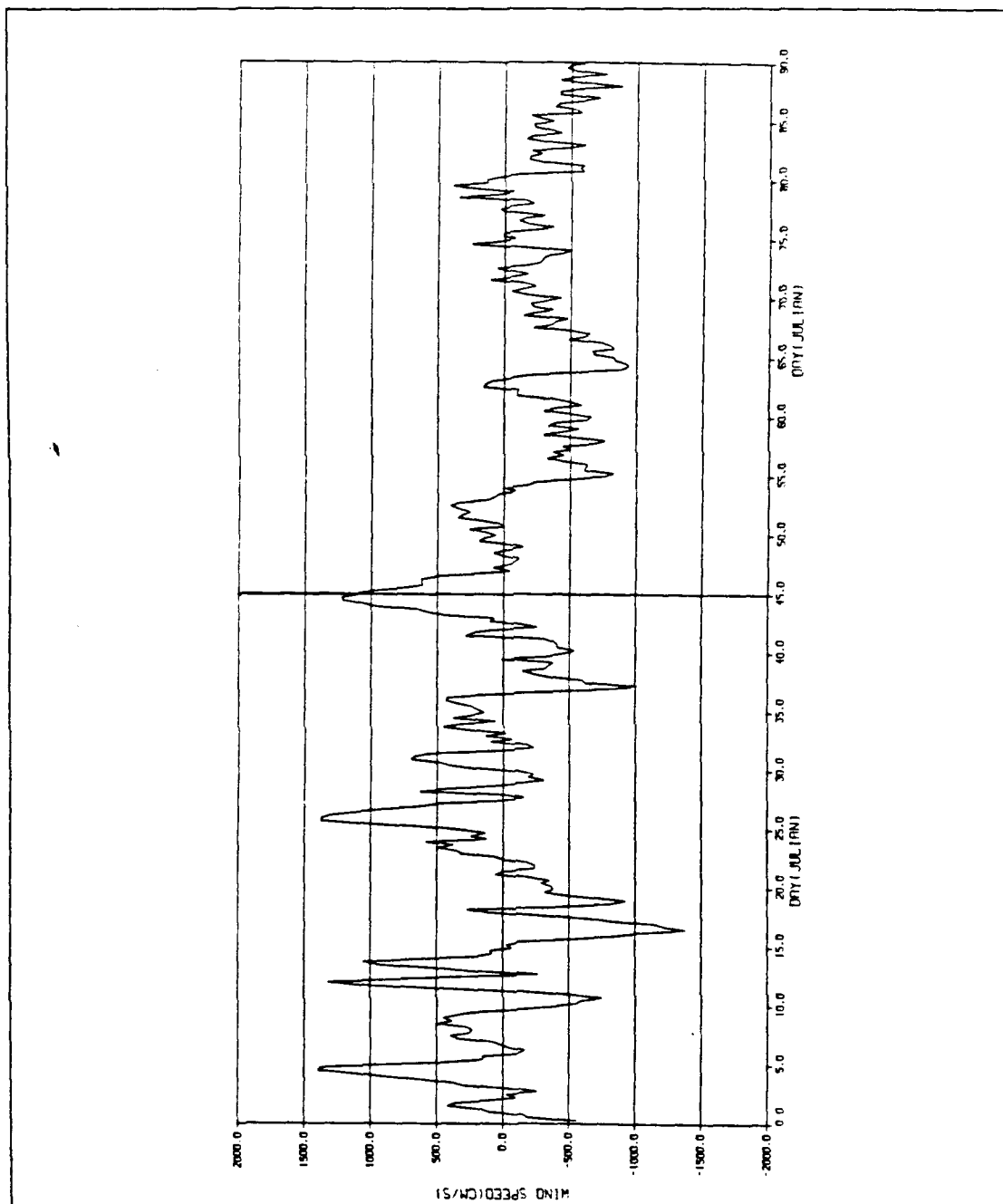
Figure 30. Expanded time series of meridional wind velocity (cm/s) for days 1-90 (1 Jan.-30 Mar.) 1988.

Figure 31. Expanded time series of meridional wind velocity (cm/s) for days 90-180 (30 Mar.- 28 Jun.) 1988.
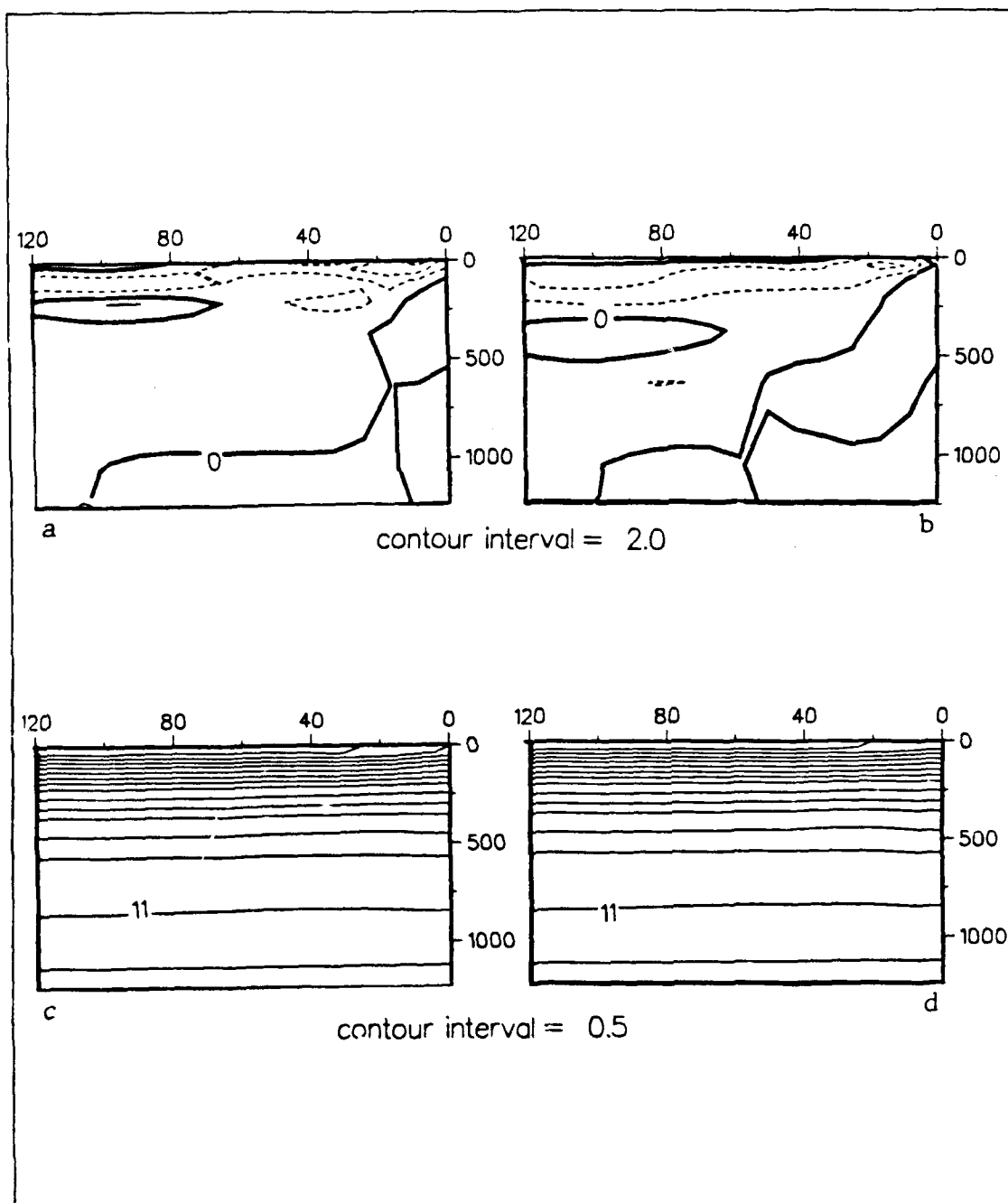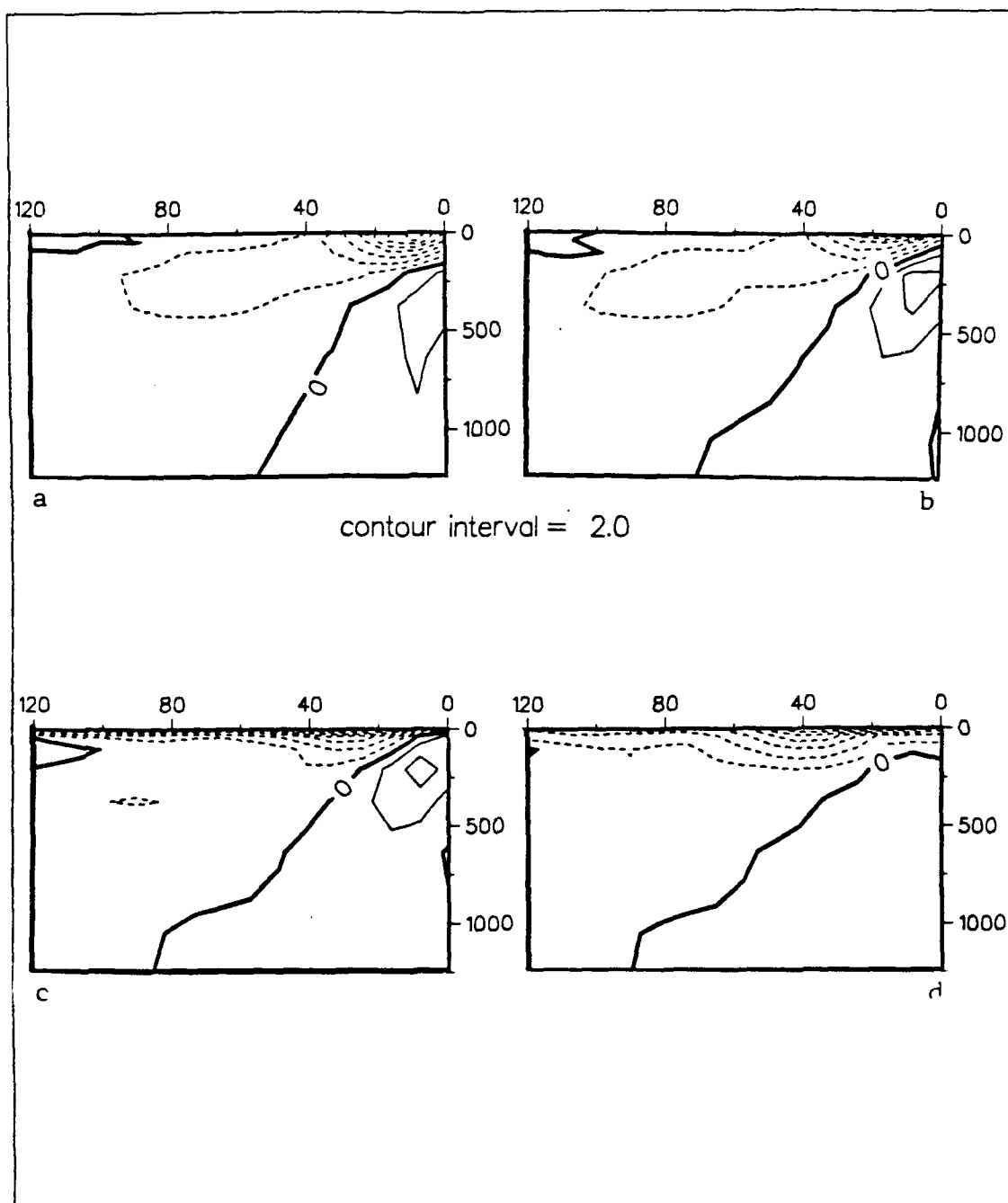
Figure 32. Expanded time series of meridional wind velocity (cm/s) for days
180-270 (28 Jun.-26 Sep.) 1988.

71

Figure 33. Vertical cross-shore sections at 40°N of temperature (°C) for **a**) 29 Apr. (day 119) and **b**) 5 May (day 126) 1988.

Figure 34. Vertical cross-shore sections at 42°N of meridional velocity (cm/s) for **a**) 11 Apr., **b**) 11 May and **c**) 10 Jun. 1988. Dashed lines=negative contours.
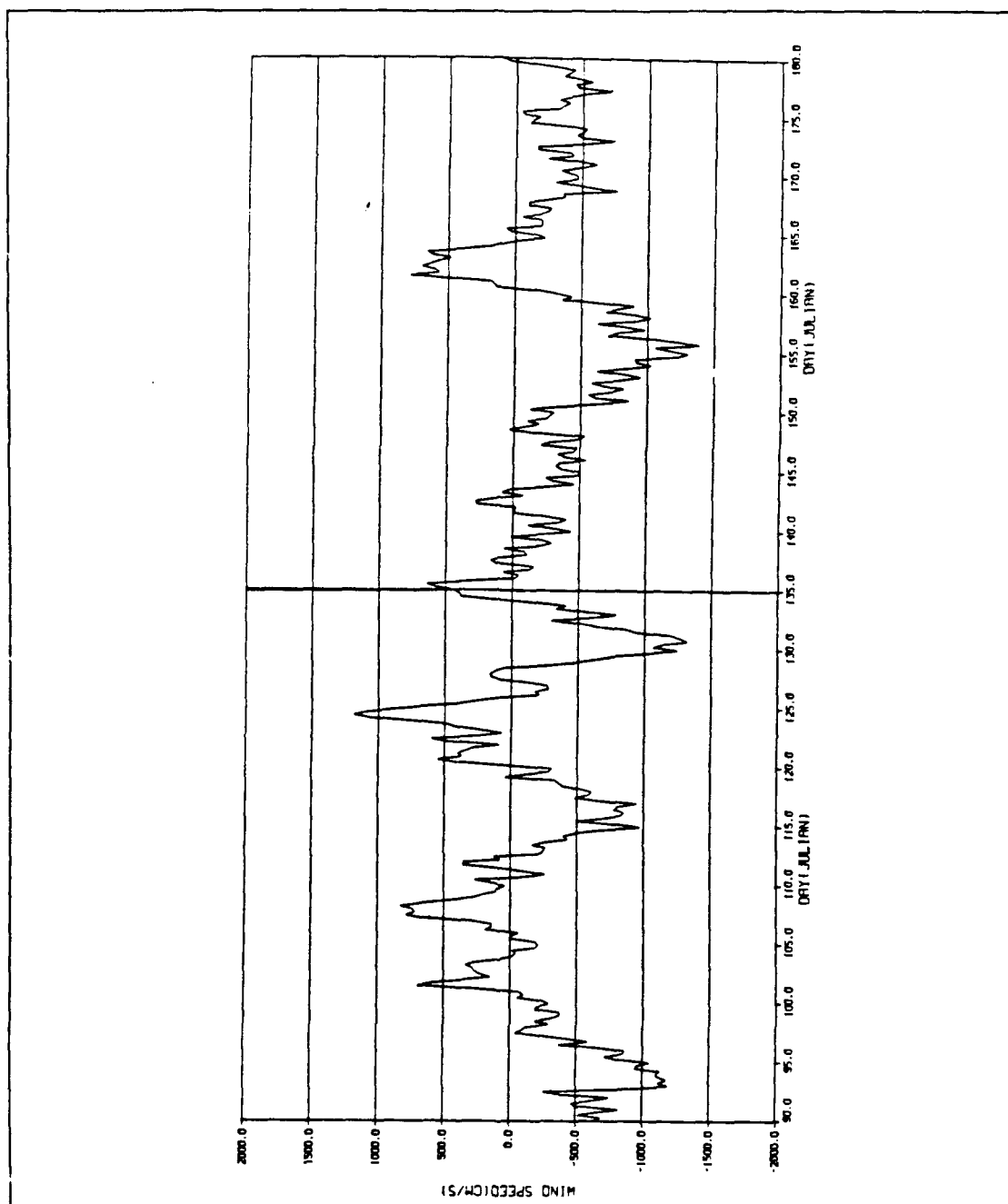
Figure 35. Expanded time series of meridional wind velocity (cm/s) for days 180-270 (29 Jun.-28 Sep.) 1987.

74
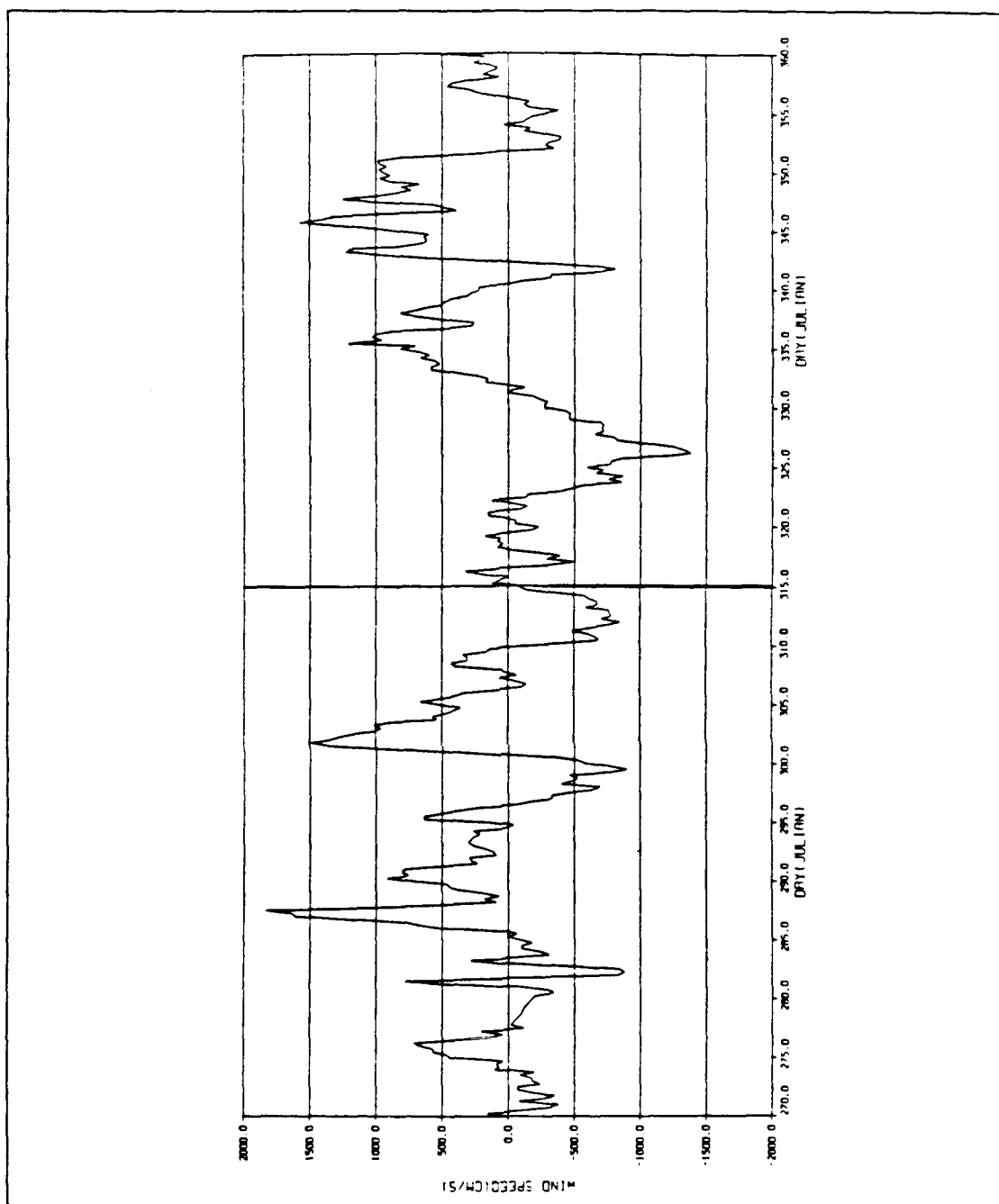
Figure 36. Expanded time series of meridional wind velocity (cm/s) for days 270-360 (28 Sep.-26 Dec.) 1987.

Figure 37. Vertical cross-sections at 40°N of meridional velocity (cm/s) for **a)** 28 Aug.,**b)** Sep., **c)** 3 Aug. and **d)** 15 Sep. 1987. Dashed=negative contours.

Figure 38. Surface isotherms (°C) for **a)** 26 Aug. (day 238) and **b)** 4 Oct. (day 277) 1987 (17 °C isotherm shown in **b**).
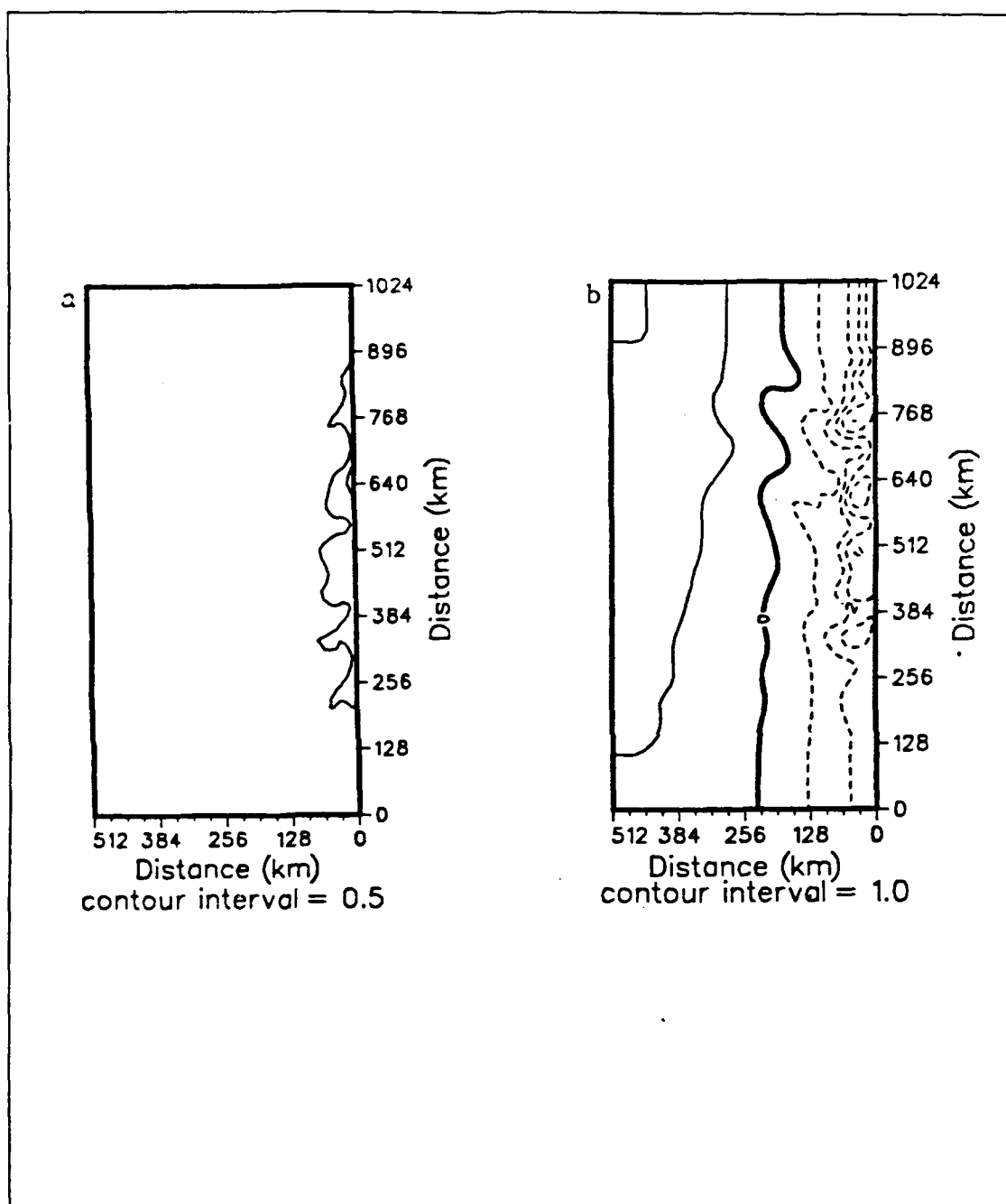
Figure 39. Surface isopleths of **a)** temperature (17°C shown) and **b)** dynamic height (cm) relative to 2400 m for 1 Sep. 1987.
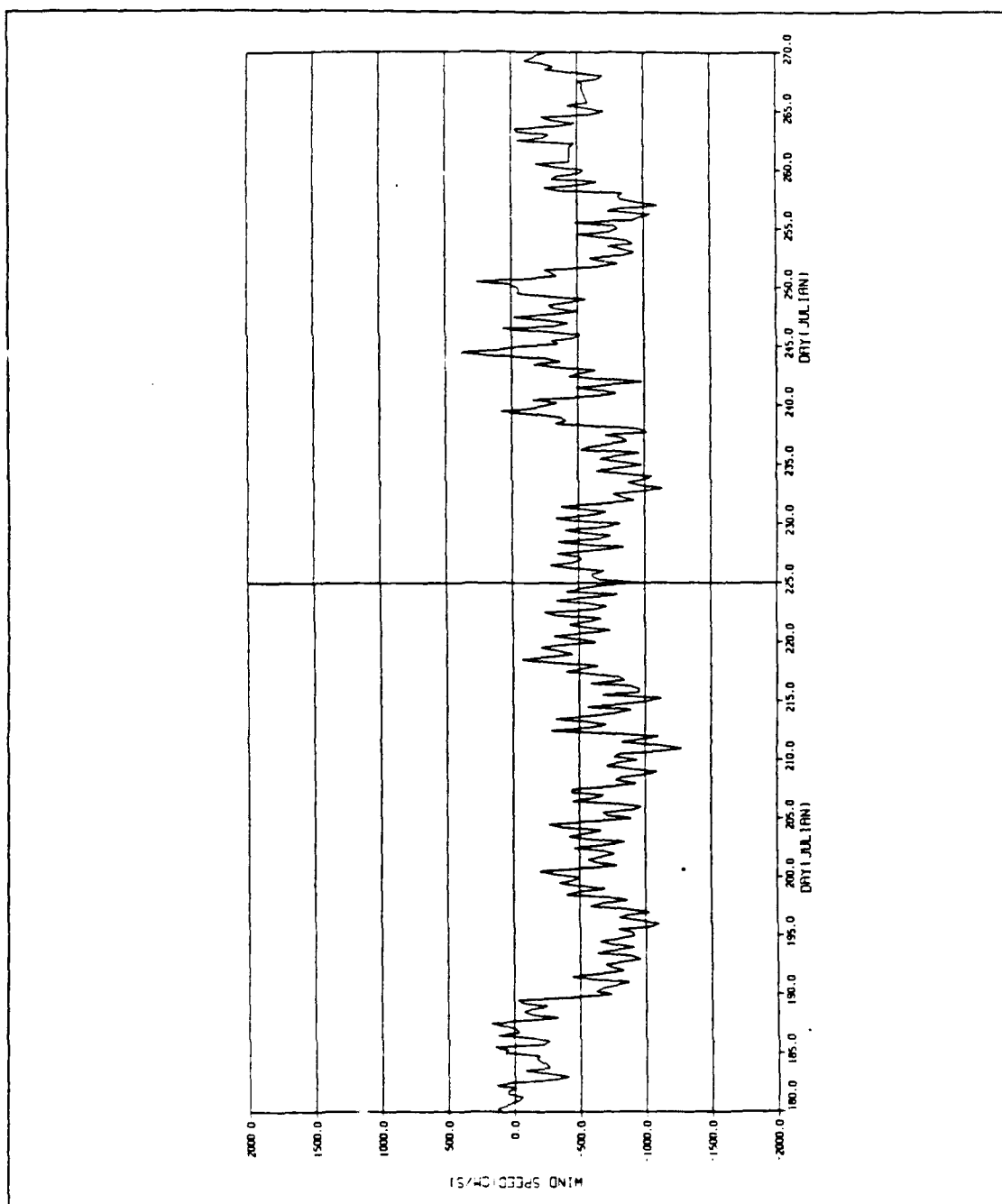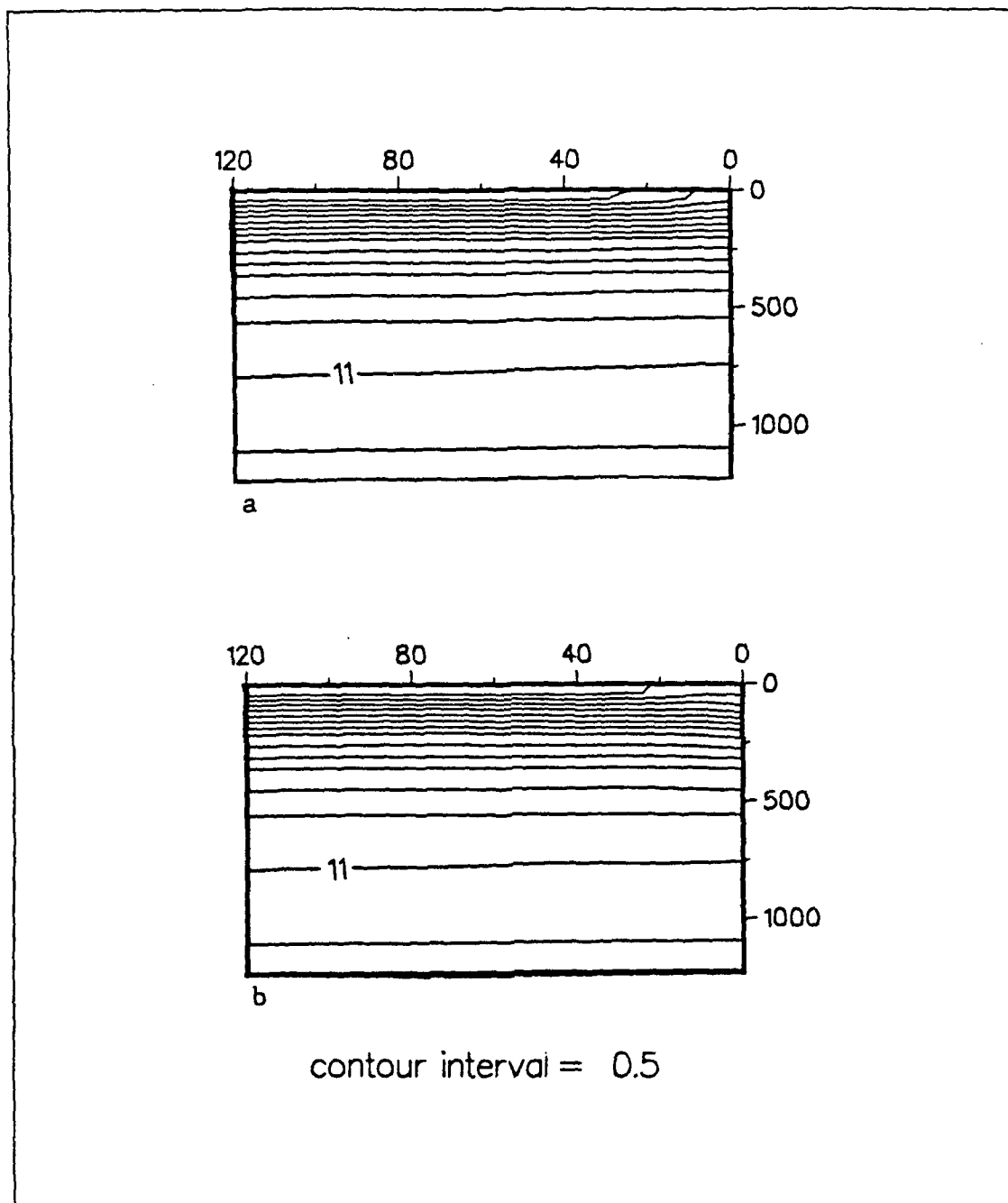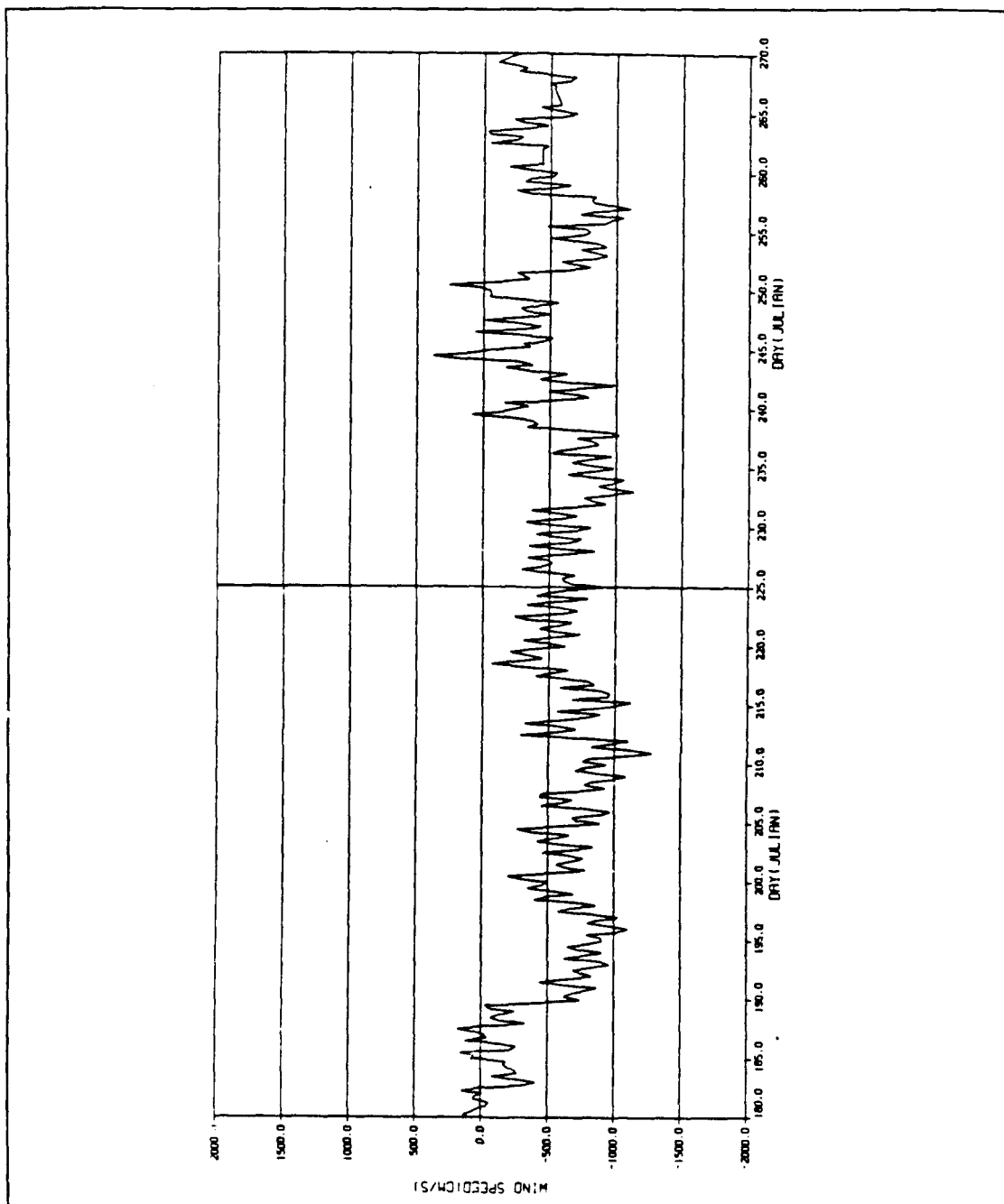
Figure 40. Expanded time series of meridional wind velocity (cm/s) for days
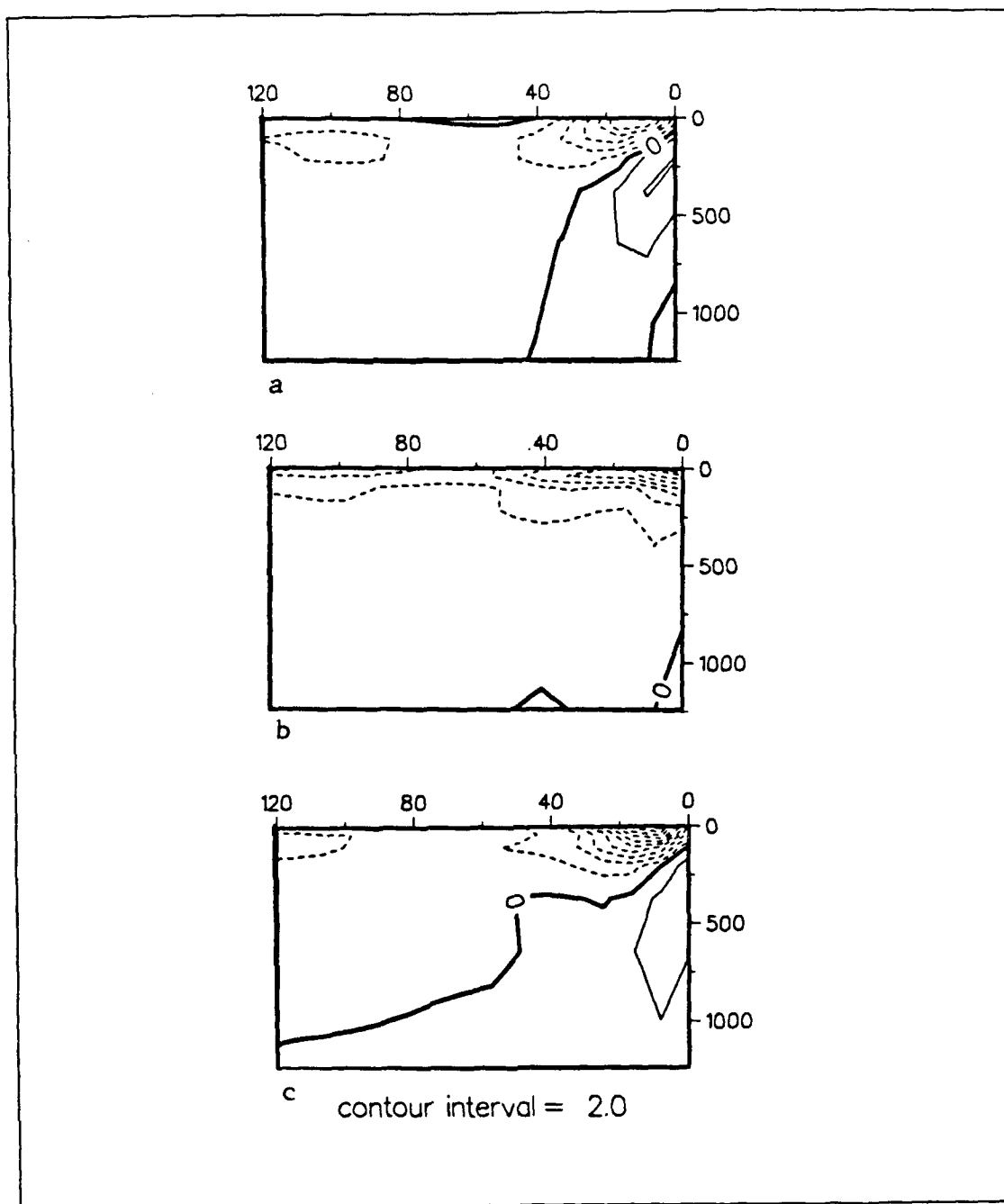180-270 (28 Jun.-26 Sep.) 1988.

79
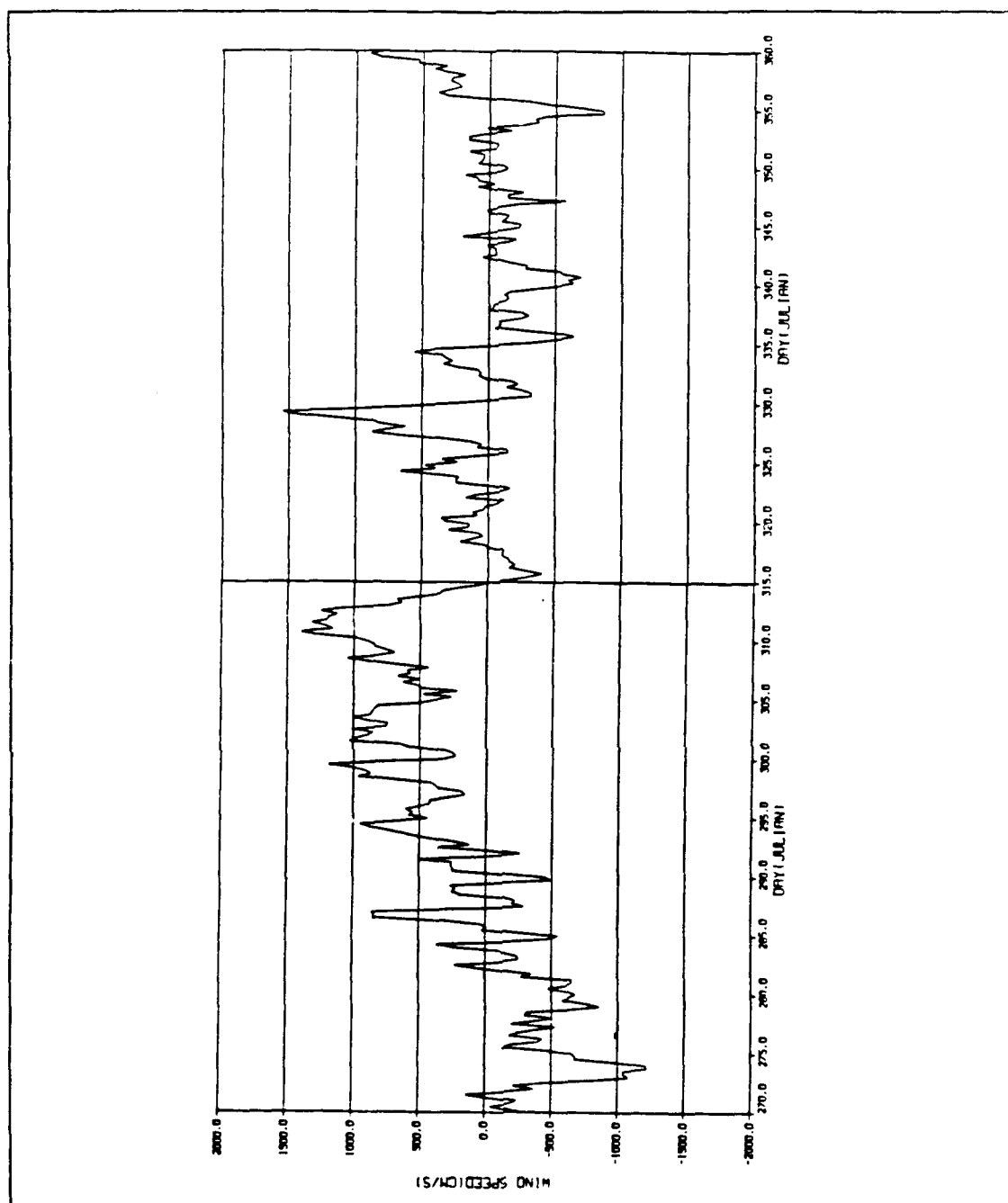
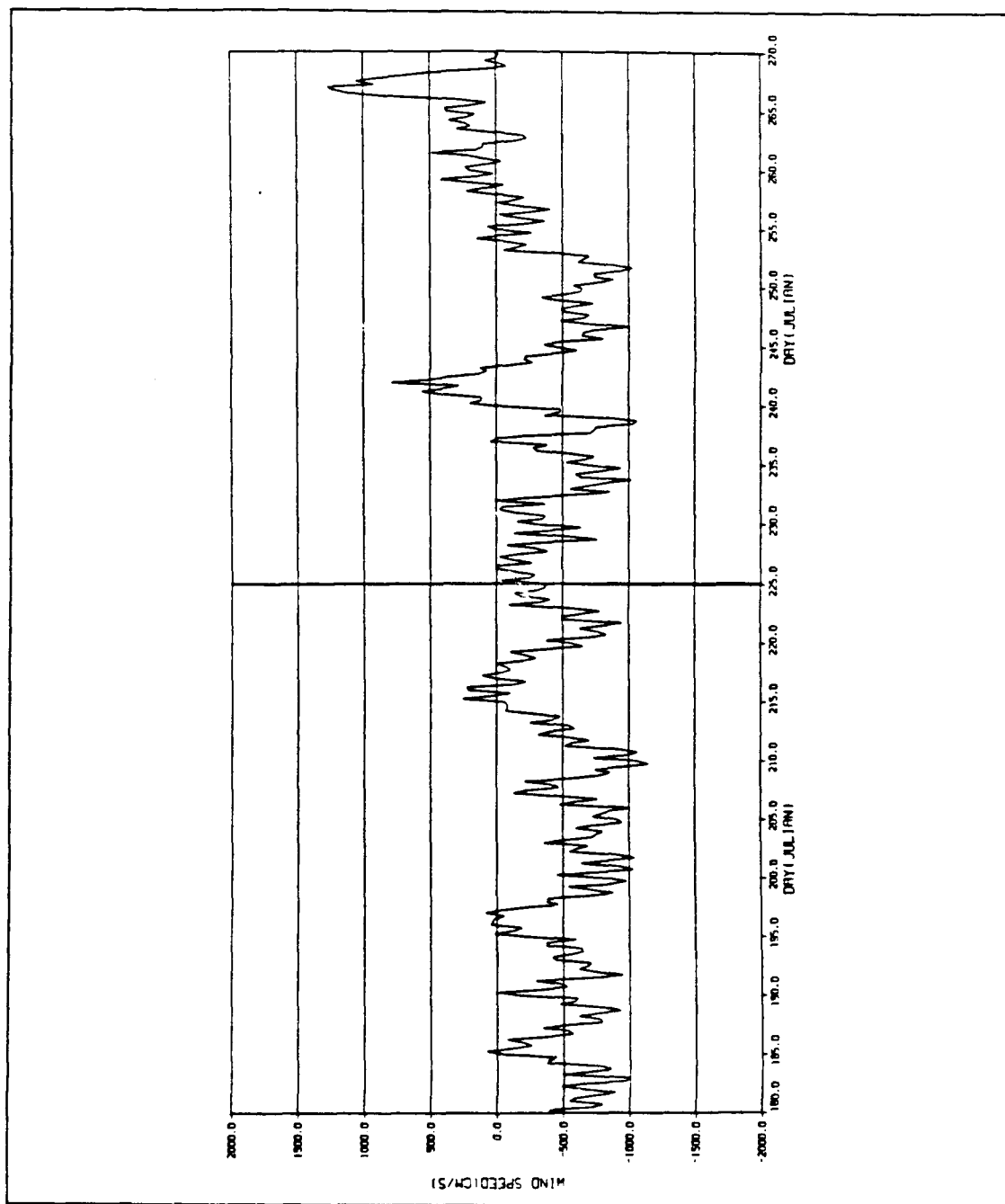**Figure 41.** Expanded time series of meridional wind velocity (cm/s) for days
270-360 (26 Sep.-26 Dec) 1988.

80
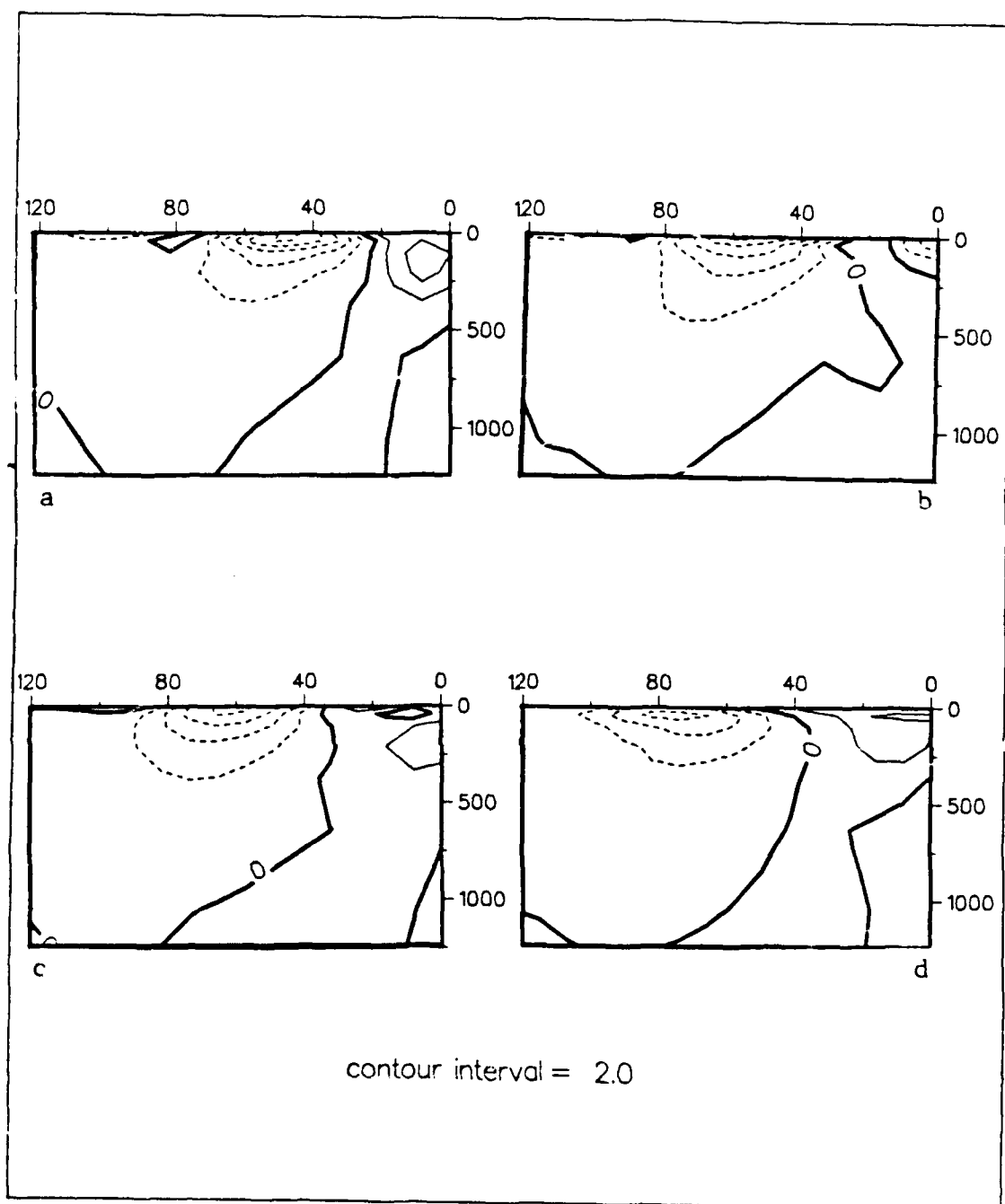
Figure 42. Vertical cross-sections at 40°N of meridional velocity (cm/s) for **a)** 3 Sep., **b)** 13 Sep., **c)** 18 Sep. and **d)** 28 Sep. 1988. Dashed=negative contours
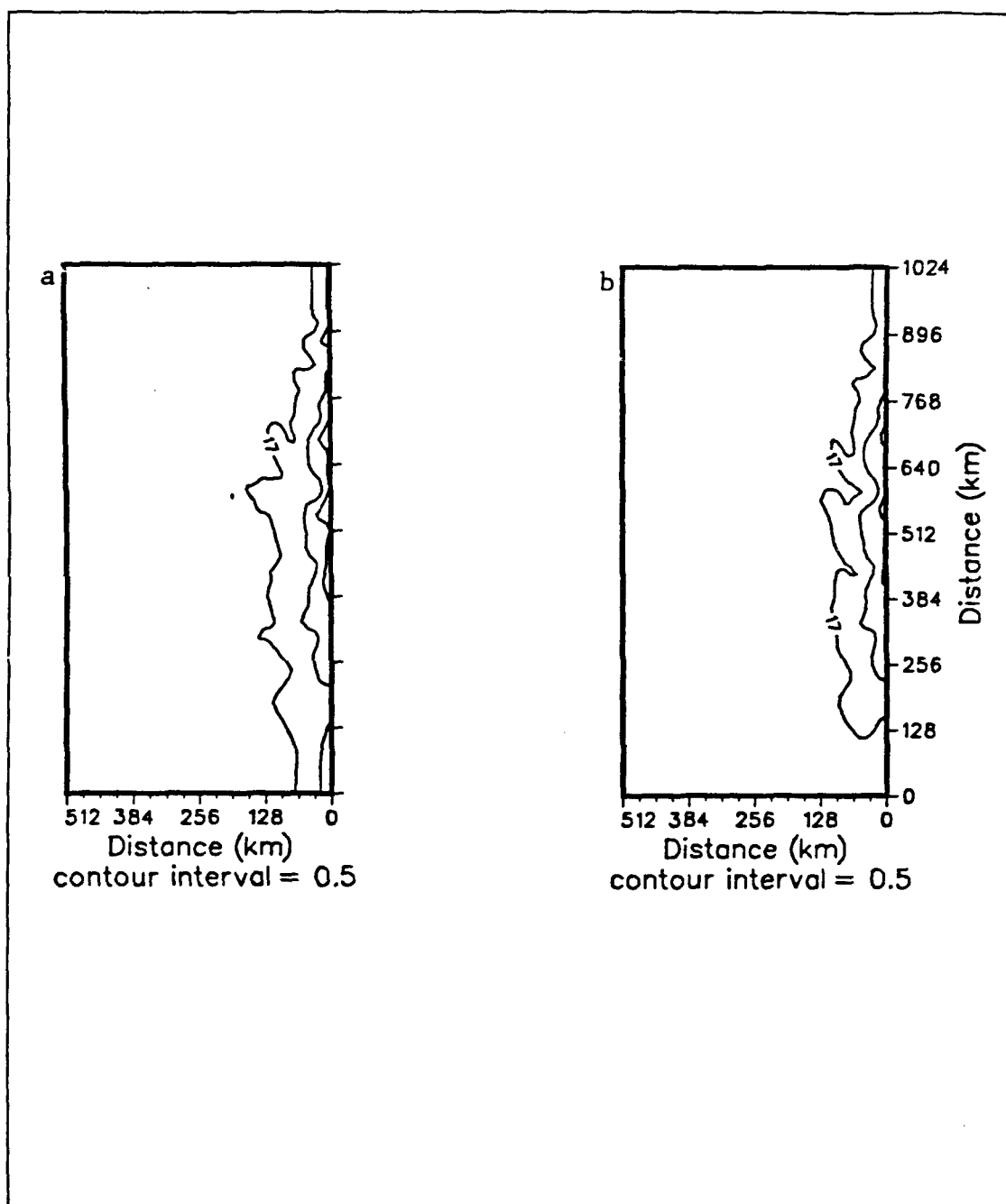
Figure 43. Surface isotherms (°C) for **a)** 1 Sep. and **b)** 29 Sep. 1988.
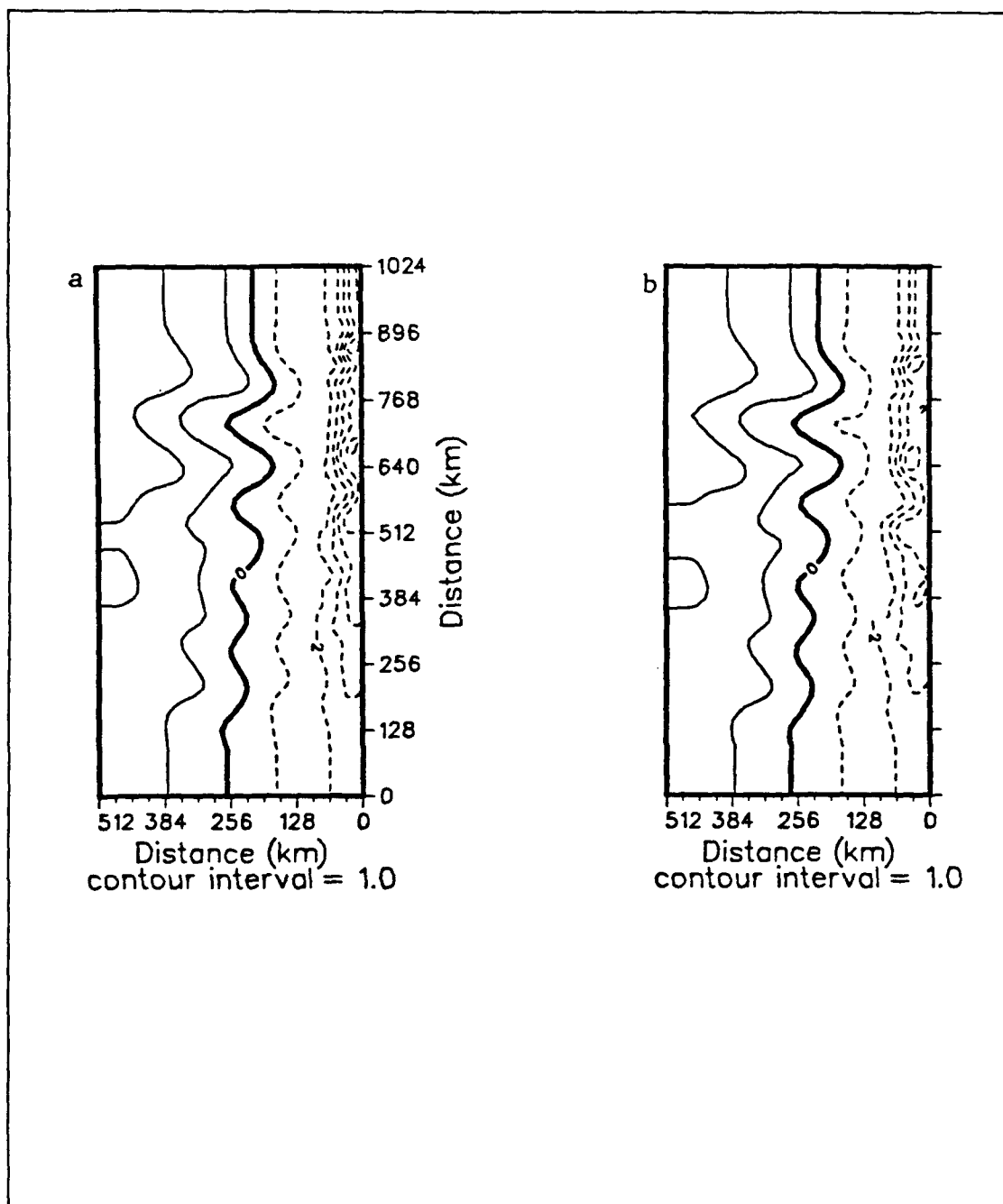
Figure 44. Surface isopleths of dynamic height (cm) relative to 2400 m for a) 1 Sep. and b) 28 Sep. 1988. Dashed lines are negative contours.

83
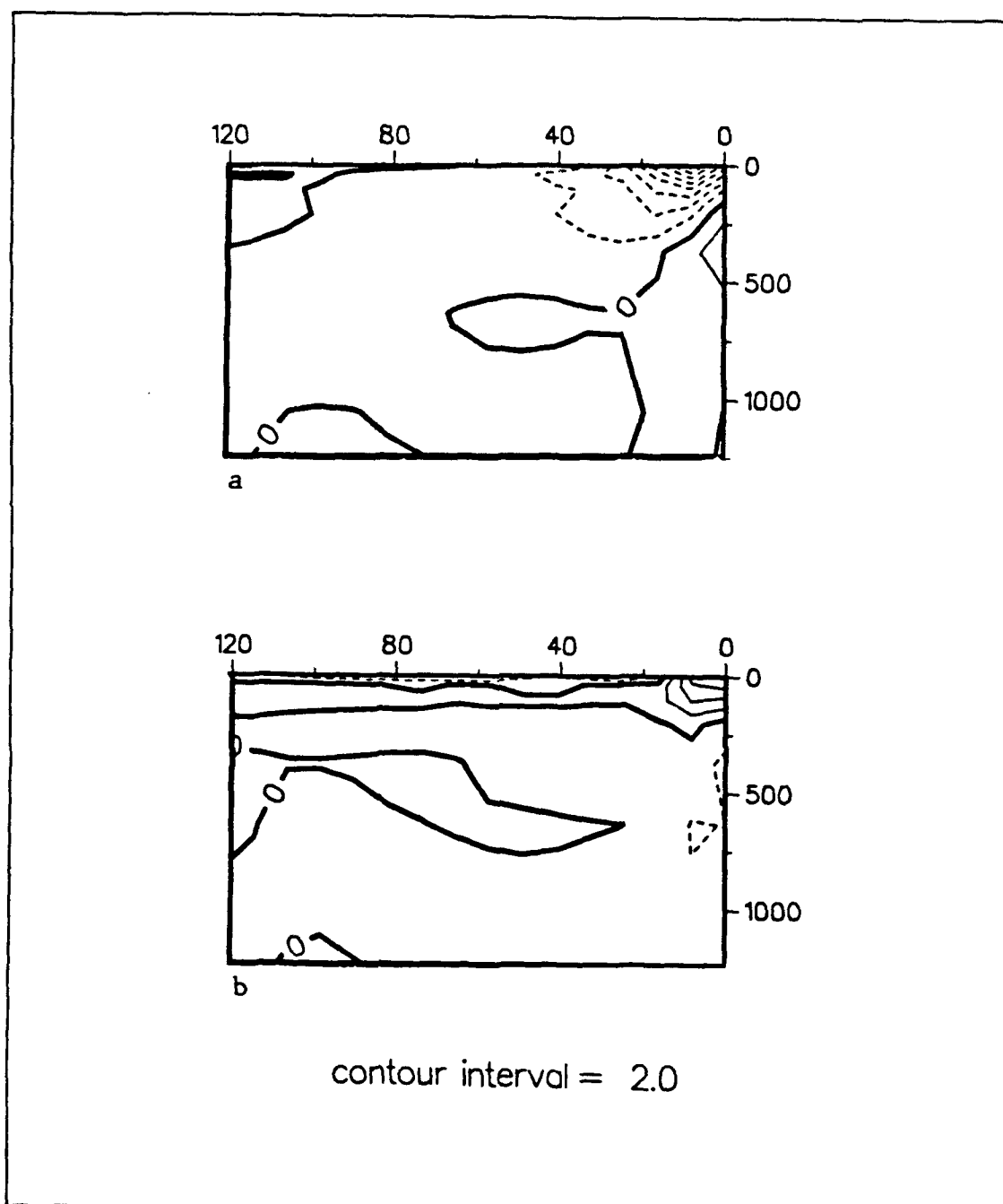
Figure 45. Vertical cross-shore sections at 40°N of meridional velocity (cm/s) for a) 27 Nov. and b) 6 Dec. 1987. Dashed lines are negative contours.
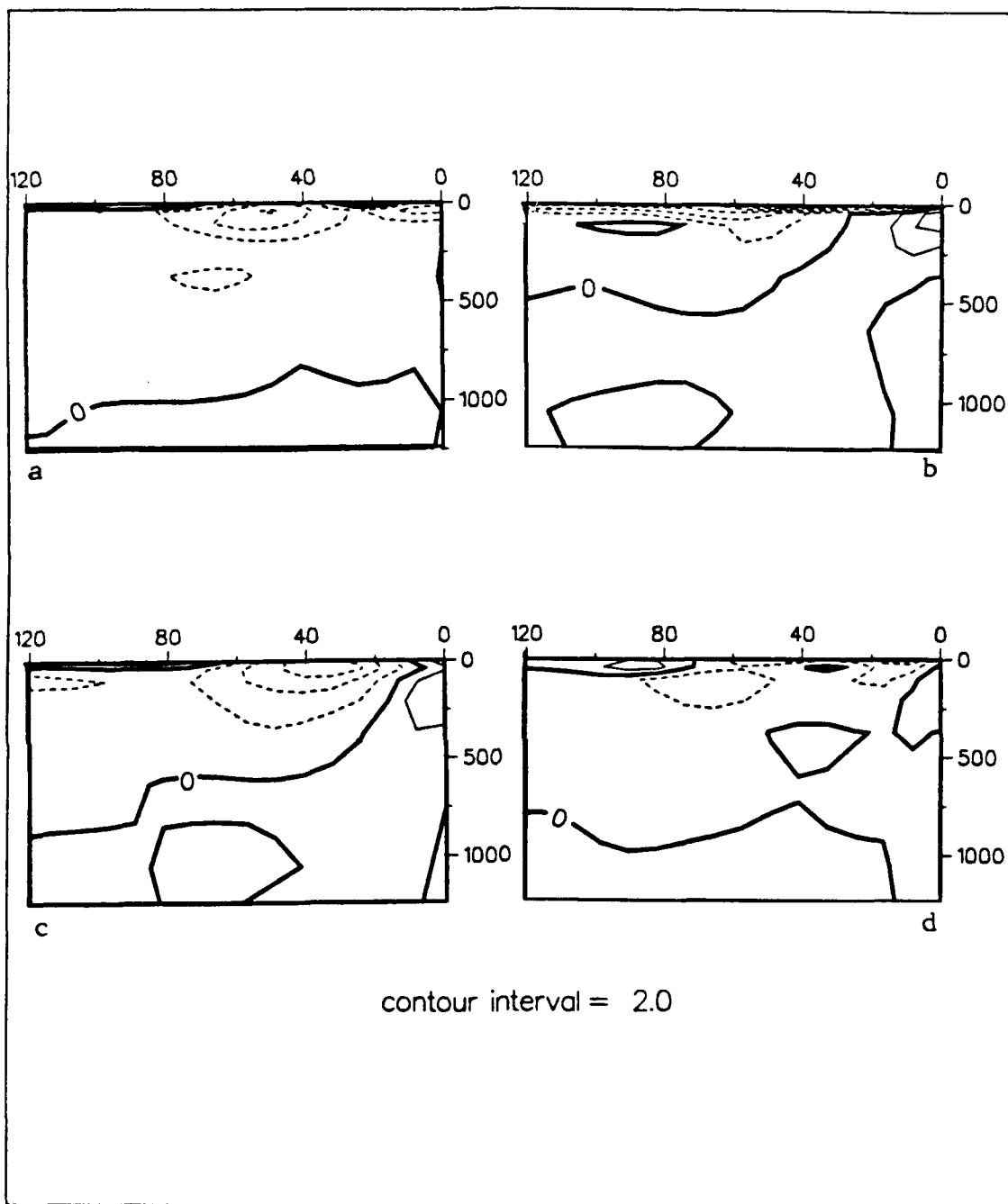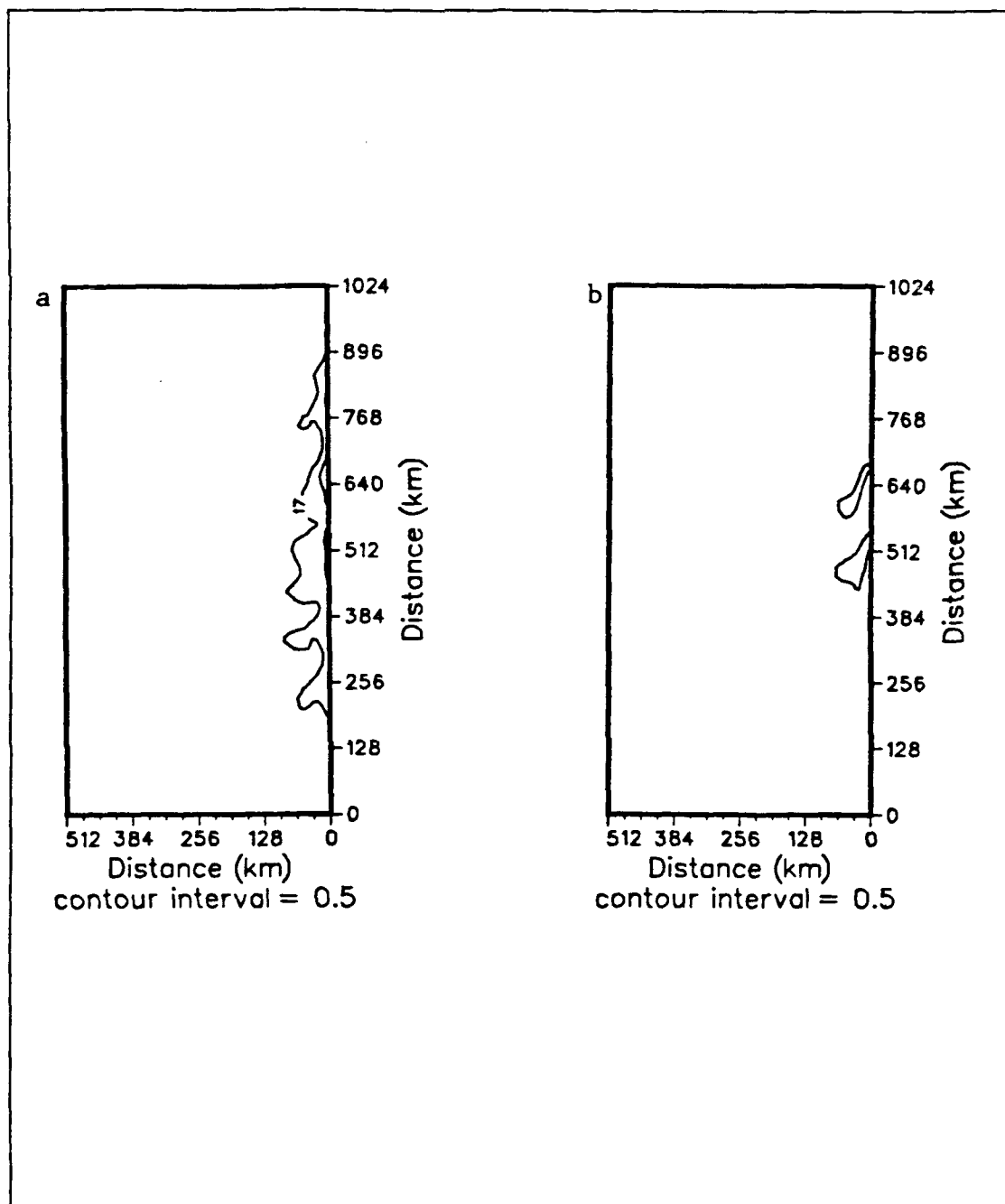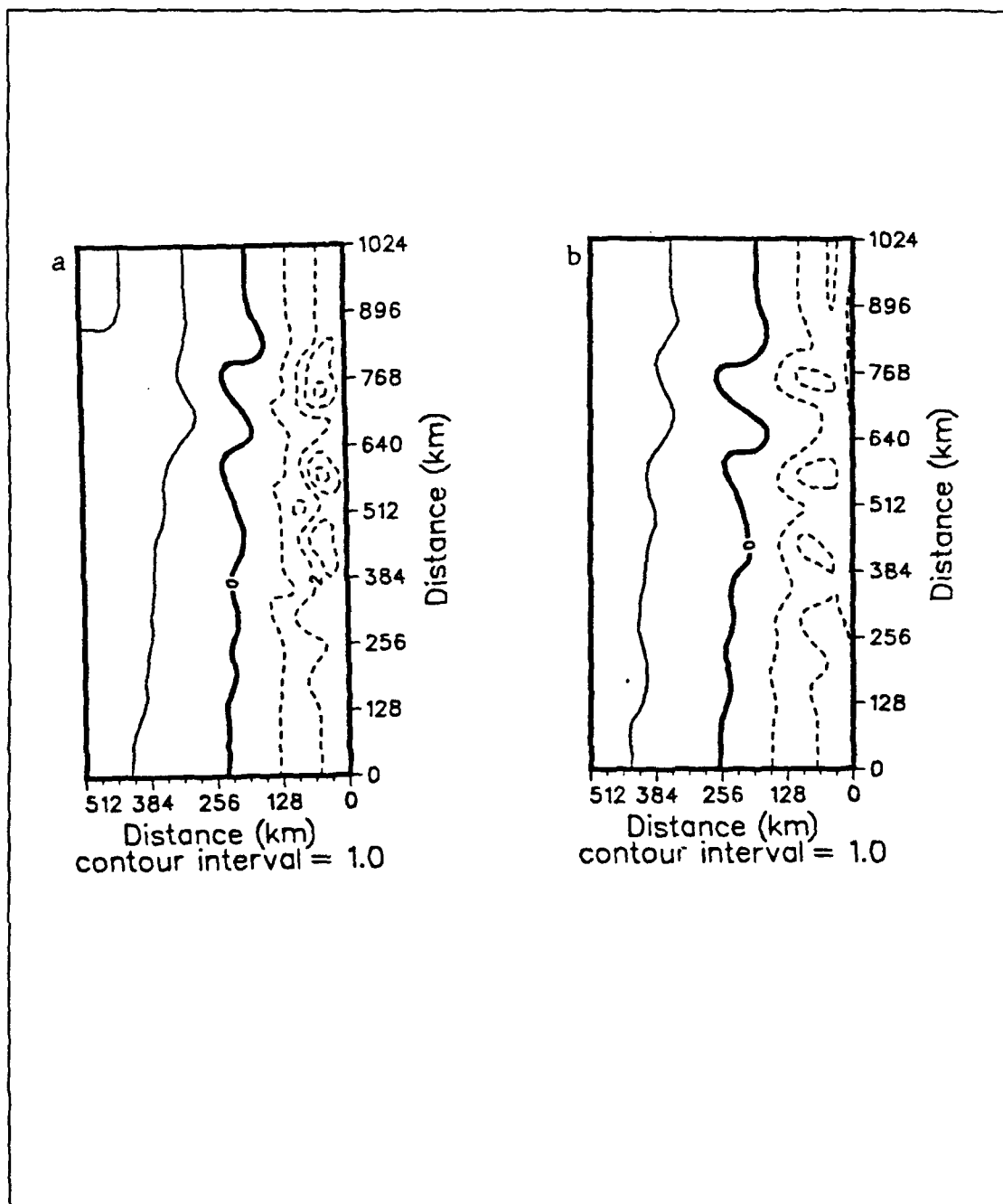
Figure 46. Surface isopleths of dynamic height (cm) relative to 2400 m for a) 14 Oct. and b) 28 Dec. 1987. Dashed lines are negative contours.
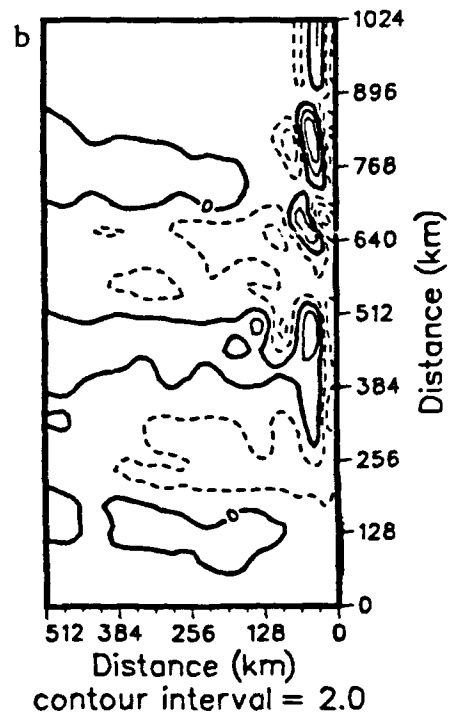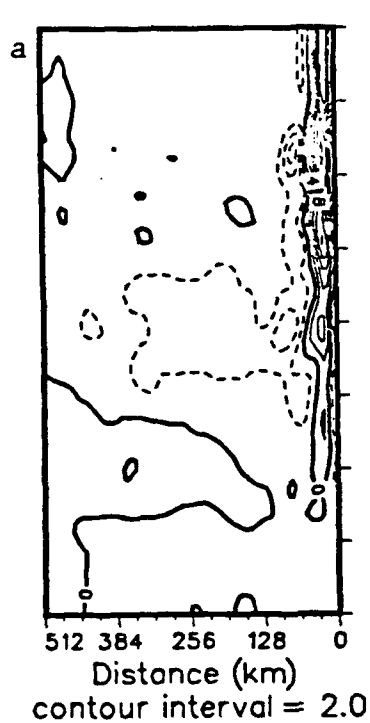
Figure 47. Isopleths of meridional velocity (cm/s) at 75 m depth for a) 12 Nov. and b) 7 Dec. 1988. Dashed lines are negative contours.
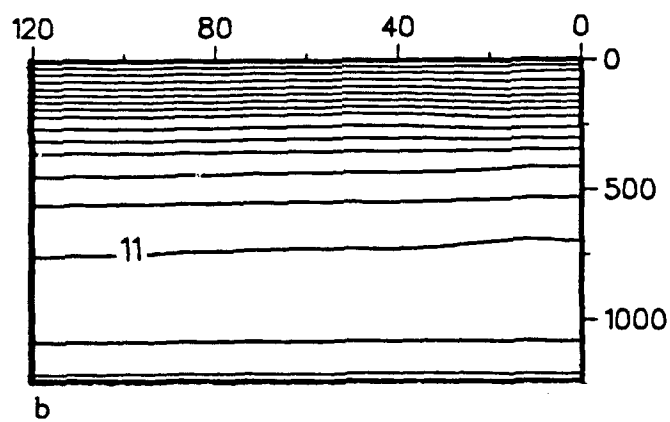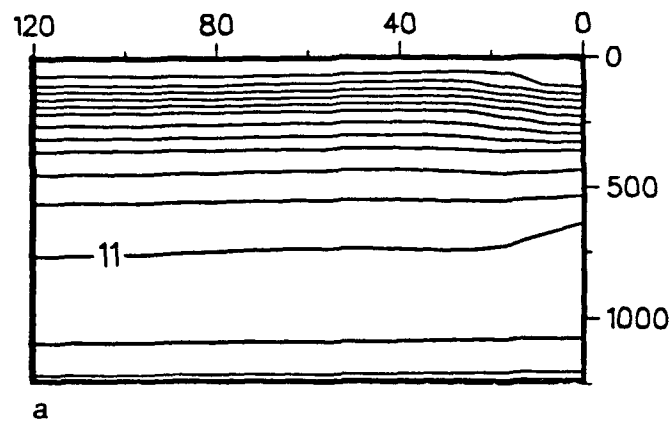
Figure 48. Vertical cross-shore sections at 42°N of temperature (°C) for a) 12 Nov. (day 317) and b) 17 Dec. (day 352) 1988.
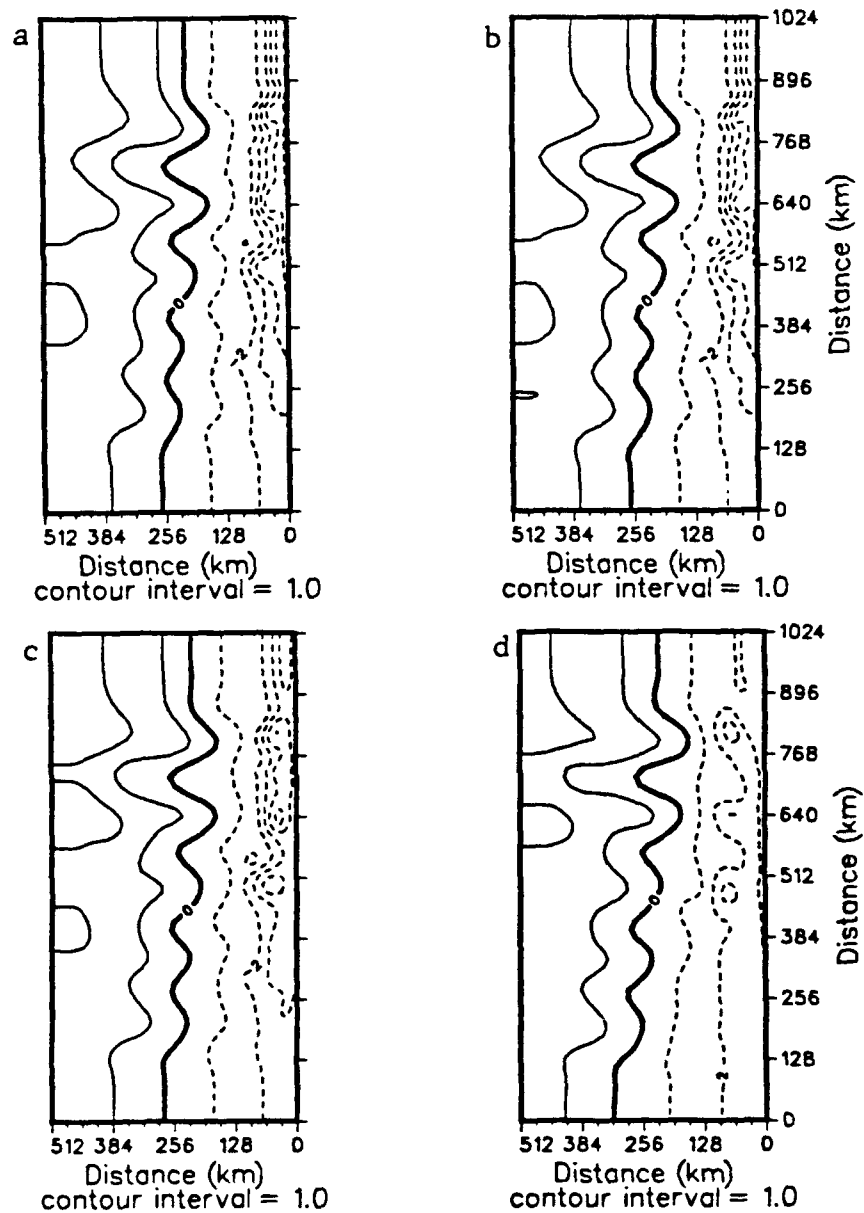
Figure 49. Surface isopleths of dynamic height (cm) relative to 2400 m for **a)** 3 Oct.,
b) 8 Oct., **c)** 18 Oct. and **d)** 31 Dec. 1988.
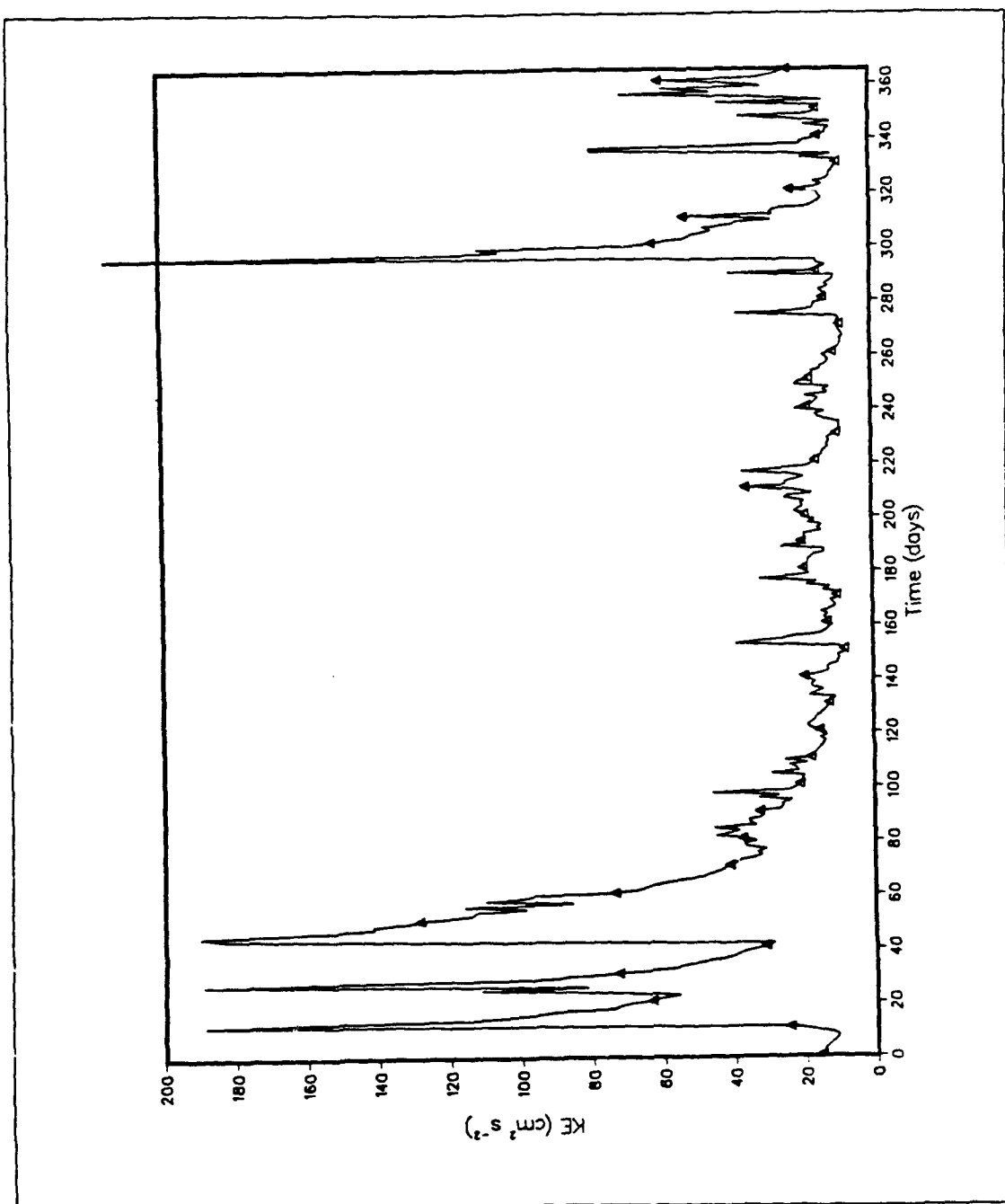
Figure 50. Kinetic energy for 1987.

BAROCLINIC TRANSFER
$(\text{ergs.cm}^{-3}.\text{sec}^{-1})$

BAROTROPIC TRANSFER
$(\text{ergs.cm}^{-3}.\text{sec}^{-1})$

a

b

Contour Interval = $1.5*10^{-6}$

Contour Interval = $1.5*10^{-6}$
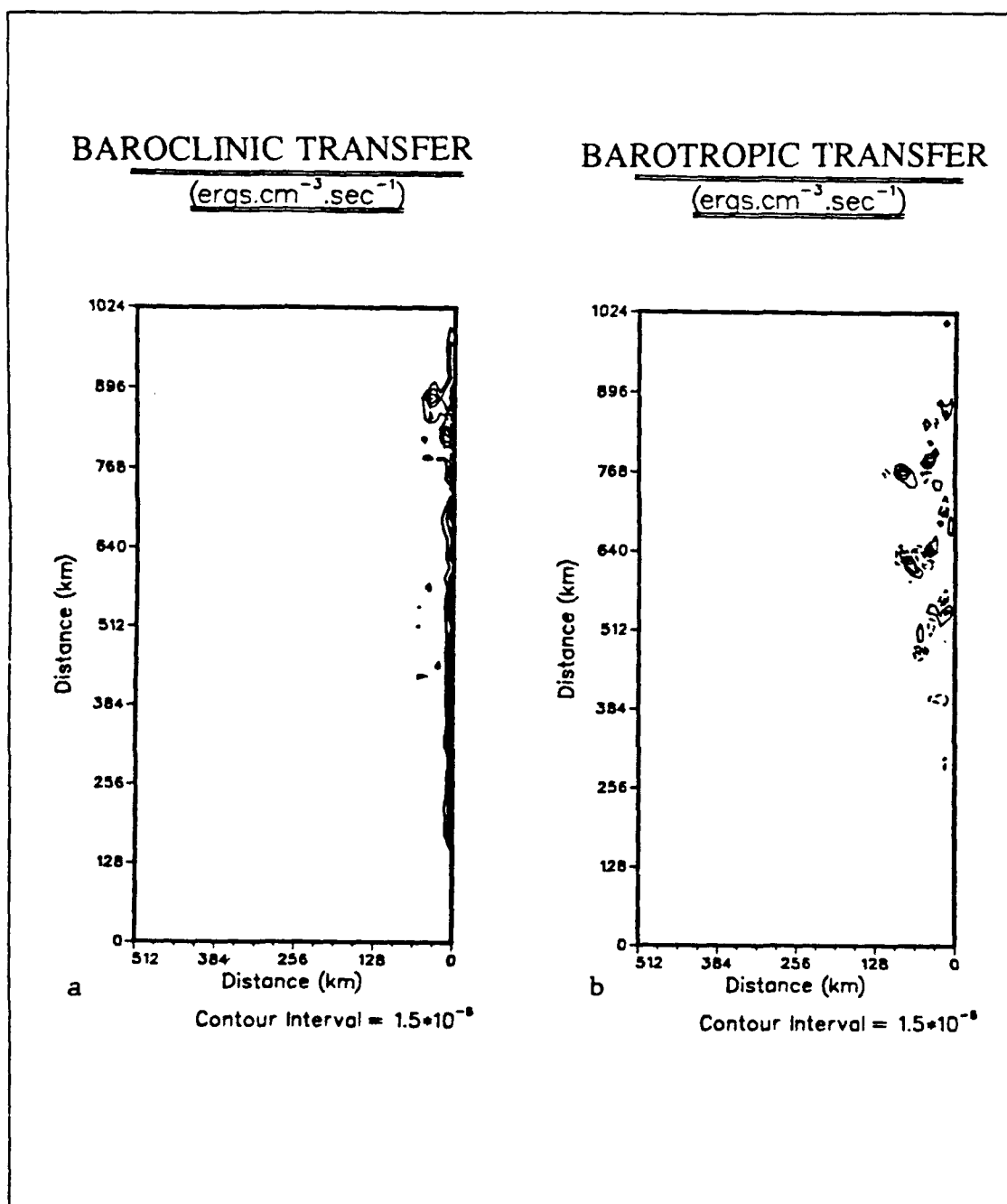
Figure 51. a) Baroclinic energy transfer for 15 Aug.-4 Sep. 1987.
b) Barotropic energy transfer for 15 Aug.-4 Sep. 1987.

90
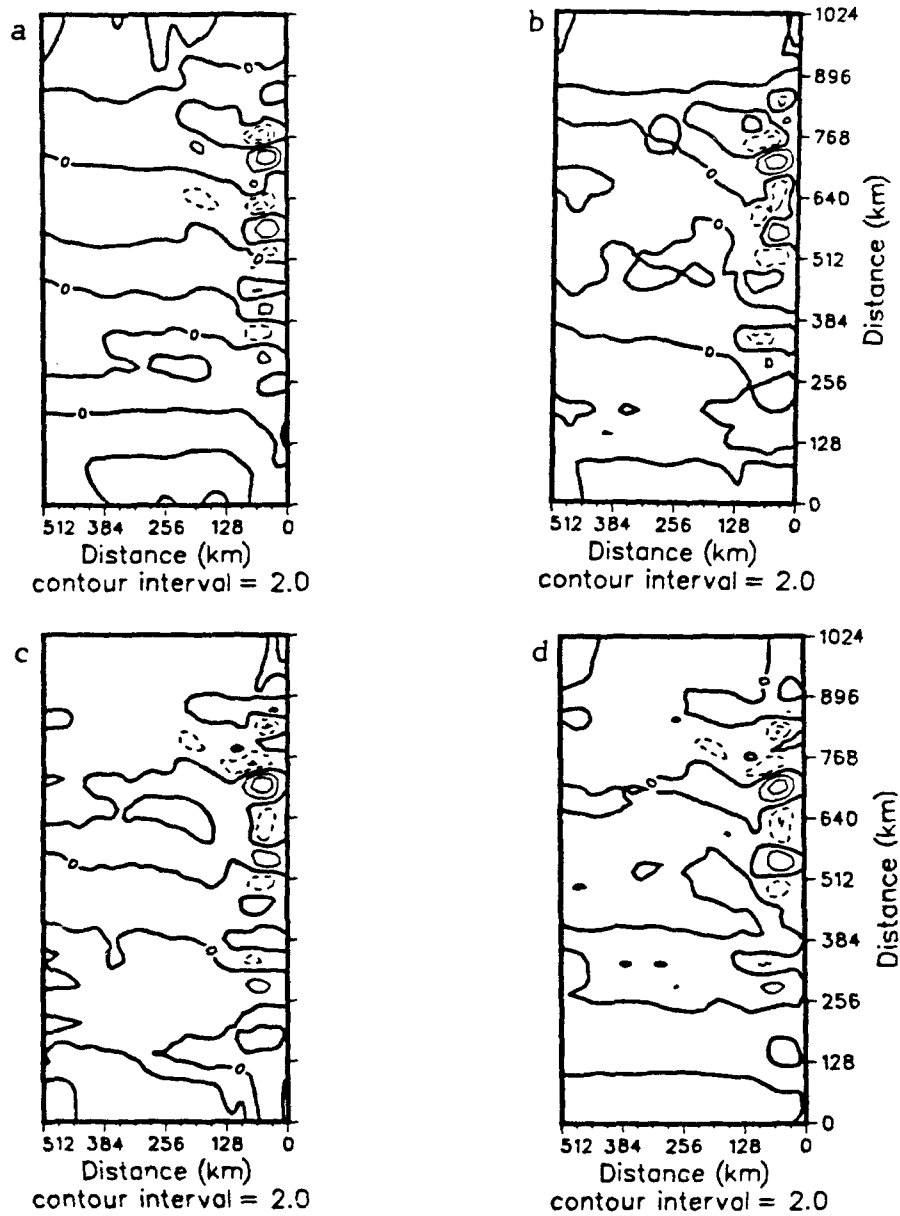
Figure 52. Isopleths of zonal velocity (cm/s) at 75 m depth for **a)** 15 Aug., **b)** 4 Sep., **c)** 14 Sep. and **d)** 24 Sep. 1987.

91
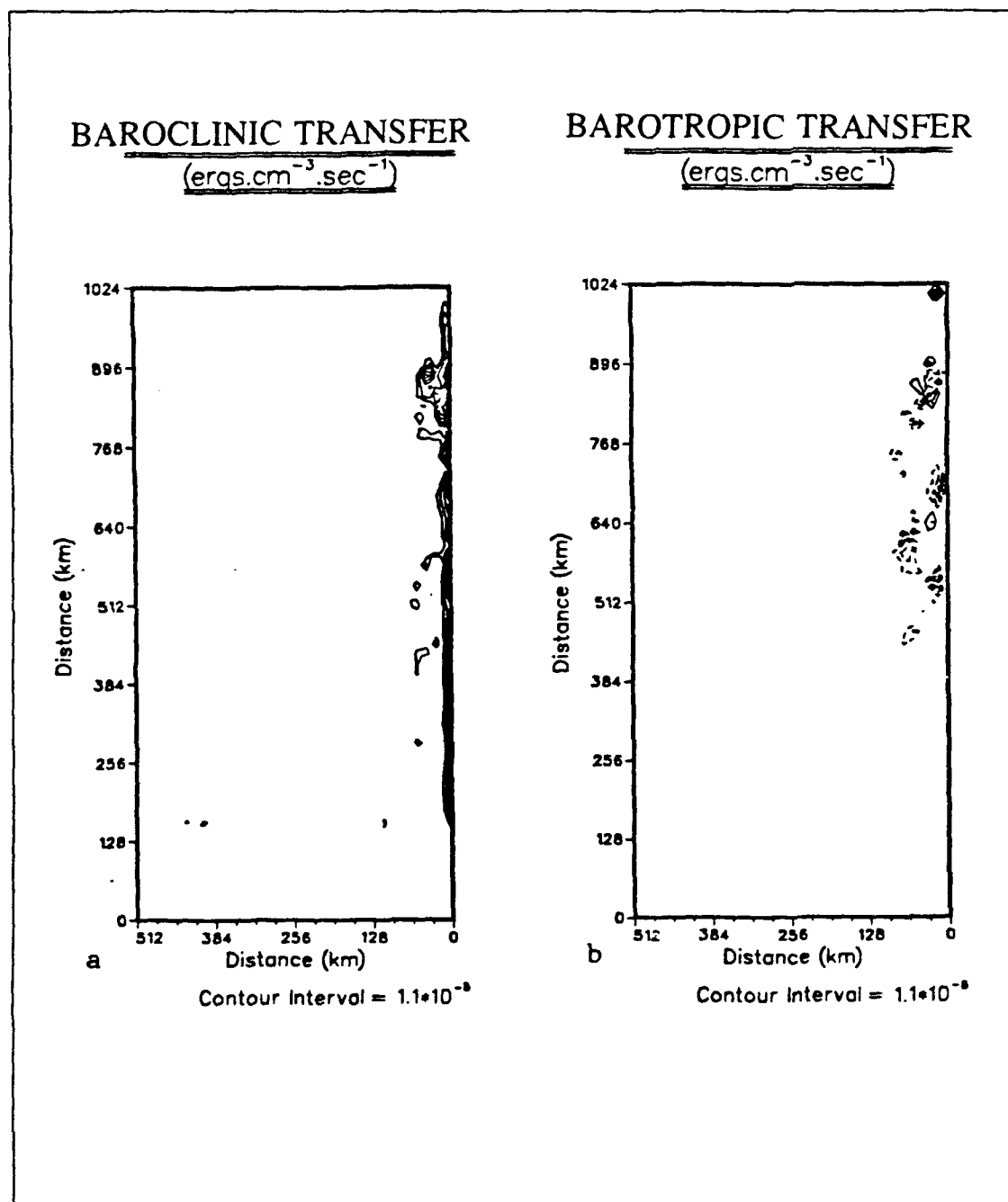
Figure 53. a) Baroclinic energy transfer for 4 Sep.-24 Sep. 1987.
b) Barotropic energy transfer for 4 Sep.-24 Sep. 1987.
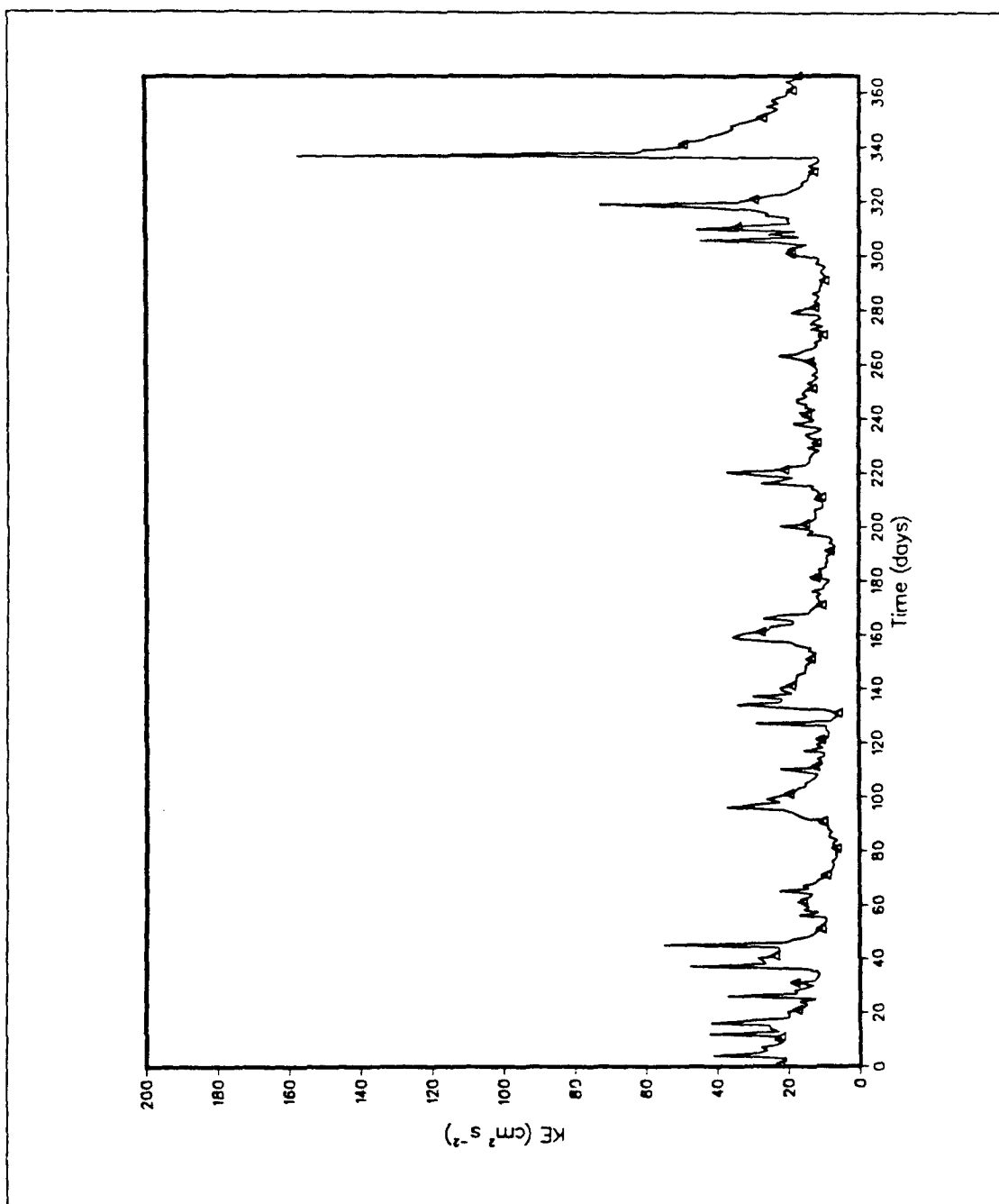
Figure 54. Kinetic energy for 1988.

93

BAROCLINIC TRANSFER
$$(ergs.cm^{-3}.sec^{-1})$$

BAROTROPIC TRANSFER
$$(ergs.cm^{-3}.sec^{-1})$$

Distance (km)

a Distance (km)

Contour Interval = $4.1*10^{-8}$

b Distance (km)

Contour Interval = $4.1*10^{-8}$
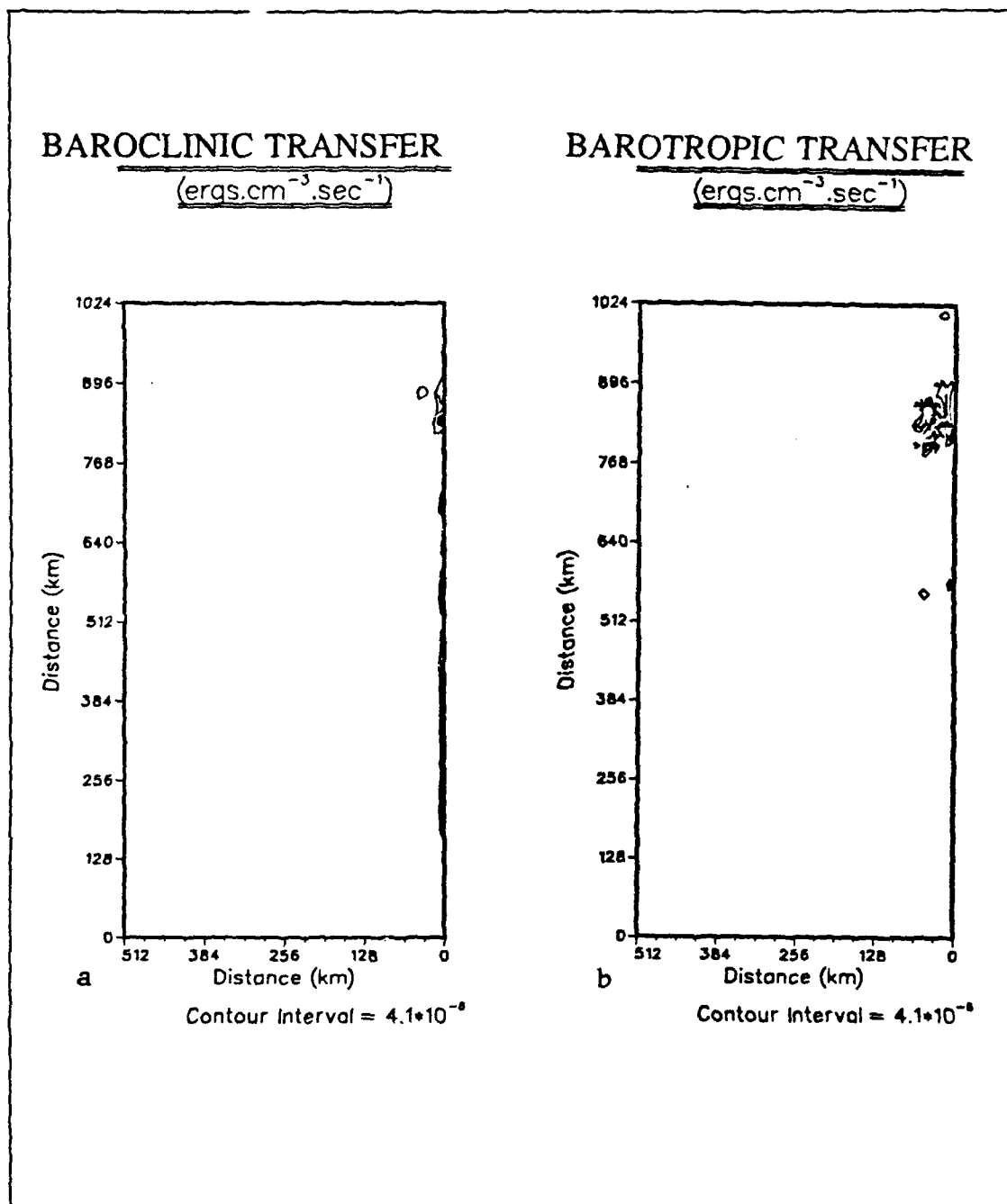
Figure 55. a) Baroclinic energy transfer for 29 Aug.-18 Sep. 1988.
b) Barotropic energy transfer for 29 Aug.-18 Sep. 1988.

94
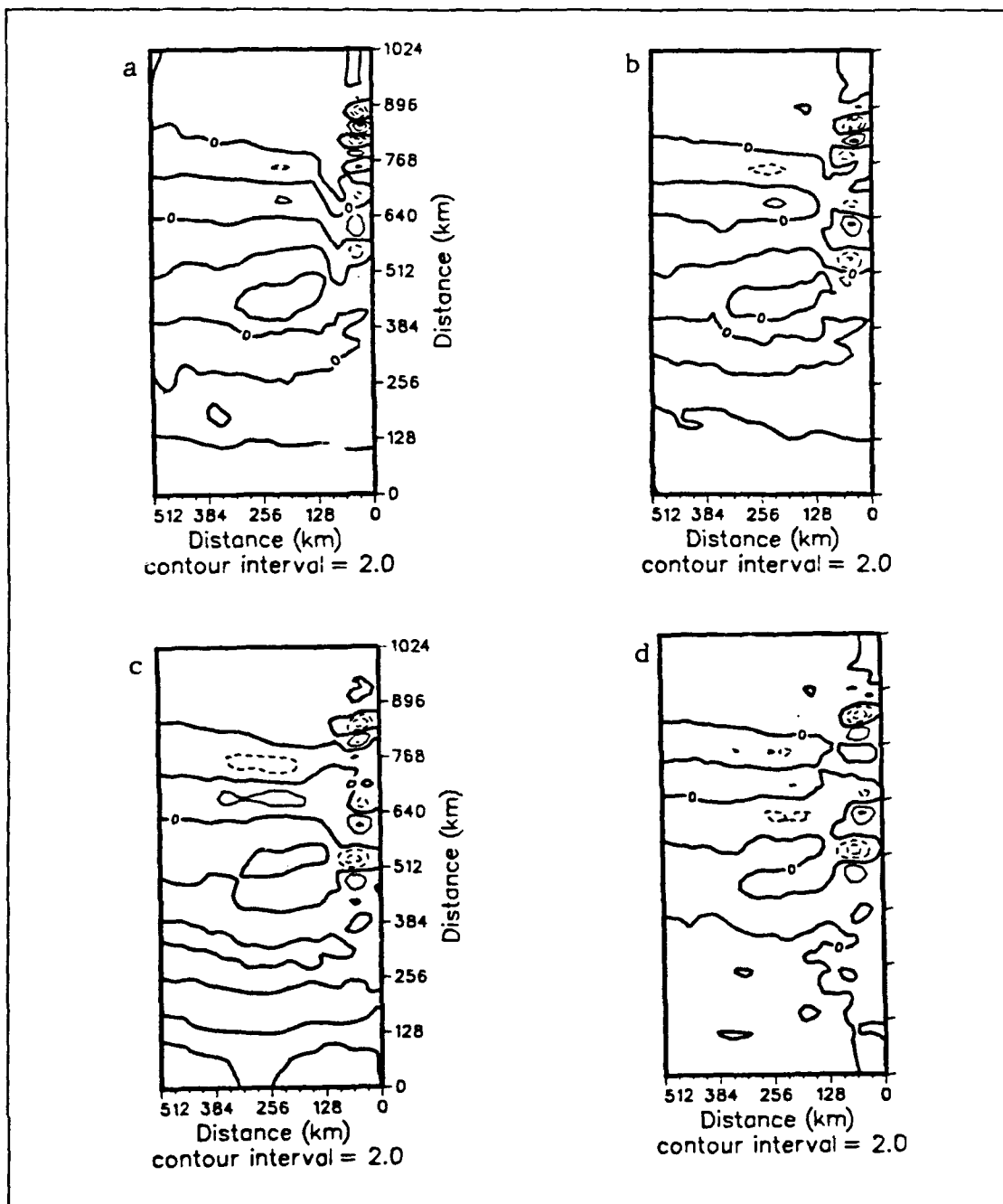
Figure 56. Isopleths of zonal velocity (cm/s) at 75 m depth for a) 29 Aug., b) 18 Sep., c) 28 Sep. and d) 8 Oct. 1988. Dashed lines are negative contours.

95
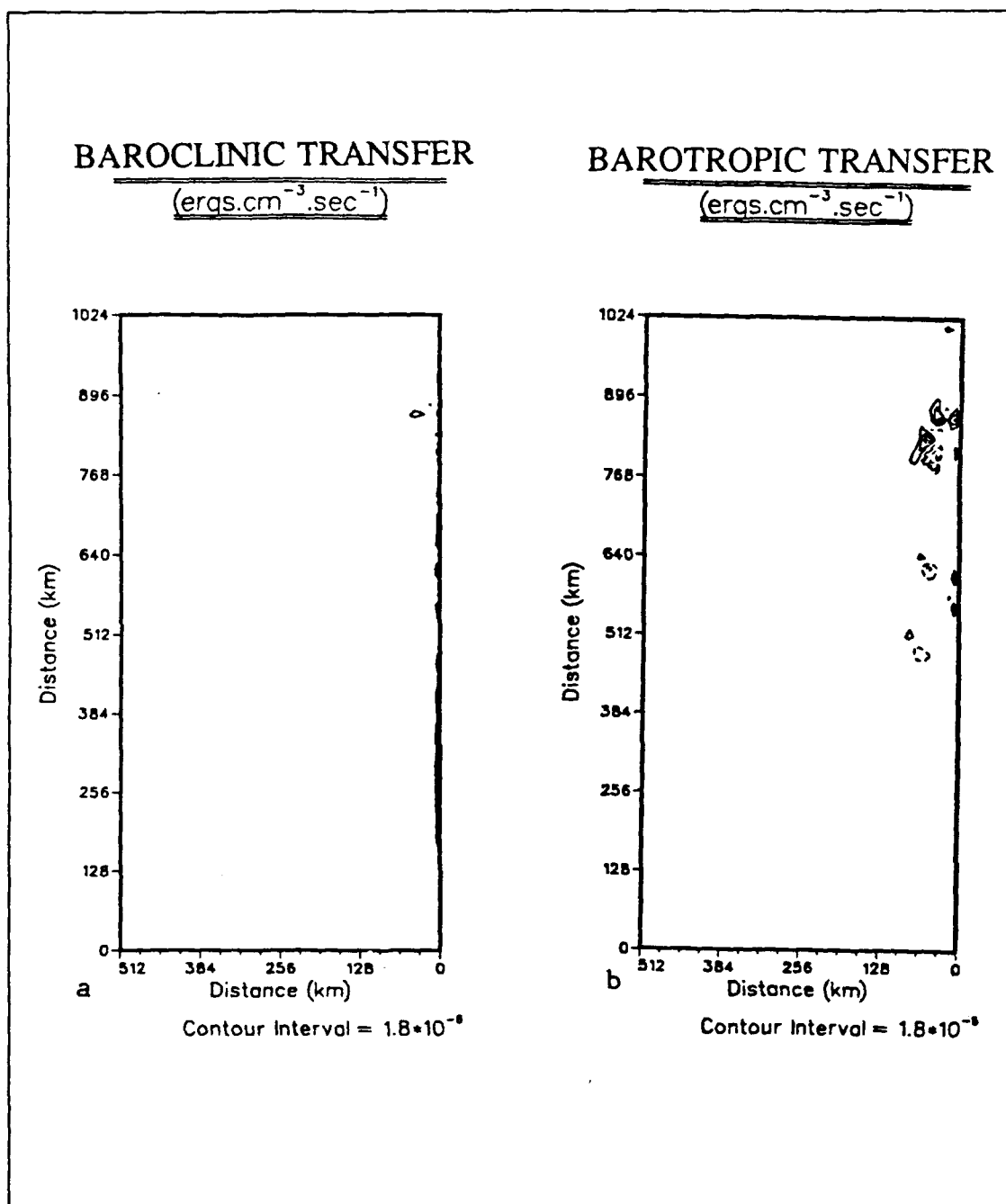
Figure 57. a) Baroclinic energy transfer for 18 Sep.-8 Oct. 1988.
b) Barotropic energy transfer for 18 Sep.-8 Oct. 1988.

IV. SUMMARY AND DISCUSSON

A. SUMMARY

A process-oriented numerical study of time-dependent wind forcing was conducted using a ten-layer primitive equation model. The model domain is geographically located off the west coast of Portugal and is rectangular in shape with a flat bottom, closed eastern boundary and open northern, southern and western boundaries.

To facilitate discussion of the model's response, the wind forcing for 1987 and 1988 was divided into four phases; Pre-Upwelling, Upwelling Favorable (Pre-Eddies), Upwelling Favorable (Eddies Present), and Post-Upwelling. These phases are defined by changes in the direction of the predominant winds.

The Pre-Upwelling phase is characterized by bursts of poleward winds superimposed on generally increasingly equatorward winds. These bursts of poleward winds cause a reduction or displacement of the surface equatorward jet and an intensification or shoaling of the poleward flow. In each year, the isotherms responded as expected indicating downwelling during periods of poleward winds and upwelling during periods of equatorward winds. At the beginning of both 1987 and 1988 there were eddies, resulting from eddy-generating mechanisms in 1986 and 1987, respectively, that completely decayed by the end of the Pre-Upwelling phase. The 1987 Pre-Upwelling phase lasted until approximately April (five months), while the 1988 Pre-Upwelling phase lasted until the end of January (one month).

The wind forcing for the Upwelling Favorable (Pre-Eddies) phase was characterized by a series of events, relaxations and reversals of the predominantly equatorward wind stress. The oceanic response to this forcing was characterized by the appearance of a quasi-steady equatorward jet (~4-13 cm/s) near the coast which was accompanied by a poleward undercurrent (~1-5 cm/s) by the end of the phase. Additionally, surfaced isotherms moved onshore and offshore in response to poleward or equatorward winds, respectively.

The wind forcing for the Upwelling Favorable (Eddies Present) phase was different for 1987 and 1988. The relaxations for 1987 were longer and of higher magnitude than those in 1988. The forcing for 1987 trended decreasingly equatorward during the phase, while for 1988 there was no noticeable trend. The third phase of 1987 lasted twice as long as the 1988 phase.

In both years, a surface equatorward jet and subsurface poleward current existed at or near the beginning of the phase. This combination persisted through the third phase of 1987 but was present only intermittently in the third phase of 1988. Cyclonic eddies were present in both years during the Upwelling Favorable (Eddies Present) phase. Eddies for 1987 were larger (60-100 km in diameter), greater in number (four-five) and more persistent than those found in 1988 (which were 20-40 km across and two-three in number). Anticyclonic eddies were absent in both 1987 and 1988. The same sequence of events preceded eddies in both years:

- The appearance of both a surface equatorward jet and a subsurface poleward current.

98

- The relaxation of equatorward wind stress.

- The shoaling and/or intensification of the poleward current.

- The formation of eddies.

The forcing during the Post-Upwelling phase was also different for 1987 and 1988. In 1987, 8-10 day bursts of equatorward and poleward winds were seen, while in 1988 the forcing was increasingly poleward until the middle of the phase when it started to become increasingly equatorward. Cyclonic eddies were present in both Post-Upwelling periods. However, in 1987 the eddies decayed, while in 1988 there were less intense eddies, which grew in size and number.

An energy analysis showed that mixed instabilities were present in the coastal, poleward region, while baroclinic instability was present in the equatorward, coastal region of the domain during both 1987 and 1988. During the early stages of eddy development in both years, barotropic instability could be present offshore. Baroclinic instability was dominant during the later stages of 1987 (i.e., late September to early October). The predominance of baroclinic instability in 1987 was not seen in 1988.

B. DISCUSSION

This process-oriented study affirms the importance of wind forcing to the overall surface circulation and eddy-generation in the coastal oceanic regime off the west coast of Portugal. The results obtained can be used to investigate the following questions:

- Do the eddies which remained at the end of 1986 and 1987 completely decay before the next upwelling season or are they simply rejuvenated and maintained by the equatorward winds?

99

- What is the generation mechanism for the eddies?

- Does the length of the upwelling season influence the characteristics of the eddies?

In response to the first question, results showed that eddies generated by mechanisms resident in the preceding year completely decayed by the end of the Pre-Upwelling phase in the succeeding year. This suggests a requirement for equatorward wind stress to maintain the eddies. It also suggests that the effects of wind forcing on eddy generation may be independent from year to year.

The generation mechanism for eddies formed in 1987 and 1988 was a combination of barotropic and baroclinic instability. This suggests that the relationship between the equatorward jet and the poleward current (existing either as a surface or subsurface current) is significant, if not necessary, for the formation of eddies in the region. For example, the results of this study show that a relaxation or reversal of the equatorward wind stress and subsequent shoaling of the poleward undercurrent preceded the formation of eddies.

The length of the total upwelling season (i.e., period of equatorward winds favorable for upwelling) does not appear to influence the characteristics of the eddies (e.g., the 1988-seven-month upwelling season produced smaller and weaker eddies than the 1987-five-month upwelling season). The results obtained do suggest, however, that there is a relationship between the characteristics of the eddies and the characteristics of the wind forcing during the Upwelling Favorable (Eddies Present) phase. The wind forcing for the third phase of 1987 was increasingly poleward with higher magnitude reversals and

relaxations and more than twice as long as the third phase of 1988. The 1987 wind forcing produced more and larger eddies than 1988 wind forcing.

The results obtained from this study suggest other questions that could be investigated to expand our understanding of the role of wind forcing on the surface circulation and eddy generation in this and other EBC regions. For example, how sensitive to the intensity of the wind forcing is the generation of eddies? Which is more important to eddy generation, the shoaling or the intensification of the poleward undercurrent? What is the relationship between the characteristics of the wind forcing during the third phase and the characteristics of the eddies generated? All these questions are important to address. With the advent of high speed computers, more process-oriented numerical studies should be conducted, which incorporate even more physical and dynamical processes (e.g., topographic forcing). The knowledge gained in such studies may well yield a better understanding of the circulation off Portugal as well as in other EBC regions.

LIST OF REFERENCES

Ambar, I., 1985: Seis meses de medicoes de correntes, temperaturas e salinidades na vertente continental Portuguesa a 40 N. *Relatorio tecnico, 1/85*, Grupo de Oceanografia, *Universidade de Lisboa*, 40 pp. (unpublished manuscript).

Arakawa, A., and V. R. Lamb, 1977: Computational design of the basic dynamical processes of the UCLA general circulation model. *Methods Comput. Phys.*, **17**, J. Chang, Ed., Academic Press, 173-265.

Bakun, A., 1973: Coastal upwelling indicies, west coast of North America, 1946-71. *U. S. Dep. Commer., NOAA Tech. Rep. NMFS SSRF-671*, 103pp.

Bakun, A., and C. S. Nelson, 1991: The seasonal cycle of wind stress curl in subtropical eastern boundary current regions. *J. Phys. Oceanogr.*, in press.

Barton, E. D., 1986: A filament programme in the Iberian upwelling region. *Coastal Transition Zone Newsletter*, **1**, 2-5.

Barton, E. D., 1989: The poleward undercurrent on the eastern boundary of the subtropical North Atlantic. In: *Poleward Flows along Eastern Ocean Boundaries*, edited by S. Neshyba, C. N. K. Mooers, R. L. Smith and R. T. Barber. Springer - Verlag Lecture Notes. 82-94.

Batteen, M. L., and Y.-J. Han, 1981: On the computational noise of finite difference schemes used in ocean models. *Tellus*, **33**, 387-396.

Batteen, M. L., and M. J. Rutherford, 1990: Modeling studies in the Leeuwin Current: The role of thermal forcing. *J. Phys. Oceanogr.*, **20**, 1484-1520.

Batteen, M. L., C .N. Lopes da Costa, and C. S. Nelson, 1991: A numerical study of wind stress curl effects on eddies and filaments off the Northwest coast of the Iberian Peninsula. *J. Mar. Systems*, submitted.

Batteen, M. L., R. L. Haney, T. A. Tielking, and P. G. Renaud, 1989: A numerical study of wind forcing of eddies and jets in the California Current System. *J. Mar. Res.*, **47**, 493-523.

Brink, K.H., 1983: The near-surface dynamics of coastal upwelling. *Prog. Oceanog.* **2**, 223-257.

Chief of Naval Research, Office of Naval Research, 1987: Fy-91/95 Naval research planning and programming guidance, letter.

Fiuza, A. F. G., 1982: The Portuguese coastal upwelling system. In: *Present problems of oceanography in Portugal, Junta Nacional de Investigacao Cientifica e Tecnologica, Lisboa,* 45-71.

Fiuza, A. F. G., and F. M. Sousa, 1989: Preliminary results of a CTD survey in the Coastal Transition Zone off Portugal during 1-9 September 1988. *Coastal Transition Zone Newsletter,* **4, 2-9.**

Frouin, R., A. F. G. Fiuza, I. Ambar, and T. J. Boyd, 1990: Observations of a poleward surface current off the coasts of Portugal and Spain during Winter. *J. Geophys. Res.,* **95,** 679-691.

Han, Y.-J., 1975. Numerical simulation of mesoscale eddies. Ph.D. thesis, University of California, Los Angeles, 154 pp.

Haney, R. L., 1985. Midlatitude sea surface temperature anomalies: A numerical hindcast. *J. Phys. Oceanogr.,* **15,** 787-799.

Haynes, R., and E. D. Barton, 1990: A poleward flow along the Atlantic coast of the Iberian Peninsula . *J. Geophys. Res.* **95,** 11425-11441.

Huyer, A., 1983: Coastal Upwelling in the California Current System. *Prog. Oceanog.,* **12,** 259-284.

Levitus, S., 1982: Climatological atlas of the world ocean. *U. S. Dept. Commer. NOAA Prof. Pap.* **13,** 173 pp.

Lopes da Costa, C., 1989: A numerical study of wind forcing in the eastern boundary current system off Portugal. M. S. Thesis, Naval Postgraduate School, 114 pp.

Meincke, J., G. Siedler, and W. Zenk, 1975: Some current observations near the continental slope off Portugal. *"Meteor" Forsch.-Ergebn.,* A, **16,** 15-22.

Naval Oceanography Command Detachment, Asheville N. C., 1989: Joint U. S. Navy/U. S. Air Force Climatic Study of the Upper Atmosphere. Vols. 2 and 8, pg 2.

Paulson, C. A., and J. J. Simpson, 1977: Irradiance measurements in the upper ocean. *J. Phys. Oceanogr.,* **7,** 952-956.

103

Phillips, N. A., 1966: The equations of motion for a shallow rotating atmosphere and the traditional approximations. *J. Atmos. Sci.,* **23**, 626.

Pickard, G. L., and W. J. Emery, 1982: *Descriptive Physical Oceanography,* Pergamon Press Fourth Edition, 249 pp.

Semtner, A. J., and Y. Mintz, 1977: Numerical simulation of the Gulf Stream and mid-ocean eddies. *J. Phys. Oceanogr.,* **14**, 623-628.

Smith, R. L., 1968: Upwelling. *Oceanogr. Mar. Biol. Ann. Rev.,* **6**, 11-46.

Weatherly, G. L., 1972: A study of the bottom boundary layer of the Florida current. *J. Phys. Oceanogr.,* **2**, 54-72.

Wooster, W. S., and J. L. Reid, Jr., 1963: Eastern Boundary Currents. *The Sea, Vol. 2* M. N. Hill, Ed., Wiley International, 253-280.

Wooster, W. S., A. Bakun, and D. R. McLain, 1976: The seasonal upwelling cycle along the eastern boundary of the North Atlantic. *J. Mar. Res.,* **34**, 131-140.

INITIAL DISTRIBUTION LIST

		No. Copies
1.	Defense Technical Information Center Cameron Station Alexandria, VA 22304-6145	2
2.	Library, Code 52 Naval Postgraduate School Monterey, CA 93943-5002	2
3.	Chairman (Code OC/Co) Department of Oceanography Naval Postgraduate School Monterey, CA 93943-5000	1
4.	Chairman (Code MR/Hy) Department of Meteorology Naval Postgraduate School Monterey, CA 93943-5000	1
5.	Dr. Mary L. Batteen (Code OC/Bv) Department of Oceanography Naval Postgraduate School Monterey, CA 93943-5000	2
6.	CAPT Craig S. Nelson, NOAA Department of Oceanography Naval Postgraduate School Monterey, CA 93943-5000	1
7.	Commander Naval Oceanography Command Stennis Space Center, MS 39529-5000	1
8.	Commanding Officer Naval Oceanographic and Atmospheric Research Laboratory Stennis Space Center, MS 39529-5004	1

105

9. Commanding Officer   1
   Fleet Numerical Oceanography Center
   Monterey, CA 93943-5005

10. Office of Naval Research (Code 420)   1
    800 N. Quincy Street
    Arlington, VA 22217

11. Dr. D. Evans   1
    Office of Naval Research (Code 1122PO)
    800 N. Quincy Street
    Arlington, VA 22217

12. LT Stephen L. Buss, USN   2
    Department Head School (Class 120)
    Surface Warfare Officer School Command
    Newport, RI 02841-5012